5-2001

Experimental Investigation of Snapover: The Sudden Increase of Plasma Current Drawn to a Positively Biased Conductor When Surrounded by a Dielectric

Clint D. Thomson

EXPERIMENTAL INVESTIGATION OF SNAPOVER: THE SUDDEN INCREASE OF PLASMA CURRENT DRAWN TO A POSITIVELY BIASED CONDUCTOR WHEN SURROUNDED BY A DIELECTRIC

by

Clint D. Thomson

A thesis submitted in partial fulfillment
of the requirements for the degree

of

MASTER OF SCIENCE

in

Physics

Approved:

Dr. John Robert Dennison Major Professor	Dr. W. John Raitt Committee Member
Dr. D. Mark Riffe Committee Member	Dr. Thomas L. Kent Dean of Graduate Studies

UTAH STATE UNIVERSITY
Logan, Utah

2001

ABSTRACT

Experimental Investigation of Snapover: The Sudden Increase of

Plasma Current Drawn to a Positively Biased Conductor

When Surrounded by a Dielectric

by

Clint D. Thomson, Master of Science

Utah State University, 2001

Major Professor: Dr. John Robert Dennison
Department: Physics

Snapover is particularly relevant to Earth-orbiting spacecraft powered by high-voltage solar arrays. During snapover, the current collected by a positively biased conductor that is immersed in a plasma suddenly increases when two conditions are met: i) there is an immediately adjacent insulator; ii) the conductor exceeds a positive threshold voltage with respect to the plasma. The enhanced current develops as a consequence of the insulator, either through secondary electron (SE) emission or by material ionization. Experiments were performed to examine snapover onset potential and current collection dependence on conductor and insulator materials, conductor size and shape, sample history, biasing rate, and contamination and smoothness of the dielectric surface. Numerous current jumps were observed between applied voltages of 100 V and 1000 V. Both surface roughening and surface coatings were found to inhibit snapover. In general, the results did not support previous simple interpretations of the SE model.

(162 pages)

ACKNOWLEDGMENTS

I wish to thank my major professor, J.R. Dennison, for his guidance and encouragement throughout my graduate work. Not only has he been a great advisor and teacher, but his personal support has greatly encouraged me in the pursuit of my physics career. Robert Davies and J.R. Dennison at USU, and Joel Galofaro and Dale Ferguson at NASA GRC should receive the majority of the credit for the initial planning, designing, and fabrication of this experimental investigation. I wish to thank all the staff at the Plasma Interaction Facility (PIF) at NASA GRC for the use of their equipment and for the gracious patience and expertise they have bestowed upon an upcoming scientist. Boris Vayner and Joel Galofaro were especially helpful in operating the PIF equipment, and in answering questions and fulfilling requests during the experimental process. I would like to thank my committee for their careful critique of my thesis, and for their insights and suggestions towards the improvement of my work. I greatly appreciate the organizations that have funded this research, including the NASA Graduate Student Research Program (awarded to Rob Davies and myself) and the Rocky Mountain NASA Space Grant Consortium (also awarded to Rob Davies and myself). Finally, I would like to thank my wife and children for the sacrifices they have made in supporting me throughout my prolonged education.

Clint D. Thomson

CONTENTS

Page

LIST OF TABLES

LIST OF FIGURES

Figure Page

Figure Page

NOMENCLATURE

A_{cond}	Area of sample conductor
A_{ins}	Snapped over insulator area
b	Planar probe fitting parameter
e	Fundamental charge
E	Emitted secondary electron energies
E_1	First crossover energy
E_2	Second crossover energy
E_{max}	Maximum yield energy
E_0	Incident electron energy
$f(E_0)$	Incident electron energy distribution function
$g(E_0,E)$	Secondary electron emission spectrum
I_b	Current before jump
I_{down}	Reverse bias collected current
I_f	Current following jump
I_f/I_b	Current jump ratio
I_{tot}	Total collected current
I_{up}	Forward bias collected current
J_e	Random plasma electron current density
J_{plasma}	Plasma contribution to total collected current density
J_{pln}	Current density to planar probe
$J_{surface}$	Secondary electron transport contribution to total collected current density
$J_{thcksphr}$	Spherical probe thick sheath current density
$J_{thcksphr2}$	Another spherical probe thick sheath current density
$J_{thnsphr}$	Spherical probe thin sheath current density
J_{tot}	Total collected current density
J_{4pln}	Current density to an infinite planar probe
m_e	Electron mass
n	Electron number density
r	Radius of conductor probe
r_s	Radius of plasma sheath
T	Mean plasma electron temperature
u_e	Mean plasma electron speed
V	Applied conductor voltage
V_{onset}	Onset voltage
α	Secondary electron collection efficiency term
γ	Forward and reverse bias current convergence parameter
ΔI	Current jump magnitude
$\Delta I/\Delta V$	I-V curve slope

δ	Secondary electron yield
δ_{max}	Maximum secondary electron yield
ε_0	Permittivity of vacuum
θ	Incident electron angle from normal
κ	Boltzmann constant
λ_D	Plasma Debye length
σ	Total electron yield
σ_{max}	Maximum total electron yield

CHAPTER 1

INTRODUCTION

1.1 Snapover and Spacecraft Power Losses

In the past, satellite solar arrays have operated at voltages of less than 100 volts. However, over the last 20 years, plans have been made to launch larger and more complex spacecraft that require much more power to operate. Most notably, massive high-voltage solar arrays are being used to power the International Space Station. This shift in interest towards high-powered spacecraft has presented new physics and engineering problems for designers. For example, operating at high currents inevitably leads to significant transmission line mass and I^2R power losses. Alternatively, operating at high voltages can result in detrimental interactions between the spacecraft and the ions and electrons that make up the space plasma environment. This is especially true in low Earth orbit (LEO) where the surrounding plasma particle densities are relatively high, ranging from $1 \cdot 10^4$ to $1 \cdot 10^6$ cm^{-3} (Hastings and Garret, 1996). Nevertheless, to reduce cabling mass, power losses, and unwanted magnetic torque and drag effects, spacecraft designers have deemed it mandatory to design arrays that operate at higher voltages and lower currents (Stevens, 1979; Hillard and Ferguson, 1993a, 1993b).

The International Space Station is an example of a high-powered spacecraft that operates at high voltages (> 100 V). In reaching equilibrium with the surrounding plasma (no net current flow to or from the environment) part of the solar arrays float positively to collect electrons while other parts float negatively to collect ions. It is estimated that the most negative end of the space station's arrays float at approximately -140 V with respect to the surrounding plasma, while the most positive ends float at voltages over +100 V (Hillard and Ferguson, 1993a, 1993b). During the process of attaining equilibrium, solar array voltages fluctuate about these two extreme values, resulting in a number of undesirable plasma interactions. First, high negatively biased solar arrays

undergo destructive arcing that can lead to both cover glass surface damage and sudden current pulses that can interfere with system instruments and control electronics (Thiemann *et al.,*1990; Thiemann and Schunk, 1994; Snyder, 1995). Second, positively biased arrays easily draw electron current from the plasma due to the relatively low mass (and high mobility) of the electrons. This current may result in either insulator surface charging, or it can be collected directly by exposed conductor interconnects or semiconductor solar cells (Hastings and Garret, 1996).

Traditional satellite arrays are composed of solar cells connected in series by a network of thin conducting interconnects. The array, along with the interconnects, is usually covered by a protective glass overcoating. The interconnects can be exposed to plasma currents when high energy meteoroids or orbital debris impact and punch tiny "pinholes" in the cover glass. In a similar manner, system power cables can develop small holes in their insulator coating, exposing the underlying wire. If the exposed conductors are at a positive potential with respect to the plasma, electron current will be drawn. Electron current drawn from the plasma cannot be utilized by the spacecraft. In fact, the system's own power supply is drained as the spacecraft reestablishes equilibrium with the surrounding plasma, resulting in power losses for the spacecraft. Consequently, plasma current drawn to the conductors is parasitic in nature. At low positive voltages, parasitic electron current is generally not a primary concern; however, above a critical positive voltage (~100 V), solar arrays can undergo a phenomenon called snapover where the electron current suddenly jumps by as much as two or three orders of magnitude (Domitz and Kolecki, 1979; Hillard and Ferguson, 1993a, 1993b; Hastings and Garret, 1996).

Snapover is a phenomenon that occurs on surfaces comprised of exposed conductors surrounded by a dielectric material in a plasma environment. In the absence of a surrounding dielectric, snapover does not occur. For this reason, it seems reasonable (and has been shown

experimentally as will be discussed in Section 1.2) that the additional collected current is generated through a combination of physical processes occurring on the insulator, and from resulting changes in the local plasma potentials. Specifically, during snapover the electron current collected by exposed conducting interconnects exhibits a sudden increase as the conductor is biased above a critical positive bias voltage. Once this voltage threshold has been reached on a solar array, the surrounding glass overlay charges positively and begins to draw electrons as though it were a conductor. Consequently, the effective current collecting surface area of the solar array is no longer limited to the conductor interconnects, but is greatly enlarged by the surrounding insulator. As mentioned before, on a spacecraft this can result in substantial power losses (Domitz and Kolecki, 1979). In addition, snapover can cause high negative counter potentials on other parts of the spacecraft solar array that can lead to destructive arcing (Hillard and Ferguson, 1993a, 1993b). Also, at times an optical glow has accompanied the phenomenon (Ferguson *et al.*, 1998).

The key elements of snapover, such as onset voltage and resulting collected current jumps, are most easily studied by plotting the current collected by the conductor against the applied voltage (referred to as an I-V curve or profile) as shown in Fig. 1.1. During this snapover investigation, numerous such I-V profiles were measured on conductor/insulator samples. Important characteristics of these data curves were the snapover onset voltage, absolute current values at a given voltage, current jump magnitudes (differences of current before and after snapover), current jump ratios (ratio of current after to before snapover), collected current slopes (first and second derivatives of I-V curve) before and after the jump, and hysteresis behavior of the I-V curve as the applied voltage was subsequently stepped down. As will be shown, these characteristics were used to study the basic material and plasma parameters that influence snapover.

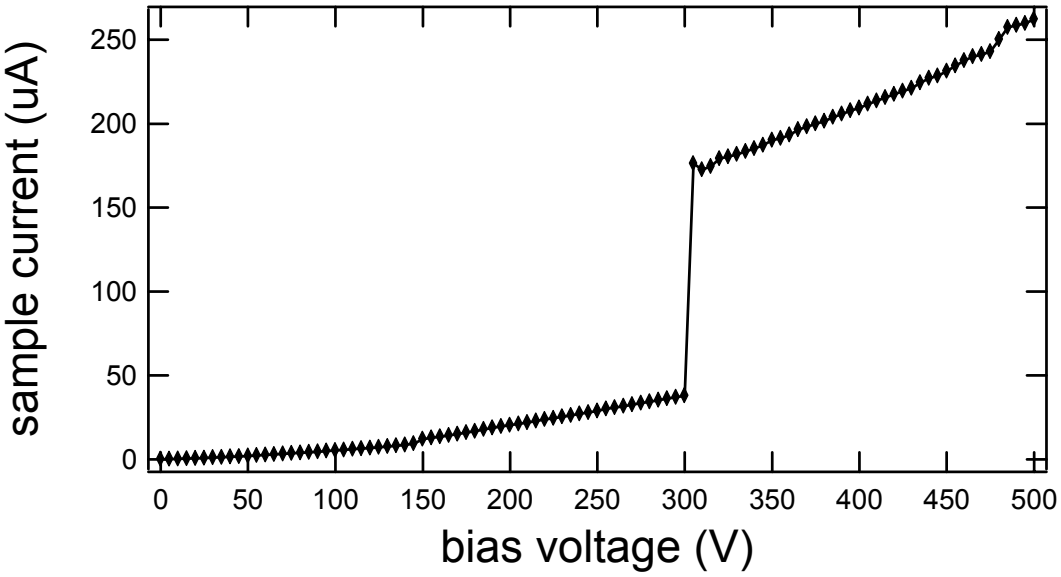

FIG. 1.1. A typical sample I-V profile showing snapover (at ~ 300 V) for a Cu-Teflon™ sample.

1.2 Previous Theoretical, Computational, and Experimental Work

Some of the first experimental studies on snapover were performed by Cole, Ogawa, and Sellen in the late 1960s (Cole *et al.,* 1969). At the time, snapover was termed the "pinhole effect" because it was noticed that tiny pin-sized holes in a solar array cover glass could increase the plasma current to an underlying conductor (in comparison to an uncovered conductor of the same area) by as much as two orders of magnitude (Stillwell *et al.*, 1985). Early ground-based experimental investigations of snapover were performed primarily at NASA Lewis Research Center (now NASA Glenn Research Center) during the 1970s and early 1980s by Stevens, Grier, Domitz, and Kennerud (Grier and McKinzie, 1972; Kennerud, 1974; Grier and Domitz, 1975; Grier and Stevens, 1978; Stevens, 1979; Domitz and Kolecki, 1979). Also, a successful space flight experiment, PIX, was launched in 1978 (Grier and Stevens, 1978; Grier, 1979). These early studies focused primarily on measuring the general features of snapover.

Most of the important findings are summarized below.

i) It was confirmed that the anomalous snapover current to a conductor only occurred in the presence of an insulator at positive voltages, and that the I-V current profile differed substantially from an isolated conductor probe with no surrounding dielectric. To verify this, isolated conductor probes were ramped to high positive voltages and no current jumps were observed in the I-V curves. Then, conductor-insulator samples (of the same conductor dimensions) were ramped to high voltages, and I-V curves were compared to those of the individual conductor probes (Grier and Domitz, 1975; Grier and Stevens, 1978; Grier, 1979). It was found that prior to snapover, current to the conductor-insulator samples was often suppressed as compared to an individual conductor probe because the insulator maintained a slightly negative charge that seemed to suppress plasma electron current collection (Grier and Domitz, 1975; Stevens, 1979). However, after snapover the current was enhanced by as much as two to three orders of magnitude as compared to the current before snapover and also to the isolated conductor probes (Grier and Domitz, 1975; Grier and Stevens, 1978; Stevens, 1979). Also, Grier and McKinzie (1972) compared the measured current (through 0.51 cm diameter hole) to planar conductor probe theory predictions and found that below ~ 1 kV the measured current fell below the computed value, but that after a current jump transition the current exceeded the computed value. Conductor-insulator samples were also ramped to high negative voltages in order to confirm the positive voltage affiliation of snapover. It was shown that at high negative voltages, snapover-enhanced current did not occur. Instead, the insulator or plasma would break down under high potentials, resulting in arc discharge (Grier and Stevens, 1978; Grier, 1979; Stevens, 1979).

ii) The range of onset voltages and magnitudes of the current jumps were studied on

conductor-insulator samples of different geometries. In some investigations (Grier and Stevens, 1978; Stevens, 1979; Grier, 1979) samples were fashioned after damaged solar array panels (with conductor interconnects exposed through tiny holes in the cover glass) in order to observe effects of snapover on large areas of solar arrays. In other investigations (Grier and McKinzie, 1972; Grier and Domitz, 1975; Gabriel *et al.*, 1983), simpler sample geometries such as disk-shaped electrodes surrounded by insulator plates were fabricated in an attempt to simplify the study of the underlying physical mechanism involved (Grier and Domitz, 1975; Gabriel *et al.*, 1983). During ground-based solar array sample experiments of snapover, Grier (1979) reported increased snapover current collection of one to two orders of magnitude at applied voltages ranging from 100 to 500 V. Stevens (1979) reported current increases of three to four orders of magnitude on solar array samples at inception voltages above 100 V. Grier and Domitz (1975) reported snapover current increases of as much as three to four orders of magnitude on copper disks surrounded by Kapton™ at voltages ranging from 100-1000 V. During the PIX flight experiment, current enhancement of one to two orders of magnitude was observed at applied voltages ranging from 400-1000 V for both solar array and disk sample geometries (Grier and Stevens, 1978).

iii) Current jump magnitude and inception voltage dependence on exposed electrode and insulator areas were studied. Grier and Domitz (1975) studied current collected to copper electrodes through 2.54-cm and 0.051-cm diameter holes in Kapton™ plates of different areas. They found that, overall, the collected current through the larger holes exceeded the current through the smaller holes by one to three orders of magnitude (depending on the insulator area) up to applied voltages of 10 kV. Additionally, the current strongly increased as a function of insulator plate area. For example, a 30.5-cm diameter plate

collected nearly 100 times the current as a 2.54-cm diameter plate through a 0.051-cm diameter hole at the same voltage. In this same study, no inception voltage dependence on hole size or sample insulator area was reported. Stevens (1979) also reported an increase in collected current as a function of surrounding insulator surface area.

iv) According to Stevens (1979), the overall collected current before and after snapover was found to increase with increasing plasma density. Additionally, the magnitude of the current jump (occurring above 100 V on a solar array sample) was found to increase by roughly an order of magnitude as the plasma density was also increased by an order of magnitude. Grier (1979) reported similar results, that the overall current increased at higher plasma electron densities.

v) Insulator surface potentials as well as local plasma potentials were measured before and after snapover. Stevens (1979) used a capacitively coupled surface-voltage probe to measure insulator surface-voltage profiles on a solar array sample, and found that prior to snapover the conductor resided at the applied bias voltage while the surrounding insulator maintained a slightly negative potential (1 to 10 V). However, somewhere between 250 to 500 V applied bias, the immediately surrounding insulator potentials jumped nearly to the applied conductor voltage, and then the surface potential gradually decreased with increasing distance from the conductor. Similar results were not observed when the sample was negatively biased (in this case, the potential of the immediately surrounding insulator dropped abruptly for all applied conductor voltages). Grier (1979) reported similar results, that at 100 V applied bias the high surface potentials were localized around the conductor solar array interconnects, while at 1000 V the entire sample array resided at high potentials nearly equal to the applied conductor bias voltage. Additionally, by coating the sample array with phosphor, it was observed that at high

voltages ranging from 900 to 2000 V the entire array glowed from electron bombardment. Finally, Gabriel *et al.* (1983) measured plasma potential profiles over pinholes on a solar array sample using an emissive probe. It was found that between 100 V and 450 V the measured sheath sizes were smaller than values calculated using standard probe theory, and increased linearly with applied voltage. This result somewhat contradicted later computational models and experimental measurements (Carruth, 1987) of snapover where the plasma sheath was shown to expand over large areas of the insulator, thus allowing increased interaction with the surrounding plasma. Unfortunately, in this study, plasma potential profiles were not measured simultaneously with I-V curve profiles. Consequently, measured changes in the plasma potentials could not be correlated with snapover events.

vi) During these early studies, qualitative physical models for snapover were proposed. Included in these models were the following: the emission of low-energy electrons (secondary electrons) from the surrounding insulator; sample insulator heating, out-gassing, vaporization, and material ionization; and plasma sheath expansion (resulting from positive insulator charging) followed by increased interactions with plasma electrons. Although evidence for all three of these mechanisms existed, individually none of these mechanisms seemed sufficient to explain all aspects of the anomalous current jumps. For example, secondary electron emission from the insulator provided a good candidate for sustained current enhancement since for incident electron energies associated with snapover onset potentials (voltages greater than 100 V) an insulator gives off more electrons than are incident, and thus charges positively. However, early experiments designed to test snapover dependence on insulator material type did not show differences in snapover inception voltages due to insulator material, but did show

differences in the overall collected current up to applied bias voltages of 10 kV (Grier and McKinzie, 1972). The failure to see an insulator dependence on inception voltages may have resulted from exceedingly large bias voltage steps used in these early investigations. Bias voltage step sizes larger than 100 V were typically used, whereas insulator secondary electron emission differences can only be detected with smaller voltage steps on the order of 1-10 V. Furthermore, a wide range of applied snapover onset voltages along with multiple sequential current jumps was reported (Grier and McKinzie, 1972; Grier and Domitz, 1975; Grier and Stevens, 1978; Stevens, 1979; Domitz and Kolecki, 1979; Grier, 1979; Gabriel *et al.*, 1983). This is suggestive of numerous out-gassing/ionization events from the surrounding insulator. Additionally, in their study, Grier and McKinzie (1972) reported significant charring and melting of the insulator immediately surrounding the conductor, providing evidence of local heating, vaporization, and possibly ionization of the surrounding insulator material. The extent of the charring was shown to be dependent on insulator type. Finally, early researchers speculated that once the insulator snapped over, and reached a potential nearly equal to the applied conductor voltage, the plasma sheath expanded allowing greater interaction between the sample and plasma electrons (Grier and Domitz, 1975; Grier, 1979; Gabriel *et al.*, 1983). As will be discussed below, subsequent computational modeling and direct plasma potential measurements confirmed plasma sheath expansion as a result of positive insulator charging.

These early investigations were invaluable for experimentally mapping the basic nature of snapover of conductor/insulator systems in a plasma. These studies provided data on the deviations of positively biased conductor/insulator system current collection as compared to standard conductor electrodes in a plasma. They also predicted detrimental parasitic current

abnormalities on high-powered spacecraft. However, these early studies failed in establishing definite dependancies on sample conductor and insulator materials, even though material characteristics (particularly of the insulator material) should play a central role in the current enhancement process. Consequently, these studies did not provide the detailed information required to formulate sophisticated models of snapover.

Since the early 1980s, a few additional ground-based experimental investigations of snapover have been conducted (Gabriel *et al.*, 1983; Stillwell *et al.*, 1985; Carruth, 1987; Ferguson *et al.*, 1998). In addition, two flight experiments (PIX II and SAMPIE) have been launched to determine LEO plasma interactions with high-voltage solar arrays (Mandell *et al.*, 1986; Hillard and Ferguson, 1993a, 1993b). Also, a number of computational and theoretical studies have been performed in an attempt to model both the abnormal I-V curve behavior of conductor/insulator systems at positive biases, and also the complicated interplay between local plasma potentials, material charging, and plasma electron current collection (Chaky *et al.*, 1981; Mandell and Katz, 1983; Brandon *et al.*, 1984; Kessel *et al.*, 1985; Mandell *et al.*, 1986; Hastings and Chang, 1989; Krauss, 1989; Thiemann and Schunk, 1990a, 1990b).

Stillwell *et al.* (1985) conducted a very thorough ground-based experimental investigation where they strongly emphasized that discrepancies in previously reported onset voltages and collection currents could be explained by the existence of two separate snapover current collection modes that they termed the "surface-enhanced" and "vapor-enhanced" collection modes. They proposed that at lower inception voltages (anywhere from 100 to 500 V), the surface-enhanced mode was triggered by secondary electrons originating from the insulator. However, at higher inception voltages ($>$ 500 V), the vapor-enhanced mode was triggered by both insulator secondary electron emission as well as electrons freed from ionized materials that were out-gassed or vaporized from the insulator. As described in their investigation, the two current collection

modes had several distinguishing characteristics. For example, the surface-enhanced mode snapover inception voltages were usually reproducible, while the vapor-enhanced snapover inceptions were not. Also, the magnitudes of the current jumps for the vapor-enhanced snapovers exceeded those of the surface-enhanced snapovers by an order of magnitude or more. Additionally, the vapor-enhanced snapovers exhibited a characteristic hook-shaped decline in the I-V curves immediately following the current jump before reestablishing roughly linear I-V curve behavior. Also, the vapor-enhanced snapovers were usually accompanied by a bluish glow over the sample, and would often discolor or damage the surrounding insulator. No onset voltage dependence on insulator type (isomica, Kapton™, and Teflon™) was mentioned for either of the collection modes, although the overall collected current to isomica was significantly higher than for Kapton™ and Teflon™ (Kapton™ and Teflon™ exhibited nearly identical I-V profiles despite the differences in their SE yield properties). It was also reported that the overall current collected from the surface-enhanced snapovers increased with increasing hole diameter, while the current from the vapor-enhanced snapovers was relatively independent of hole diameter. Finally, both of the current collection modes were found to be diminished by insulator surface texturing.

In another ground-based experimental study, Carruth (1987) used two emissive probes to map the plasma potentials around two conductors (with slit geometry) separated by two and three centimeters of Kapton™ insulation. He found that at positive biases of 100 to 150 V the plasma potentials (initially localized around the conductor slits) expanded to envelop both the conductors and intermediate insulator. Finally, Ferguson *et al.* (1998) observed an accompanying glow for snapovers with onset voltages ranging from ~ 200 to 400 V.

Most of the computational and theoretical studies to date have only modeled current contributions from the surrounding plasma and from insulator secondary electron emission. Very few, if any, have attempted to include effects from out-gassed and ionized materials originating

from the surrounding insulator or conductor/insulator junction. From these plasma and secondary electron emission models, it has been shown that after including insulator charging effects (due to secondary electron emission) as well as local plasma potential responses to changing surface potentials, sudden current increases in the I-V curves can be simulated once the insulator begins to emit a net positive number of secondary electrons. These models have shown that after the snapover threshold condition is reached, the surrounding insulator potential increases to a positive value nearly equal to the applied conductor potential (which then gradually decays further away from the conductor), and the plasma sheath expands to allow greater interaction with plasma electrons (Chaky *et al.*, 1981; Mandell and Katz, 1983; Brandon *et al.*, 1984; Mandell *et al.*, 1986; Hastings and Chang, 1989; Thiemann and Schunk, 1990a, 1990b). Brandon *et al.* (1984) reported that after the snapover condition was reached (at voltages > 100 V), the sheath continued to expand with increasing applied voltage (the sheath area at 500 V was 10 times larger than at 100 V), and that the collected current was proportional to the sheath area. Qualitatively, this was consistent with previous measurements where Gabriel *et al.* (1983) experimentally showed that the sheath area expanded linearly with applied voltage throughout this same voltage range. Brandon *et al.* (1984) and Kessel *et al.* (1985) both argued that at voltages just over the insulator first crossover energy (the energy or associated voltage where more electrons are emitted from the insulator than are incident), significant current collection would result from a plasma electron focusing effect set up by the positive-charge gradient created on the surrounding insulator.

After taking into account plasma current contributions, combined with secondary electron emission from the insulator, Hastings and Chang (1989) argued that near the insulator first crossover energy, two stable current equilibrium conditions (and one unstable condition) could exist. The first stable condition was equivalent to the experimentally observed condition before snapover where the insulator maintained a slightly negative charge and repelled most plasma

electrons. The second condition involved a sudden transition to a new equilibrium state where current was maintained between incoming plasma and outgoing secondary electrons from the insulator that propagated towards the conductor. They argued that since both conditions were stable near the first crossover energy, some variation could occur in measured snapover onset voltages. The model also predicted that at ~ 700 V the current collected to Kapton™ samples would level off since Kapton™ may cease to emit more electrons than were incident (this energy is termed the second crossover energy). It should be mentioned that supporting experimental observations of this behavior for Kapton™ were reported earlier by Grier and Domitz (1975) at voltages above 1 kV, but at the time, were attributed to finite plasma chamber size. Furthermore, according to their model Hastings and Chang predicted that the snapover inception voltage for spherical geometries should be greater than those for planar geometries. Finally, the authors stated that the snapover inception voltage should depend strongly on insulator material type since first crossover energies vary among insulators.

Qualitatively, the computational and theoretical models described above have been consistent with experimental measurements in that they have predicted the sudden current enhancement of snapover at some positive threshold voltage, and they have also simulated positive insulator charging and plasma sheath expansion after a snapover event. However, quantitatively these models have generally predicted snapover inception voltages and current collection magnitudes significantly lower than measured values (modeled values of ~ 100 V compared with measured values typically ranging from 200-1000 V), and have been unable to account for multiple current jumps that have been observed experimentally. This suggests that these models, along with the simple secondary electron emission mechanism on which they are based, are somehow incomplete. Most likely, the inadequacy of these models results from a failure to incorporate desorption and ionization of materials originating from the sample, as well

as the ionization of any surrounding neutral background gas of the plasma environment.

To date, although a number of snapover experimental studies have been undertaken with the aim of determining the general nature of snapover and its detrimental effects on spacecraft, there have been very few comprehensive experimental investigations performed to explore the material-related mechanisms involved. In fact, as of yet no ground-based or flight investigation has successfully determined the detailed role played by secondary electron emission from the insulator, or the role played by insulator out-gassing and ionization on the multiple current transitions observed in snapover I-V curves. Additionally, researchers who have explored material effects have reported few (and rather inconsistent) results concerning the dependence of onset voltages and collection current magnitudes on conductor and insulator types (Grier and McKinzie, 1972; Stillwell *et al.*, 1985). Consequently, there remains an insufficient amount of detailed experimental data needed to develop convincing theoretical and computational models that accurately incorporate material properties. A summary of significant experimental studies to date is provided in Table 1.1.

Our investigation was undertaken to expand on the existing experimental database by testing some of the fundamental parameters of snapover, which include the importance of conducting material, insulating material, size and shape of the conductor, sample history, surrounding plasma density, biasing rate, and condition of the dielectric surface (contamination and smoothness). A careful study of material effects (especially of the insulator secondary electron emission properties on snapover) was a principal aim of this investigation, and will continue to be a principal aim in any future investigations undertaken by our group.

Table 1.1. A summary of significant snapover experimental investigations.

Researchers	Details of the investigation	Pertinent findings
Cole *et al.*, 1969	Objective: demonstrated the "pinhole effect" on an electrode beneath a Kapton™ sheet.	In the presence of an insulator, the electron current is two orders of magnitude higher than probe theory predictions at high voltages.
Grier and McKinzie, 1972	Objective: current collection dependence on insulator type. Bias Voltage Range: 0-2 kV. Materials: Parylene™, Teflon™, Nomex™, quartz, Mylar™, and Kapton™ on copper disks with 0.05-0.076 cm diam. holes. Electron Densities: 1-2$\times 10^6$ cm^{-3}.	Onset Voltages: 300-1000 V. Current Enhancement Factor: 10. • charring and melting of insulators. • comparable onset voltages and currents for all insulators. • suppression of current before snapover (as compared to computational model). Proposed Mechanism: insulator out-gassing and ionization.
Grier and Domitz, 1975	Objective: effects of conductor and insulator area on current collection. Bias Voltage Range: 0-10 kV. Materials: Kapton™ on copper disks with 0.051 cm and 2.54 cm diam. holes. Electron Densities: 10^2 cm^{-3} and 10^4 cm^{-3}.	Onset Voltages: 100-1000 V. Current Enhancement Factor: 10^3. • no current enhancement at negative biases. • 2.54 cm conductors collected three times the current of 0.051 cm conductors. • lower onset voltages and higher collected current for larger area insulators: "area effect". • current collection saturated after 1000 V for Kapton™ samples. Proposed Mechanism: attractive electrode potential breaks through plasma repulsive potential.

Table 1.1. (Continued)

Researchers	Details of the investigation	Pertinent findings
Grier and Stevens, 1978	Objective: ground-based study and PIX flight results comparisons. Bias Voltage Range: 0-1 kV (four voltage steps). Materials: Kapton™ sheet with 3 cm diam. gold plated disk, and a small solar array segment. Electron Densities: 2-3 $\times 10^4$ cm^{-3}.	Onset Voltages: 500-1000 V. Current Enhancement Factor: 10^1-10^2. • space flight results are comparable to ground study results. • Kapton™ suppressed current collection before snapover (< 260 V) as compared to plain conductor disk for both ground and space experiments. After ~ 500 V, the current was enhanced. Proposed Mechanism: not mentioned.
Grier, 1979	Objective: pre-flight ground study and PIX flight results comparisons. Bias voltage range: 0-10 kV (for ground study) and 0-1 kV (for flight study). Materials: fused silica glass overlay with exposed interconnects. Electron Densities: 1-4 $\times 10^4$ cm^{-3}.	Onset Voltages: 100-500 V. Current Enhancement Factor: 10^1-10^2 . • space flight results are comparable to ground study results. • glass overlay potential is near 0 V before snapover and nearly equal to interconnects after snapover. • array coated with phosphor revealed electron bombardment of entire array between 900-2000 V. • current jump magnitude increased with electron densities. Proposed Mechanism: secondary electron emission from insulator.

Table 1.1. (Continued)

Researchers	Details of the investigation	Pertinent findings
Stevens, 1979	Objective: snapover behavior on a solar array segment including insulator surface potentials. Bias Voltage Range: 0-10 kV. Materials: solar array segment with exposed interconnects, and a Kapton™ sheet on a conductor with a 0.038 cm diam. hole. Electron Densities: 10^3-10^4 cm^{-3}.	Onset Voltages: ~ 100 V. Current Enhancement Factor: 10^2 to 10^3. • glass overlay potential is near 0 V (slightly negative) before snapover and nearly equal to interconnects (50 V less than applied voltage) after snapover. • negative voltage on cover glass seemed to suppress current collection before snapover. Proposed Mechanism: not mentioned.
Gabriel *et al.*, 1983	Objective: measured plasma sheath potentials about a pinhole. Bias Voltage Range: 50-450 V. Materials: brass disc covered by Kapton™ with 0.1, 0.32, 0.64, and 1.27 cm diam. holes. Electron Densities: 2-6$\times 10^4$ cm^{-3}.	Onset Voltage: not mentioned. Current Enhancement Factor: current suppressed throughout measured voltage range. • no I-V curve data was reported. • between 100-450 V the measured sheath sizes were smaller than calculated values for all hole sizes. • sheath grew linearly with applied voltage for all hole sizes. • charring of surrounding insulator. Proposed Mechanism: "surface conduction across the insulator due to secondary electron emission and electron hopping."

Table 1.1. (Continued)

Researchers	Details of the investigation	Pertinent findings
Stillwell *et al.*, 1985	Objective: general experimental snapover study including material effects. Bias Voltage Range: 0-10 kV. Materials: brass covered by Teflon™, Kapton™, and isomica with 0.035, 0.1, 0.2, 0.3, 0.5 cm diam. holes. Electron Densities: 8×10^4 to 4.3×10^5 cm^{-3}.	Onset Voltages: ~ 400 V. Current Enhancement Factor: 10 (first mode) and 10^2 (second mode). • two distinct collection modes were identified: surface-enhanced, and vapor-enhanced modes. • the vapor-enhanced mode was not as reproducible as the surface-enhanced, and exhibited a healing effect in I-V curve, and was accompanied by a bluish glow. • the vapor-enhanced mode discolored surrounding insulator and diminished current collection in subsequent runs. • current collection in surface-enhanced mode was almost proportional to conductor area. • isomica collected significantly more current than Teflon™ or Kapton™. • hole size was not important in the vapor-enhanced mode. • roughening insulators suppressed current collection by 20-60% for surface-enhanced mode; radial lines reduced current by 75%. • increasing sample temperature decreased current collection for both modes. Proposed Mechanism: secondary electron emission for surface-enhanced mode, and out-gassing/ionization stimulated by electron bombardment for vapor-enhanced mode.

Table 1.1. (Continued)

Researchers	Details of the investigation	Pertinent findings
Carruth, 1987	Objective: measured sheath potentials surrounding two slit geometries. Bias Voltage Range: 0-330 V. Materials: Kapton™ sheets with two open slits; slit widths: 0.32 cm and 0.64 cm with slit spacings: 2.0 cm and 3.0 cm respectively. Electron Densities: 2-4 $\times 10^6$ cm^{-3}.	Onset Voltages: 100-300 V. Current Enhancement Factor: not mentioned. • sheath expands at positive voltages to encompass both slits, but is localized around individual slits at negative voltages. Proposed Mechanism: secondary electron emission from insulator.
Ferguson *et al.*, 1998	Objective: visual observation of the snapover glow. Bias Voltage Range: 0-400 V. Materials: small solar array samples mounted on Kapton™. Electron Densities: 10^5-10^6 cm^{-3}.	Onset Voltages: 200-400 V. Current Enhancement Factor: factor of two at 200 V. • glows coincided with current jumps in I-V curves. • glow revealed the insulator area over which snapover was occurring as well as an estimate for the potentials on the solar array surface. • approximately linear relationship between collection current and glow area. Proposed Mechanism: secondary electron emission from insulator.

1.3 Objectives and Contributions of This Research

In summary, the specific overall objectives and contributions of this research are as follows:

i) Review previous theoretical, computational, and experimental investigations on snapover and identify the physical mechanisms believed to be responsible for the anomalous current collection.

ii) Obtain an understanding of the plasma environment that existed during our experiments and determine any possible anomalous current-collecting behavior of the conductor, insulator, and surrounding plasma system.

iii) Obtain an understanding of insulator surface mechanisms that play a role in snapover, such as charging due to electron emissions, as well as surface out-gassing and ionization.

iv) Design and conduct a series of experiments to test environmental and material conditions that may affect snapover.

v) Use the experimental results to evaluate the present models of snapover–focusing primarily on the insulator secondary electron emission model.

vi) Explore possible methods of suppressing snapover current and associated spacecraft parasitic power losses.

vii) Make suggestions for further snapover studies.

Chapter 2 provides an overview of the insulator secondary electron emission model of snapover along with the associated plasma models for current collection to planar and spherical conductor probes. Next, a description of the experimental methods will be given in Chapter 3, followed by our general experimental results and data analysis in Chapter 4. Finally, suggestions

for proposed future work will be given in Chapter 5 along with a summary and conclusions in Chapter 6.

All experiments were performed by myself, Joel Galofaro, and Boris Vayner at the Plasma Interaction Facility (PIF) at NASA Glenn Research Center (GRC) at Lewis Field in March, 1999. The initial experimental design and prefabrication for these experimental studies was done prior to my participation in the project by Robert Davies and John Robert Dennison at Utah State University, and by Joel Galofaro and Dale Ferguson at NASA GRC. Independent analysis of the data was performed both at NASA GRC and by myself at Utah State University.

CHAPTER 2

MECHANISMS OF SNAPOVER

This chapter begins by outlining the theory of plasma current collection to planar and spherical conductor probes at positive applied voltages. Next, a basic description of secondary electron emission from insulators due to incident electron bombardment is given. Then, plasma probe theory and secondary electron emission theory are combined to give a simple qualitative model of secondary electron emission involvement in snapover based, in large part, on previous interpretations. Finally, the secondary electron characteristics of some materials used in our experimental investigation are presented.

2.1 Classical Plasma Probe Theory

In order to appreciate the effects of a surrounding insulator on the current collection to a conductor in a plasma, it is important to first understand the model of current collection to an isolated conductor probe in a plasma. The simplest model is considered where it is assumed that the plasma is isotropic, collision free (a good approximation for low density plasmas) and follows a Maxwellian velocity distribution function. Additionally, it is assumed that no magnetic fields are present. Then, the average thermal electron velocity far from the probe can be written as:

$$u_e = \left(\frac{8\kappa T}{\pi m_e} \right)^{1/2} \tag{2.1}$$

where κ is the Boltzmann constant, T is the absolute temperature of the plasma (κT can be taken as the approximate thermal energy of the plasma), and m_e is the electron mass. Using Eq. (2.1),

the random electron current density can be expressed as:

$$J_e = \frac{neu_e}{4} = ne\left(\frac{\kappa T}{2\pi m_e}\right)^{1/2} \tag{2.2}$$

where n is the electron number density and e is the electron charge.

In a charge neutral plasma (where the number of electrons is approximately equal to the number of ions) in thermal equilibrium (where the ion and electron average thermal kinetic energies are approximately the same), the average electron velocity will exceed the average ion velocity by a factor of the square root of the ratio of their masses (typically greater than 43) as a result of the comparatively small electron mass. Consequently, when an isolated probe is introduced into the plasma, the initial thermal electron current to the probe will exceed the initial thermal ion current until equilibrium is established between incoming and outgoing electrons and ions. As a result, there will typically be a potential difference between the probe surface and the far-field plasma. The region of plasma across which the potential drop (between the probe and plasma) takes place is the sheath region.

In a collisionless plasma approximation at moderate voltages (eV . κT), the thickness of the sheath can be estimated by the Debye shielding length (Lochte-Holtgreven, 1995):

$$\lambda_D = \left(\frac{\varepsilon_0 \kappa T}{ne^2}\right)^{1/2} \tag{2.3}$$

where ε_0 is the permittivity of free space (Uman, 1964). Outside of the sheath region, charged

particles are unaffected by the probe potential. However, once a particle enters the sheath (by its own thermal motions) it will either be attracted or repelled by the probe (for example, an ion will be repelled from a probe at a positive potential).

Once a charged particle experiences an attractive potential to the probe, two general approximations for current collection exist. These two approximations are dependent on the relative size of the probe with respect to the plasma sheath:

i) *The thin-sheath limit* ($r_s << r$): The radius of the sheath, r_s, is much smaller than the radius of the probe, r. In this regime, sheath effects dominate current flow to the probe, and current collection is independent of probe voltage. Nearly all particles entering the sheath are collected by the probe (Lochte-Holtgreven, 1995). In our investigation, at low voltages this regime may be more applicable to samples with conductor diameters greater than two centimeters.

ii) *The thick-sheath limit* ($r_s >> r$): The radius of the sheath, r_s, is much larger than the radius of the probe, r. The probe current depends on the probe voltage. At low voltages, this regime may be more applicable to smaller samples with conductor diameters smaller than one centimeter.

For planar probe geometries (as used almost exclusively in this experimental investigation), an infinite plane surface represents the extreme of the thin-sheath limit. Although this limit will most likely not apply to samples used in our investigation, the current collected to an infinite conductor should serve as a limiting case, and is therefore useful to study. For an infinite plane, the sheath radius for a Maxwellian velocity distribution can be derived from Poisson's equation for attracted species, and can be expressed by the Child-Langmuir length as:

$$r_s = \frac{2\lambda_D}{3\pi^{1/4}}\left(\frac{eV}{\kappa T}\right)^{3/4} \tag{2.4}$$

where V is the probe potential with respect to the neutral plasma (Hastings and Garret, 1996). The sheath thickness should always be on the order of the spherical Debye length, which requires that the probe potential energy (eV) be greater than the plasma electron energy (κT) so that repelled species current (in the form of ions) can be ignored (Hastings and Garret, 1996). In our experiment, this condition was reached after only a few volts of potential bias. The expression for the Child-Langmuir length implies that at high voltages, the electric field about an infinite conductor extends much further into the plasma than at lower voltages. The current flow (neglecting ion current) to a positively biased infinite conductor plane can be expressed in terms of the Child-Langmuir law as:

$$J_{\infty p\ln} = \frac{4\varepsilon_0}{9}\left(\frac{2e}{m_e}\right)^{1/2}\frac{V^{3/2}}{r_s^2} \tag{2.5}$$

Combining Eqs. (2.3), (2.4), and (2.5) yields a constant current flux to the infinite plane, equal to twice the thermal electron flux given by Eq. (2.2). Thus, for the infinite plane thin-sheath limit the collected random electron current density can be written as:

$$J_{\infty p\ln} = 2J_e = \frac{neu_e}{2} = ne\left(\frac{2\kappa T}{\pi m_e}\right)^{1/2} \tag{2.6}$$

It is also beneficial to write thick- and thin-sheath approximations for the current collection to spherical probes, since finite planar probes should collect similar currents, and because a hemispherical conductor sample was included in this experimental investigation. For the thin-sheath approximation, the current to a spherical probe is constant as with the infinite plane, and is just the random electron current density (Lochte-Holtgreven, 1995):

$$J_{thnsphr} = J_e = \frac{neu_e}{4} \tag{2.7}$$

For the thick-sheath approximation, the collected current depends linearly on applied voltage as (Lochte-Holtgreven, 1995):

$$J_{thckshpr} = J_e\left(1 + \frac{eV}{\kappa T}\right) \tag{2.8}$$

Furthermore, Al'pert *et al.* (1965) have given a thick-sheath solution that better approximates the current collection to a spherical probe at high voltages:

$$J_{thckshpr2} = (0.951)J_e\left(\frac{eV}{\kappa T}\left(\frac{\lambda_D}{r}\right)^{4/3}\right)^{6/7} \tag{2.9}$$

Since the majority of the samples used in this study were comprised of 0.32- to 5.1-cm diameter conductor planes surrounded by insulator sheets, it is also necessary to provide current

collection estimates for small planar probes. Although no analytical solution exits for the current collected to finite planar probes, Parker and Whipple (1967) have given an approximation written in terms of a parameter, b, that characterizes both the trajectory of the incoming electrons and the current collection regime (thin- or thick-sheath). This approximation is given as:

$$J_{p\ln} = J_e\left(1+\frac{b^2}{4}+\frac{eV}{\kappa T}\left(1-\frac{b^2}{4}\right)\right) \tag{2.10}$$

where 0<b<2. As shown in Fig. 2.1, according to Eq. (2.10) the collected current density is linearly dependent on the applied probe voltage with the slope determined by the parameter, b. As b60, a maximum slope is attained corresponding to a function equivalent to the spherical thick-sheath solution (Eq. (2.8)). Alternatively, if b62 one attains a constant current density corresponding to the thin-sheath infinite plane result (Eq. (2.6)). Also, as can be seen in Fig. 2.1 and Eq. (2.10), the y-intercept of the current also depends weakly on the parameter, b, (increasing with increasing b). As will be shown in more detail in the data analysis of Chapter 4, based on calculations involving plasma properties such as the electron number density, random current density, and the Debye length, the plasma sheath dimensions at low voltages were roughly equal to the sample conductor dimensions. Consequently, it was expected that the plasma electron current to the samples would lie somewhere between the thick- and thin-sheath regimes (or, alternatively have an intermediate value for the characteristic b parameter somewhere between 0 and 2 depending on the sample conductor size).

Finally, in these treatments for probe current collection, it is worth it to once again summarize the assumptions on which the simple current collection equations given above are

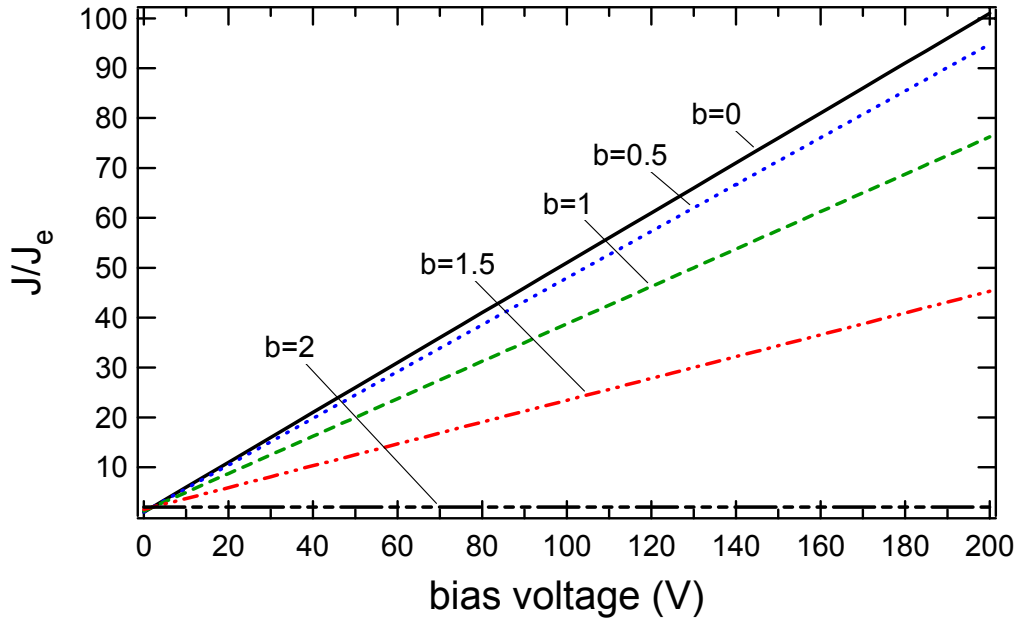

FIG. 2.1. Normalized current density to planar probes. The current density is a function of the planar probe parameter, b. The collected current is linear with applied voltage, where the parameter, b, determines the slope and the y-intercept. The slope is maximized for b=0, and is zero for b=2. These two extremes provide theoretical bounds to planar probe current collection as given by Parker and Whipple (1967).

based. These approximations included: i) a collision-free, fully ionized plasma; ii) an isotropic, Maxwellian velocity distribution (although this simplifying assumption has been used, it is not entirely accurate in the presence of an electric field); iii) equal electron and ion average kinetic energies; iv) exclusion of ion current contributions; and v) absence of magnetic fields (the Earth's magnetic field effects were assumed to be negligible). Also, it should be pointed out that the thin- and thick-sheath are extreme approximations used only when the sheath and probe dimensions differ substantially. All of these approximations represent the simplest scenarios for the plasma/sample conditions in our experiments, and as a result may display errors in modeling our current collection data.

2.2 Secondary Electron Emission

When an insulator or a conductor surface is bombarded by incident electrons, several electron-electron interactions can occur either on or just below the surface of the material. Through these processes, the material can release electrons–some with energies equal to (elastic) or nearly equal to (quasi-elastic), and some with energies below (inelastic) the incident electron energy. At a constant incident electron energy, an emitted electron energy spectrum can be measured as shown in Fig. 2.2. By convention, all electrons emitted with energies greater than 50 eV are termed backscattered electrons (BSE's). Those electrons that escape with energies less than 50 eV are designated secondary electrons (SE's). Although by this definition, any electron with an energy below 50 eV is termed a secondary electron, the vast majority of SE's possess energies less than 20 eV (see Fig. 2.2. and Nickles *et al.*, 1999).

The total number of BSE's and SE's produced as a result of incident primary electron (PE) bombardment depends on the material, incident angle, and incident energy of the incident electrons. This quantity can be expressed as a ratio of the number of emitted electrons over the number of incident electrons (or alternatively as the ratio of outgoing to incoming current), and is known as the total electron yield, σ (measured yield values range from 0 to 30 or more for insulators). Similar ratios can be expressed individually for the backscattered yield, η, and the secondary electron yield, δ.

Typical plots of the total, SE, and BSE yields for an insulator (for electron-induced emissions only) are plotted as a function of primary electron (PE) energy in Fig. 2.3. In general, the total current can consist of electron-induced SE's, BSE's, and emitted ions, as well as ion-induced and photon-induced emitted electrons. However, in our laboratory studies, ion emission as well as ion-induced and photon-induced electron emissions were assumed to be negligible due

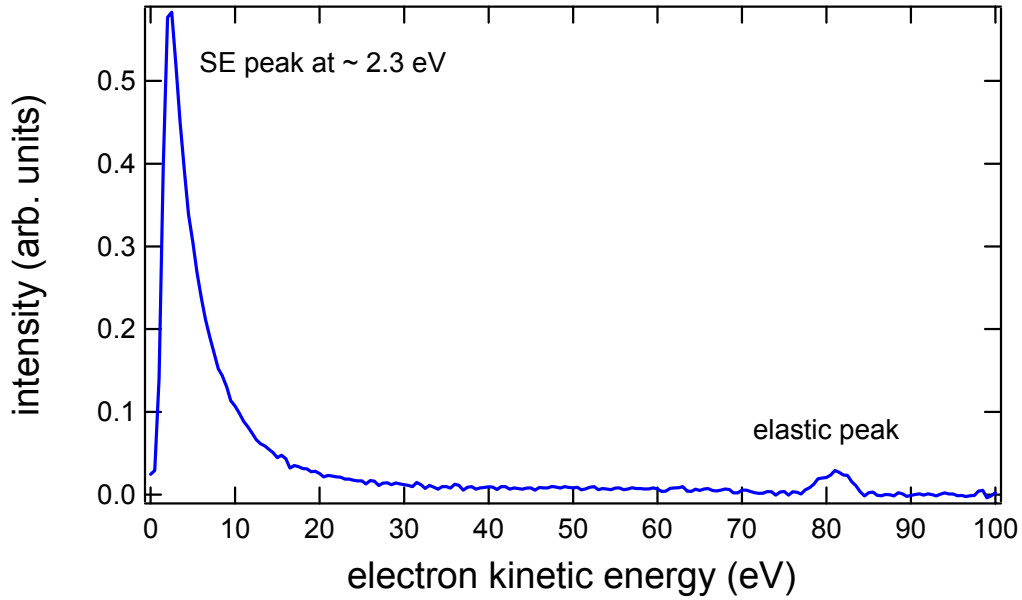

FIG. 2.2. The energy spectrum of emitted electrons for polycrystalline gold for an incident beam energy of 80 eV. By definition, secondary electrons are those electrons that are emitted with energies < 50 eV while back-scattered electrons are those electrons emitted with energies

to positive bias repulsion and low-intensity radiation near the sample. Also, the BSE yield is roughly constant above a few hundred electron volts of incident energy, with typical yield values ranging from 0.2 to 0.6 (see Fig. 2.3). From Fig. 2.3 it can be seen that at low incident energies (< 75 eV for most insulators) both the total and SE electron yields are less than one. Hence, for this energy range, electron bombardment of insulators will cause negative charging until surface charge repulsion becomes sufficient to balance incoming and outgoing electron currents. At some critical incident energy (ranging from 30 eV to 80 eV for most insulators) termed the first crossover energy, E_1, (as shown in Fig. 2.3) an insulator begins to emit more than one electron for each primary electron, producing a net outward flux of electrons away from the surface that can lead to positive charging of the insulator. As the incident energy is increased further, this outward flux of electrons is continued with increasing incident energy until the incident electron

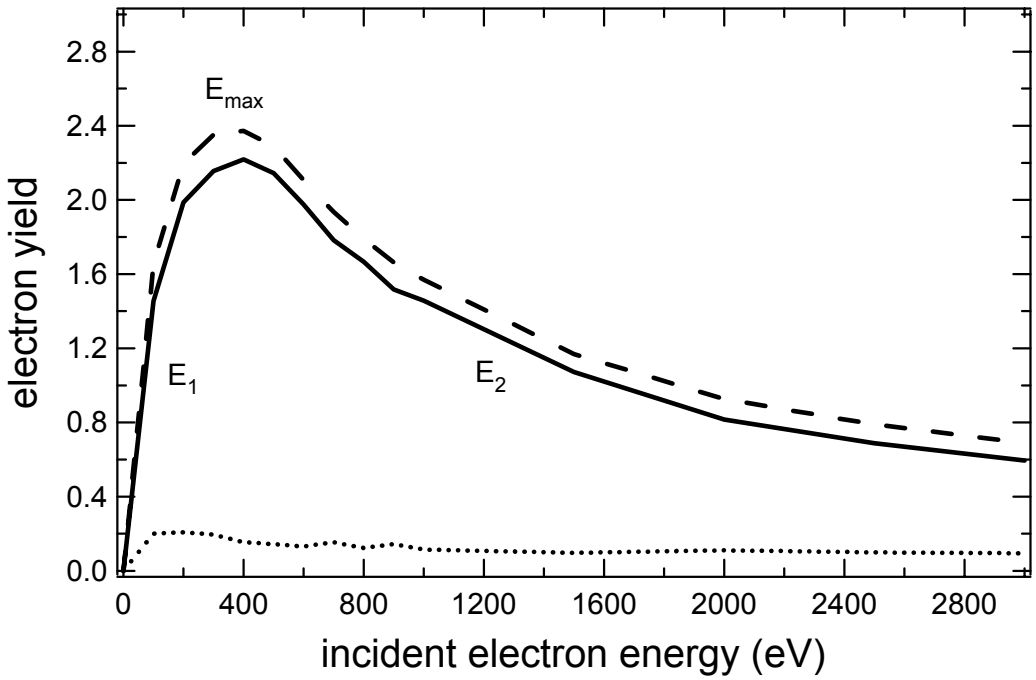

FIG. 2.3. Curves of the total yield (dashed), SE yield (solid), and BSE yield (dots) versus incident electron energy for untreated Teflon™ (Krainsky *et al.*, 1981). The vertical axis represents the ratio of emitted electrons to incident electrons. The first crossover energies (E_1) occur at the energy (~ 70 eV) where the total and SE yield ratios rise above unity. From the graph, the energies where the total and SE yield ratios are a maximum (E_{max} at ~ 400 eV) and where the ratios eventually fall back below unity (E_2 at ~ 1600 eV) can also be seen. Other insulators have similar total, SE, and BSE yield curves.

energy reaches a second crossover energy, E_2, where the direction of net current is once again reversed to a net inward flux of electrons.

In general, when studying snapover, one is concerned with the total electron yield of an insulator since all electrons (either incident or emitted) can potentially contribute to sample insulator charging and also to current collected by the conductor. BSE's by convention have energies greater than 50 eV, and as a result at high applied voltages ($ 50 V), they may be emitted from the surrounding insulator and eventually be collected by the nearby biased conductor (see the emitted energy spectrum of Fig 2.2). Nevertheless, in theoretical and computational models,

it has been customary to only consider SE emission contributions to calculate onset voltages, current collection, and local sheath and insulator surface potential profiles (Chaky *et al.*, 1981; Brandon *et al.*, 1984; Kessel *et al.*, 1985; Hastings and Chang, 1989).

An estimate for the SE current density from the surface of the insulator as a function of incident electron energy and angle is given by Hastings and Garret (1996) as:

$$J_{SE} = \frac{2\pi e}{m_e^2} \int_0^\infty dE \int_0^\infty f(E_0) g(E_0, E) dE_0 \int_0^\pi \delta(E_0, \theta) \sin\theta d\theta \tag{2.11}$$

where $g(E_0,E)$ is the normalized emission spectrum of SE's at emission energy, E, with an incident electron energy E_0. Generally, the mean SE emission energy is ~2 eV and Chung and Everhart (1974) have offered a semi-empirical theory for modeling the SE energy distribution. The function $f(E_0)$ is the energy distribution function of primary electrons, and in general depends on the electron source, but in the presence of the plasma can most likely be approximated with a Maxwellian distribution centered about the surface potential, eV, with a width of κT. Finally, $\delta(E_0,\theta)$ is the SE yield as a function of incident electron energy and angle, θ. The SE yield, δ, can be approximated fairly well by the Sternglass equation (Hastings and Garret, 1996):

$$\delta(E_0, \theta) = \delta_{\max} \frac{E_0}{E_{\max}} \exp\left[2 - 2\sqrt{E_0 / E_{\max}}\right] \exp\left[2\left(1 - \cos\theta\right)\right] \tag{2.12}$$

or by a semi-empirical model given by Young (1956) for normal incidence as:

$$\delta(E_0) = c_1 \delta_{\max} \left(E_{\max} / E_0 \right)^{0.35} \left\{ 1 - \exp\left[-c_2 \left(E_0 / E_{\max} \right)^{1.35} \right] \right\} \qquad (2.13)$$

and is typically measured by taking a ratio of SE current over PE current (as described above). The formalism of Eqs. (2.11) through (2.13) provides a useful representation of the secondary electron current for computational models of snapover. Davies (1999) and Nickles *et al.* (1999) provide further detail on measuring the SE yield properties of materials.

2.3 Secondary Electron Emission Model of Snapover

The majority of the theoretical formulations proposed over the past 20 years have involved speculations that secondary electron emission–specifically from the dielectric surrounding the positively biased conductor–is the dominant physical process responsible for the anomalous snapover enhanced currents (Chaky *et al.*, 1981; Mandell and Katz, 1983; Stillwell *et al.,* 1985; Mandell et al., 1986; Carruth 1987; Hastings and Chang, 1989; Vayner *et al.*, 2000). As described in Chapter 1, computer simulations of conductor/dielectric interfaces in the presence of secondary electrons (SE) and a plasma generally support the SE hypothesis by producing several results that agree with measurement, such as the anomalous snapover I-V curve current jump, local plasma sheath expansion, and the charging of large areas of the surrounding insulator through SE emission. However, these models generally predict snapover onset voltages much lower than measured values, and do not account for the multiple current jumps that are observed in measured I-V curves (Chaky *et al.,* 1981; Brandon *et al.,* 1984; Mandell *et al.,* 1986; Hastings and Chang, 1989).

As revealed by experiments, the physical dynamics of snapover appear more complicated than simulated results provided by simple computational SE models. However, SE emission from

the surrounding insulator (and subsequent insulator charging) most likely still plays a very significant role. Consequently, it is important to understand the simple SE model of snapover before attempting to propose variations that can account for other experimental observations such as high onset voltages and multiple current jumps. In the most basic SE model of snapover, as supported by measurement and computer simulation, the role of SE emission is proposed to behave as follows:

i) Before snapover, the conductor/dielectric maintains equilibrium with the plasma primarily through a balance between incoming ion and electron currents regulated by an approximately spherical sheath above the positively biased conductor (Gabriel *et al.*, 1983; Brandon *et al.*, 1984; Thiemann and Schunk, 1990a, 1990b; Davis and Gardner, 1995). Ambient electrons enter the sheath region by their own thermal energies, and once inside they accelerate radially inward towards the positively biased conductor. At this time, the surrounding dielectric (primarily outside of the conductor sheath region) remains at a near zero (slightly negative) potential through a self-regulating process where electrons hit the insulator surface, accumulating negative charge, which limits the total number of electrons that can reach the insulator surface (Stevens, 1979; Chaky *et al.,* 1981; Brandon *et al.*, 1984; Kessel *et al.*, 1985; Mandell *et al.*, 1985; Hastings and Chang, 1989; Thiemann and Schunk, 1990a). The slightly negative (but relatively large area) insulator surface may also act to further suppress plasma electrons reaching the conductor, thereby reducing the total collected current before snapover (Stevens, 1979; Thiemann and Schunk, 1990a). Refer to Fig. 2.4 for a rough schematic of the conductor/insulator/plasma system under these conditions.

ii) Inside the conductor plasma sheath region, some of the incident electrons strike the

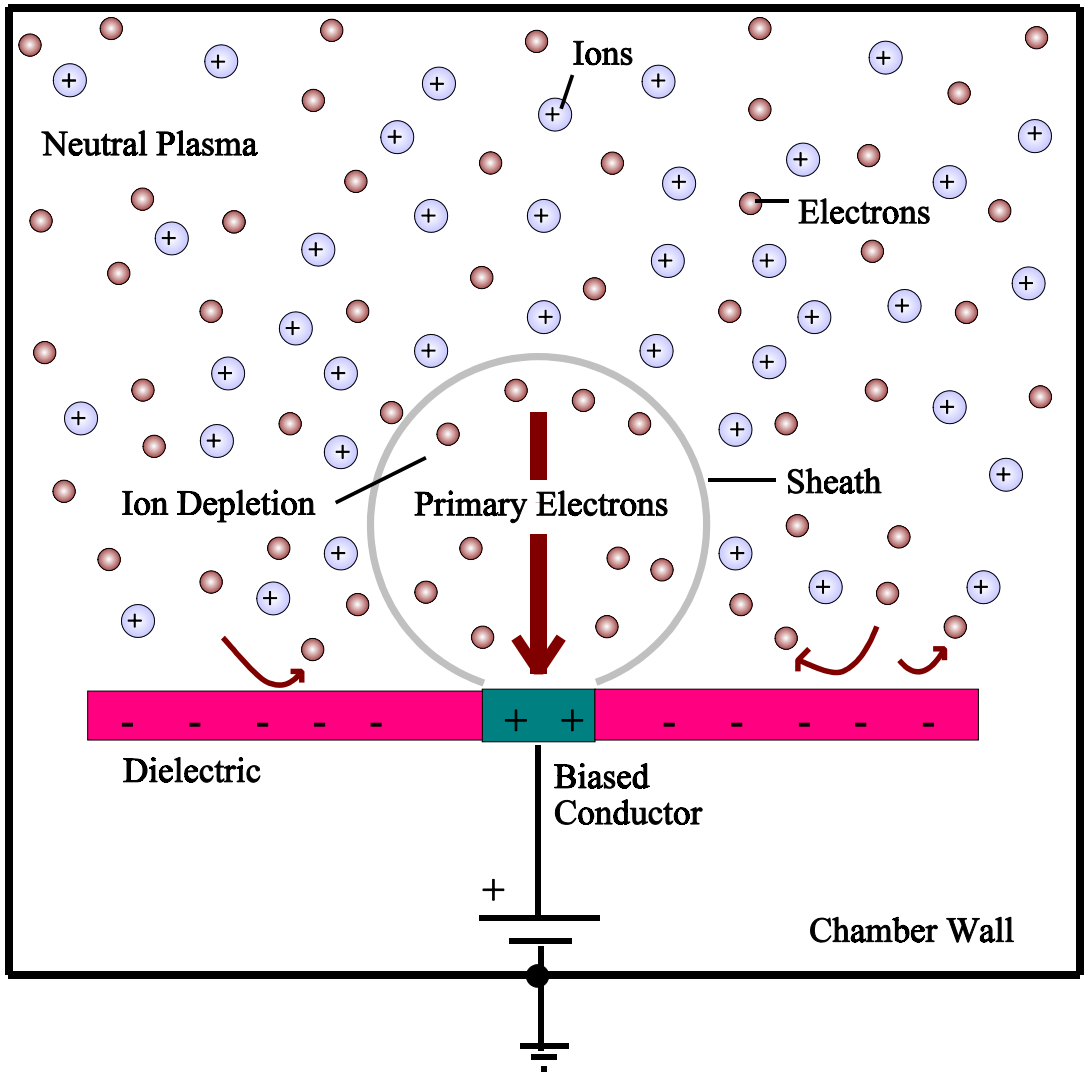

FIG. 2.4. Plasma and surface charge profiles before the onset of snapover. The illustration is based on experimental measurements and computer modeling. After current equilibrium is established, the surrounding plasma responds to the conductor applied voltage by forming an ion depleted sheath region about the conductor. Also, the insulator outside of the conductor sheath charges slightly negative to repel thermal electrons from the surrounding plasma. Plasma electrons can enter the conductor sheath region by their own thermal motion, and once inside they accelerate to the conductor and are registered as collected current. Depending on the extent of the conductor sheath, plasma electrons can also hit the surrounding insulator, causing local charging that may eventually trigger snapover.

dielectric immediately adjacent to the conductor with an energy equal to or somewhat less than the conductor bias (i.e., for a conductor bias of +100 V, the electron kinetic energy upon striking the adjacent dielectric is E_0 . 100 eV), producing secondary electrons from the dielectric. The conductor sheath can extend over nearby portions of the dielectric if the dielectric has a finite resistivity such that the applied conductor voltage damps out across a finite region of the insulator. As the conductor bias is increased, so too is the energy with which the plasma electrons strike the edges of the dielectric, increasing the number of emitted SE's. Above some critical conductor bias, the ratio of SE's to PE's (SE yield, δ) from the immediate adjacent dielectric becomes greater than unity and the insulator can begin to charge positively.

iii) Many of the SE's emitted from the nearby dielectric are drawn in to the more positively biased conductor, although some are recaptured by the insulator in the process (Brandon *et al.*, 1984; Kessel *et al.,* 1985). Alternatively, these SE's can be transported through a thin contamination layer on the insulator surface in an ohmic fashion. If a sufficient number of SE's reach the conductor before they are reabsorbed by the insulator, portions of the dielectric nearest the conductor will accumulate a positive charge (slightly less positively charged than the conductor) (Grier, 1979; Stevens, 1979; Chaky *et al.,* 1981; Brandon *et al.*, 1984; Kessel *et al.*, 1985; Mandell *et al.*, 1985; Hastings and Chang, 1989; Thiemann and Schunk, 1990a, 1990b). Thus the positively charged dielectric can itself begin to attract electrons from within the conductor plasma sheath, with several important consequences. First, the number of SE's being produced by the now positively biased portion of the dielectric increases–the result of an increased flux of ambient plasma electrons to the surface. Second, the increased positive surface area has a tendency to extend the sheath surrounding the conductor, encompassing more of the

surrounding insulator, and thus exposing more insulator area to high energy plasma electrons (Chaky *et al.*, 1981; Gabriel *et al.*, 1983; Brandon *et al.*, 1984; Kessel *et al.*, 1985; Carruth, 1987; Thiemann and Schunk, 1990a, 1990b). Third, some of the plasma electrons attracted by the positively charged dielectric strike the immediately adjacent, uncharged portions of the dielectric; these portions then begin to emit SE's and can become positively biased themselves, cascading the process until a larger region of the dielectric surface is positively charged as shown in Fig. 2.5 (Brandon *et al.*, 1984; Kessel *et al.,* 1985; Thiemann and Schunk, 1990a, 1990b).

iv) This entire process can potentially lead to a sudden transition in the current collection by the conductor in two ways: First, before snapover the charge on the dielectric remains somewhat less than that on the conductor. The low energy SE's emerging from the dielectric surface are drawn radially inward across the insulator surface toward the conductor (as discussed above) where they are collected, thus leaving the insulator positively charged. Second, with a larger region of the dielectric surface positively charged, the radius of the sheath surrounding the conductor/dielectric assembly expands (as discussed above) and more of the plasma electrons "see" or are attracted both to the biased conductor and positively charged insulator, continuing the increased plasma electron flux to these surfaces. Additionally, due to the charge gradient across the insulator, plasma electrons that are attracted to the conductor/insulator assembly may be funneled in towards the more positive conductor.

After a snapover current jump has been initiated, a new equilibrium is established primarily through a current balance between incoming plasma electrons and outgoing secondaries

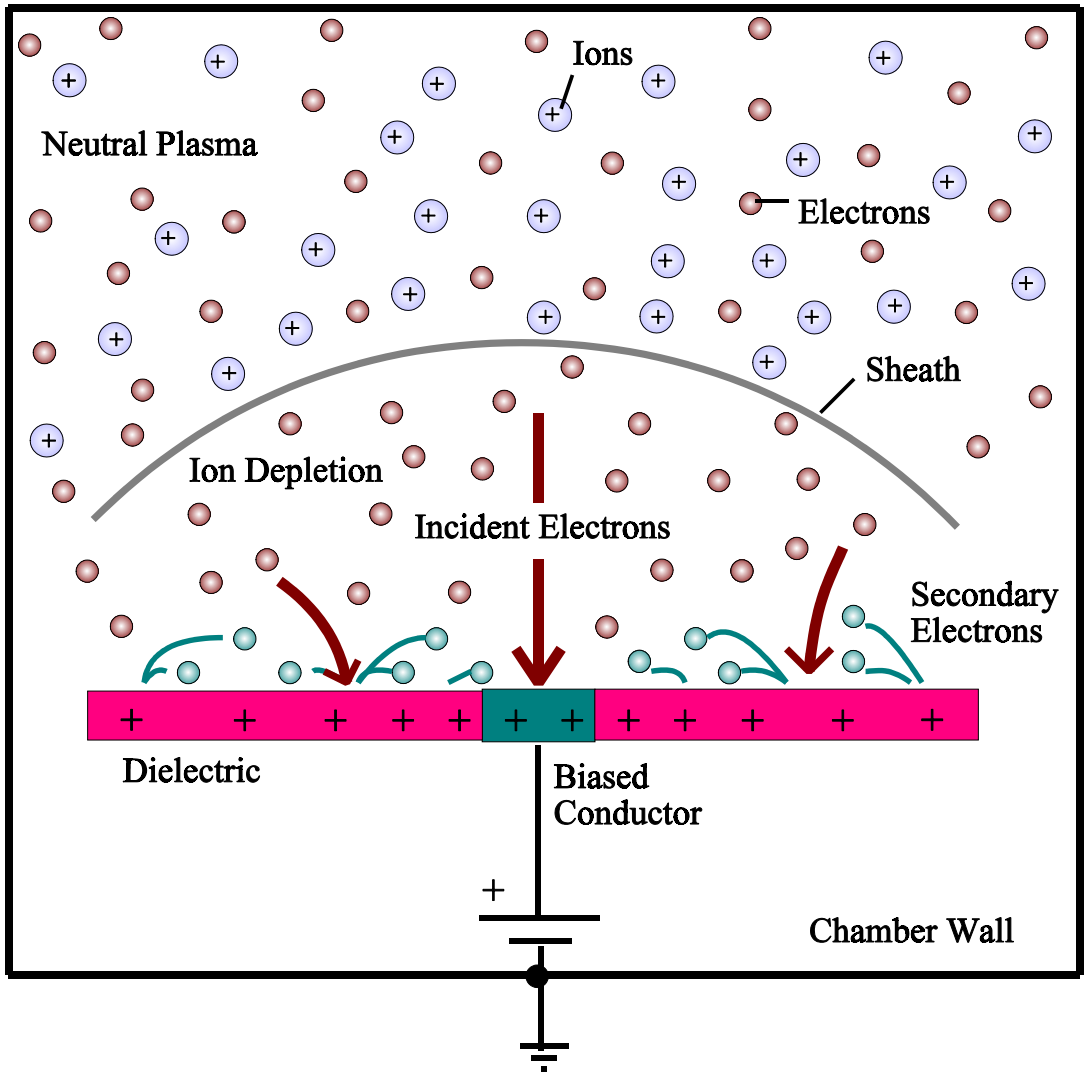

FIG. 2.5. Plasma and surface charge profiles after the onset of snapover. This illustration is based on experimental measurements and computer modeling. During snapover inception, the surrounding insulator emits more electrons than are incident from the surrounding plasma leaving the insulator positively charged. In response to the charged insulator, the plasma sheath expands, allowing greater interaction between the sample and surrounding plasma electrons. Very quickly, a new quasi-steady state current equilibrium is established where the conductor collects more overall current.

which are collected by the conductor (Hastings and Chang, 1989; Thiemann and Schunk, 1990a, 1990b). This abrupt transition in current collection equilibrium is snapover.

Finally, it must be emphasized that although insulator first crossover energies are less than 100 eV, snapover onset voltages could potentially be delayed to higher bias voltages since the SE cascading effect, insulator charging, and associated sheath expansion may all be suppressed by the self-regulating negative bias on the rest of the surrounding insulator (outside of the conductor sheath region) before snapover. As a result, even though near portions of the insulator have crossed the SE first crossover energy and have begun to charge positively (as outlined above), the surrounding sheath and insulator may still not make the transition to an amplified current collection mode. Hence, snapover onset voltages may not correspond in magnitude to the associated insulator first crossover energies.

Before snapover has occurred one would expect the collected current to be dominated by plasma electrons drawn directly to the conductor as a result of the applied bias (more or less following planar probe current collection theory). However, as mentioned, some current suppression (as compared to probe theory predictions) may exist due to the slightly negative potential on the surrounding insulator. After snapover has occurred, one would expect the collected current to increase as a consequence of the expanded sheath and the positively charged surrounding insulator. Additionally, one might expect a decrease in the overall effective impedance of the plasma-sample current loop if secondary electrons can propagate (or hop) along the insulator surface towards the conductor while continually being replenished by an outside electron source (i.e., the plasma). A similar breakdown process called flashover has been shown to occur on insulator surfaces (and has been more thoroughly studied than snapover) where an SE avalanche propagates from a cathode to an anode in a vacuum (Hawley, 1968; Miller, 1989). During flashover, high electric fields (10-100 kV/cm) along the cathode/insulator gap induce field

emission of electrons that act to feed a continual SE avalanche breakdown (Pillai and Hackam, 1982; Hendriks *et al.*, 1997, 1999). It is conceivable that a similar physical process occurs after snapover (without field emitted electrons, but instead through plasma electrons) at much lower potentials since an alternate electron source exists (i.e., plasma electrons instead of field emissions from the cathode/insulator junction) to sustain SE emission and hop transport process across the insulator surface. If this were the case, the total current to the conductor after snapover could be written in terms of a direct plasma component, J_{plasma}, as well as an indirect plasma component, $J_{surface}$, that reaches the conductor by way of the insulator surface as:

$$J_{tot} = J_{plasma} + J_{surface} \tag{2.14}$$

Eq. (2.14) can be further evaluated by considering that after snapover the insulator surface behaves much like a conductor (attracting plasma electrons directly). Hence, the effective surface area of the sample probe increases, although the plasma electron current to the insulator diminishes gradually further from the conductor due to a decreasing charge gradient along the insulator surface. Nevertheless, treating the conductor and the entire positively charged insulator as an enlarged planar probe, and assuming that current incident on the snapped-over insulator is in some way collected by the conductor (either through finite surface conductivity or through SE hop transport), then the total current to the system can be evaluated using Eq. (2.10) and written in terms of a direct plasma component as well as a surface component from the insulator. Considering only insulator SE contributions to the surface current term, the number of secondaries can be approximated by knowing the incident plasma electron current (estimated from Eq. (2.10)), the incident electron energy (on the order of the conductor bias potential energy close

to the conductor but will decrease with distance from the conductor), and the insulator SE yield function, $\delta(E_0,\theta)$ (since δ is just the ratio of SE current over PE current). Then, an estimate for the total collected current (neglecting ion and BSE current) can be written in terms of Eqs. (2.10) through (2.14) as:

$$J_{tot} A_{cond} = J_{plasma}(r) A_{cond} + \alpha\delta(E_0,\theta) J_{plasma}(r) A_{ins} \qquad (2.15)$$

where A_{cond} is the conductor area, J_{plasma} is the incident current density from the plasma to the entire sample (now a function of sample radius since in general it will fall off with increasing distance from the conductor), A_{ins} is the snapped-over insulator area (not known *a priori*), $\delta(E_0,\theta)$ is the SE yield (dependent on incident plasma electron energy and incident angle), and α is a unitless collection efficiency constant (ranging from zero to one, zero if no SE's make it to the conductor, one if all make it) that could depend for example on the average energy and angle of emitted SE's, on the local electric fields (strength and direction) from the charged surface and biased conductor, and on the insulator surface topology. In principle, by decreasing the collection efficiency, α, (for example by roughening the insulator surface) the overall collected current could be suppressed.

It should be emphasized that Eq. (2.15) is by no means considered complete. It was merely derived for demonstration purposes, and has not yet been used in any of the analysis for this experimental investigation. In the future, a model built upon Eq. (2.15) may be further investigated and, if necessary, modified to calculate collection currents before and after snapover.

The basic SE model presented in this section qualitatively describes many of the key features attributed to snapover. However, other physical mechanisms may contribute to the onset

voltage and current collection. As mentioned above, a more thorough understanding of both the charge gradient along the dielectric and of the coupled sheath dynamics is required to better model the phenomena. Also, one should consider BSE contributions to insulator charging. Furthermore, insulators may exhibit surface conductivity from adsorbed contamination films (such as water or diffusion pump oil) that affect the overall surface charge and current to the conductor. However, if the general notions of the secondary electron snapover model are correct, the voltage required to initiate snapover should depend in some ways on the SE properties of the dielectric material. Specifically, one would expect it to depend on the PE incident energy (and, therefore, the closely related conductor bias voltage) above which the insulator's electron yield, σ, is greater than unity–that is, on the total yield (or closely related SE yield) first crossover energy, E_1 (see Fig. 2.3) (Hastings and Chang, 1989).

Table 2.1 lists E_1 for the various materials used in this study, along with the maximum SE and total electron yields, δ_{max} and σ_{max}, the energy E_{max} at which δ_{max} and σ_{max} occur, and the second crossover energy E_2. The variations in the reported yield values were a great concern in this investigation. Particularly, the reported E_1 value variations for an individual insulator sometimes exceeded the E_1 differences in dissimilar insulators, making it potentially impossible to establish a relationship between snapover inception and insulator first crossover energies.

TABLE 2.1. Secondary electron emission properties and total electron yield properties (indicated by *) of materials used in this investigation. Listed yield and energy values for Teflon™, Kapton™ , SiO_2, Al alloy 2024-T3, and OFHC copper were measured on as received samples that were cleaned by methods similar to those used in this investigation. Listed yield values for insulators were measured using a pulsed beam method to reduce dielectric charging effects. Alternate values and references for Teflon™, Kapton™, and SiO_2 are given in parentheses. The wide variation in insulator SE and total yield values was a crucial concern in testing the SE model of snapover.

Material	δ_{max}, σ_{max}*	E_{max} (eV)	E_1 (eV)	E_2 (eV)	References
Teflon™	2.2, 2.4* (3*)	396, 370* (300*)	69, 60* (50*)	1640, 1847* (1850*)	Krainsky *et al.,* 1981 (Willis and Skinner, 1973)
Kapton™	1.6, 1.75* (2.1*)	222, 212* (150*)	75, 67* (30*)	651, 738* (500*)	Krainsky *et al.,* 1981 (Willis and Skinner, 1973)
SiO_2	3.3, 3.4* (2.3)	404, 308* (400)	45, 42* (40)	3606, 3942* (2400)	Krainsky *et al.,* 1981 (Mueller, 1945)
Al alloy 2024-T3 (oxidized)	3.3	370	50	3670	Chase *et al.,* 1979
Aluminum (clean)	0.70-0.75	350-400	--	--	Thomas and Pattison, 1970
OFHC copper	1.14	790	370	1480	Chase *et al.,* 1979
Microcrystalline graphite (Aquadag™)	0.45	500	--	--	Bruining, 1938
MgO thin film	18	1200	30	> 4000	Whetten and Laponsky, 1959
Diffusion pump oil (Dow Corning 704)	1.8-2.0	140-150	<75	900-1000	Goto and Ishikawa, 1968

CHAPTER 3

EXPERIMENTAL METHODS

3.1 Key Parameters Measured in This Study

Considering the extensive computational and theoretical work done on snapover during the 80s and 90s, it is interesting that previous ground-based and in-flight experiments have been unable to fully uncover the detailed nature of snapover or the role played by SE emission (refer to Chapter 1). Additionally, too few comprehensive experimental studies have been performed over the last 20 years to fully explore the most essential parameters involved in snapover. Consequently, the necessary information needed to effectively compare measurements with modeled results is sparse (refer to Chapters 1 and 2). With this in mind, our experimental investigation was designed to systematically explore the importance of:

i) Cycling a given sample through multiple snapovers to study the effects (if any) on snapover onset voltage and current jump due to sample surface alterations.

ii) The effect of conductor biasing ramping rate (step size and time delay) on surrounding plasma dynamics, temporal sample current response rate, and the snapover onset voltage or current jump.

iii) The effect of surface contamination (such as diffusion pump oil) of both insulator and conductor surfaces on snapover occurrence, onset voltage, and current jump. Even monolayer contaminant films have been shown to significantly modify SE emission (Davies and Dennison, 1997; Chang *et al.,* 2000; Dennison *et al.*, 2001).

iv) The effect of the ambient plasma density on plasma sheath formation, pre-snapover current collection, and snapover onset voltage and current jump.

v) The type of insulating material surrounding a fixed conducting material–and particularly

the insulator's first crossover energy–on the snapover onset voltage or current jump. Teflon™, Kapton™, and $Si0_2$ insulators were chosen for this study based on their range of E_1 values (see Table 2.1).

vi) The type of conductor material (e.g., Al and Cu) surrounded by a common insulator on the snapover onset voltage or current jump. Al and Cu were chosen because of there distinctly different SE emission characteristics (see Table 2.1).

vii) The effect of the conductor size or shape (flat versus spherical) on plasma sheath formation and the snapover onset voltage or current jump. Hastings and Chang (1989) suggested that the snapover onset voltage should be significantly larger for a planar geometry than for a spherical one; hence, a hemispherical conductor sample was included for comparison.

viii) The effect of roughening a strip of the surrounding insulator to try to inhibit SE collection by the conductor and possibly delay the insulator charging cascade, and thus the snapover phenomenon. Previous experimental studies have reported inconsistent results for roughened surfaces (Stillwell *et al.,* 1985; Krauss, 1989).

ix) The effect of coating the surrounding insulator with colloidal microcrystalline graphite (Aerodag™) or MgO to try to modify the snapover phenomenon.

x) The optical spectra of the glow that sometimes accompanies the phenomenon. This may allow determination of the materials (e.g., plasma, insulator, conductor, or out-gassed species) involved in snapover or gas discharge.

3.2 Experimental Setup and Procedure

An array of 20 samples of various predetermined materials, shapes, and sizes was constructed as shown in Fig. 3.1. Fig.3.1 is a key to the individual samples mounted in the array. Each sample was comprised of a 10 cm x 10 cm dielectric plate (either 0.32 cm thick Teflon™, 0.32 cm thick Teflon™ covered with Kapton™ tape, or 0.32 cm thick SiO_2) with a conductor press fit in the center, flush with the front surface. Either OFHC copper or aluminum alloy (Al 2024-T3) rods of 0.32 to 5.08 cm diameter conductors were used. Sample 17 was an aluminum alloy (Al 2017-T4) 1.27 cm diameter hemispherical conductor. The back sides of the conductors were insulated to avoid snapover of the back side. The samples were cleaned with isopropyl alcohol each time the vacuum chamber was opened to remove accumulated contaminants.

The sample array (see Fig. 3.2) was mounted vertically in the center of a 3 m high x 1.8 m diameter plasma chamber at the Plasma Interaction Facility (PIF) at NASA Glenn Research Center (GRC) (Vayner *et al.*, 1998) (see Fig. 3.3). The chamber was pumped to a base pressures (monitored with an ionization gauge) of $\sim 10^{-6}$ Torr using three liquid nitrogen cold trapped oil diffusion pumps. Using argon pressures of $\sim 6.5 \cdot 10^{-5}$ to $3 \cdot 10^{-4}$ Torr (most measurements were performed between $6.5 \cdot 10^{-5}$ to $8.0 \cdot 10^{-5}$ Torr), plasmas were produced with two standard Penning sources. A two centimeter diameter Langmuir probe determined typical plasma densities of $\sim 1 \cdot 10^{5}$ to $4 \cdot 10^{5}$ cm^{-3} and electron thermal energies of ~1 to 3 eV. By carefully monitoring the background pressure from one run to the next, the pressure was found to fluctuate by no more than ~ 3% during each series of measurements. At any given pressure it was found that the electron number density and thermal energies were consistent to within a factor of two. A simple block diagram of the experimental setup is provided in Fig. 3.4.

Starting at bias voltages of -100 V and typically ending at +600 V, a series of current

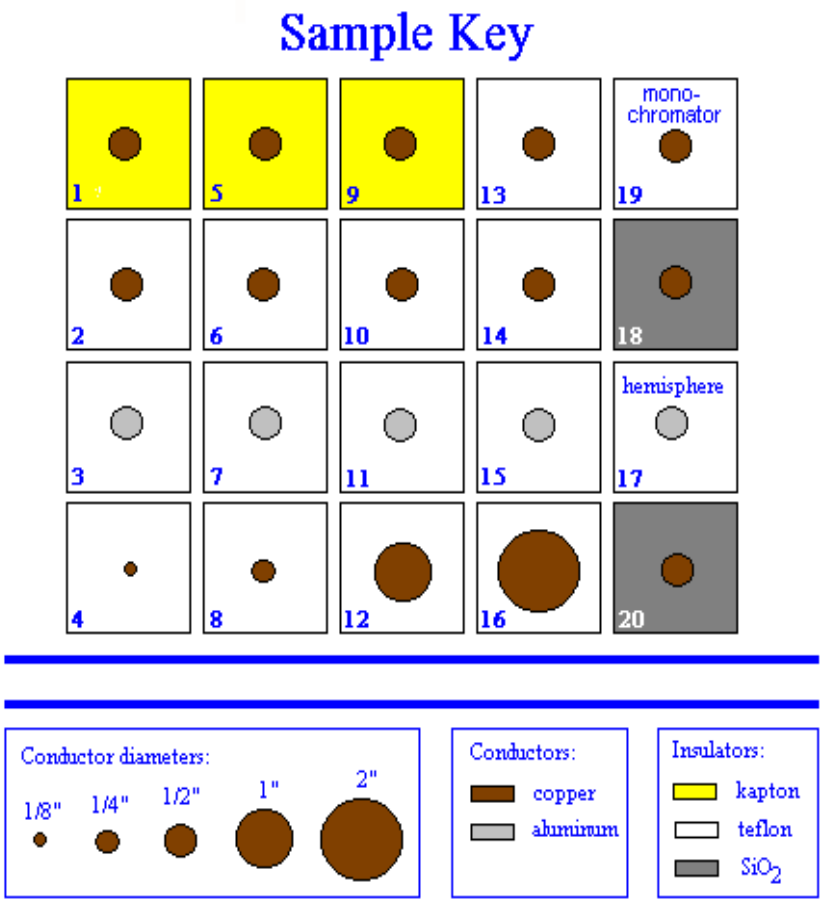

FIG. 3.1. Sample key. This shows the conductor materials, shapes and sizes and insulating materials used in the sample array.

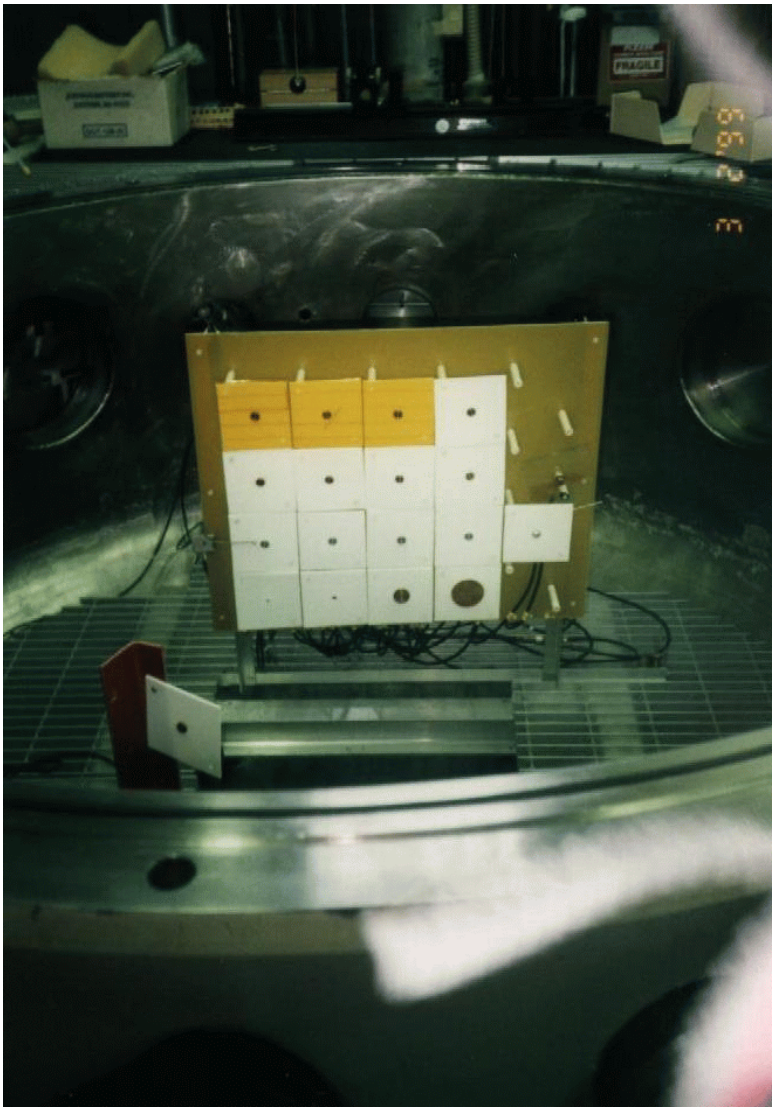

FIG. 3.2. Sample array mounted vertically in the plasma chamber.

FIG. 3.3. NASA GRC Plasma Interaction Facility (PIF) (NASA Space and Environment Effects Branch Web Site, 2001). Of the two large plasma chambers shown, our experiments were performed in the chamber on the left.

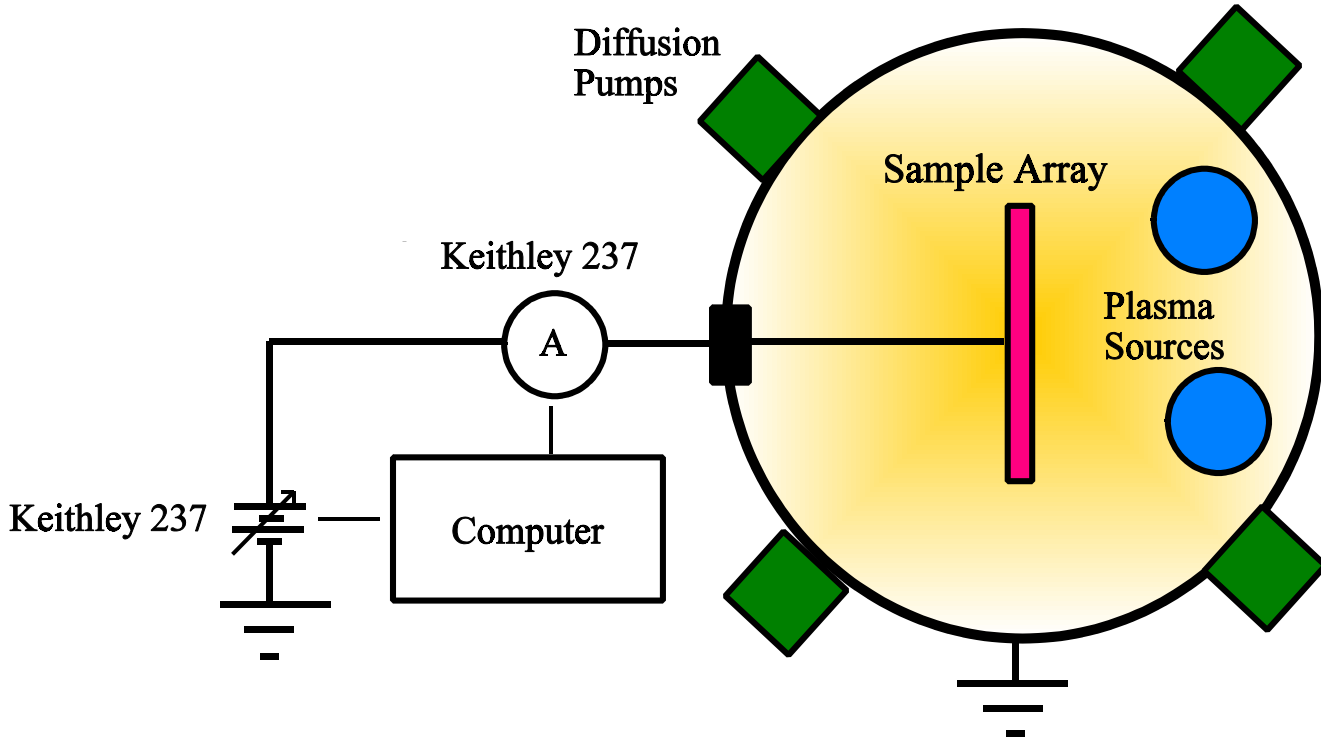

FIG. 3.4. Simple block diagram of the plasma chamber, samples, and measuring apparatus.

versus conductor bias curves, or I-V curves, (typically 10 sweeps per run) was recorded for each conductor/dielectric pair. Although the step size and ramping rate were varied from 1V/s to 50 V/s on a number of samples, 10 V/s (5 V steps with 500 ms delays) was standard. From this ramping rate, it was estimated that a ~ 15 V voltage lag existed between the sample/plasma potential as compared to the applied conductor bias voltage as will be discussed in detail in Section 4.6. The bias ramping was controlled using a Keithley 237 power source/measurement instrument interfaced to an IBM compatible personal computer using a GPIB interface. Currents up to 10 mA were measured using a computer interfaced with a Keithley 237. For normal operating temperatures of 18E to 28E C, the Keithley 237 operator's manual reported an uncertainty in the applied voltage of ± 0.04% and an uncertainty in the measured current of ± 0.035% and a source-delay-measure cycle of 1 Fs.

One additional sample was mounted in view of an optical spectrometer to analyze the glow that often accompanies the discharge phenomenon (see Fig. 3.5). Details of the spectrometer setup are reported by Galofaro *et al.* (2000), but are summarized here. The sample was positioned 85 cm in front of a 10-cm diameter double convex lens (focal length of 24 cm). The lens was enclosed in a black cylinder to shield out stray light, and light from the glowing sample was focused to a spot just outside a 15.2-cm diameter quartz window of the chamber (see Fig. 3.5). The spectrometer was placed to intercept the focused spot onto a 50-µm entrance slit. The spectrometer used a Czerny-Turner optical design, where the light undergoes three specular reflections, once off of a single grating with 1200 grooves/mm, before exiting. The spectrometer operated properly for wavelengths of 190 nm to 600 nm with a reported resolution of 1 nm. The light exited to a charge-coupled device (CCD), and the electrical signal was processed by an IBM compatible personal computer. In this way, the optical spectrum (350 nm to 600 nm) of a sample

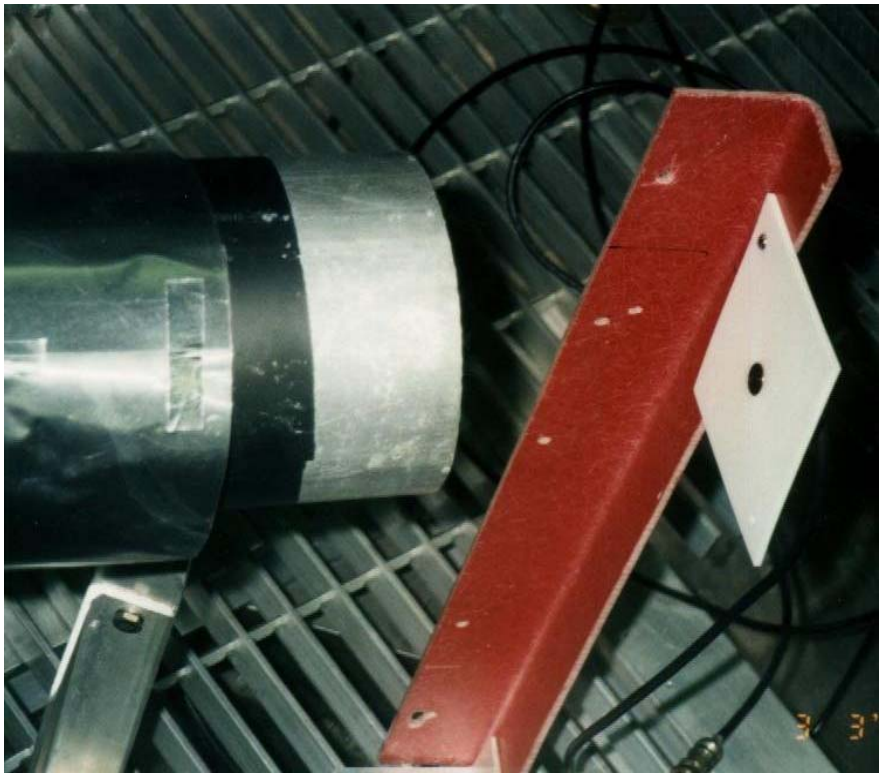

FIG. 3.5. Sample mounted in view of a spectrometer. This was done to analyze the glow that often accompanies the gas discharge phenomenon.

undergoing discharge was recorded.

Finally, it should be mentioned that after several measurements were made on a sample, yellow stains formed on the sample insulator surrounding the conductor electrodes. These stains were determined visually to be diffusion pump oil. Additionally, after approximately 48 hours of being in the chamber all samples would develop a thin oily residue (due to diffusion pump oil) on their surfaces that had to be wiped off with a cloth and methyl alcohol. It was later reported that the abundance of diffusion pump oil contamination could have been due to a faulty valve discovered by the PIF staff after the measurements were performed (Galofaro *et al.,* 2000).

CHAPTER 4

EXPERIMENTAL RESULTS AND DISCUSSION

This chapter describes the results of our experimental investigation. First, a general discussion of the measured I-V curves will be given. A classification scheme for several snapover current jumps, differing in onset voltage and current jump magnitude, will be introduced so that further references can be made throughout the thesis to the numerous current anomalies that were observed. Then, the current collecting behavior of the samples before and after snapover will be compared to plasma probe theory. Next, the results of the basic parameter studies will be presented by the addressing each of the parameters outlined in Chapter 3 in the following order: i) changes to the sample surfaces as a result of snapover and gas-discharge; ii) general hysteresis behavior; iii) effects of varying ramping rate; iv) surface contamination; v) plasma background pressure dependence; vi) a general comparison of collected current to samples of different material types; vi) insulator-type dependence; vii) conductor-type dependence; viii) conductor size dependence; ix) conductor shape dependence; x) effects of sample surface treatments; and xi) optical spectra of the gas-discharge glow. Chapter 5 will summarize a number of improvements that can be made in future snapover experiments along with suggestions for entirely new experiments that will further our understanding of snapover.

4.1 A General Discussion of the Results

Examination of the I-V profile data for various samples under a variety of conditions revealed that most samples exhibited more than one current jump over the voltage range of approximately +50 V to +1000 V (Thomson *et al.*, 2000). After viewing the I-V curves for each sample (over 400 I-V curves in number), general patterns were observed that allowed

categorization of the current jumps using the following criteria:

i) Value of onset voltage

ii) Magnitude of current jump

iii) Comparison of trends in the I-V curves for consecutive measurements on a given sample;

iv) Dependence of current transition behavior on conductor diameter (as discussed in more detail in Section 4.12)

v) Shape of the snapover I-V curves and their derivatives.

By classifying each current jump using the above criteria, four major categories over the voltage range of 150 V to 1000 V were identified using sweep rates of 10 V/s (5 V steps with 0.5 s delays).

i) Preliminary Snapover: First, a small current jump (~ 1 μA to 10 μA for 1.27-cm diameter conductors) could often be distinguished and occurred quite frequently over the voltage range of 150 V to 200 V, depending on the sample. Preliminary snapover almost always occurred in conjunction with a larger snapover current jump as shown in Fig. 4.1 (a). Initial analysis of these current jumps indicated minimal dependence of current jump magnitude and onset voltage on ambient plasma conditions. Although some more insignificant and irregular current jumps occurred at voltages less than preliminary snapover, this was the first significant current jump found to be somewhat repeatable for all samples. Due to their low onset voltage, these current jumps were believed to be closely related to SE emission of the sample insulators, but did not consistently occur often enough to warrant a thorough study.

ii) Primary Snapover (often referred to as just snapover in subsequent sections): The second major current jumps (~ 10 μA to 100 μA for 1.27-cm diameter conductors) occurred

(a)

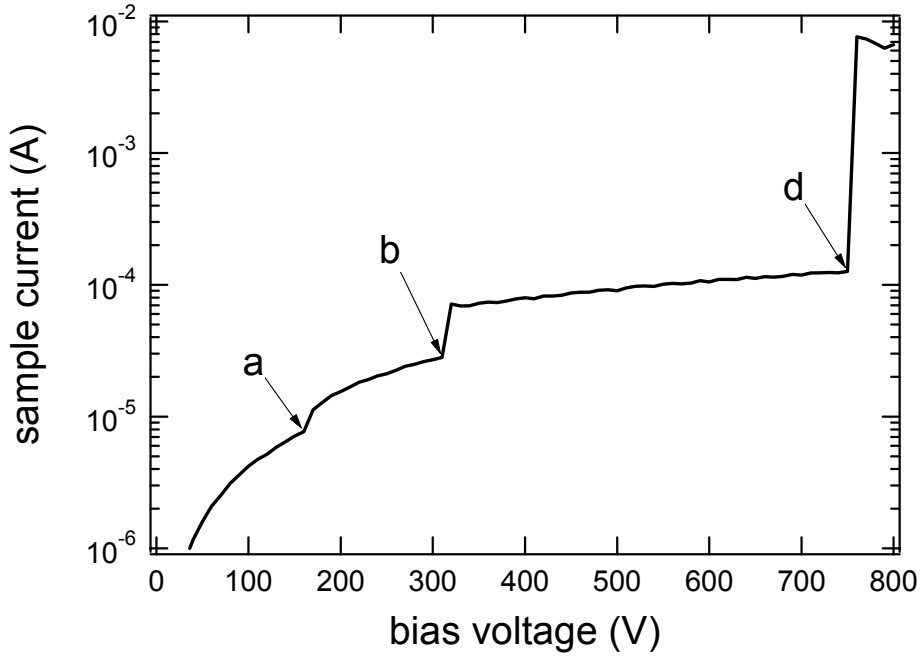

(b)

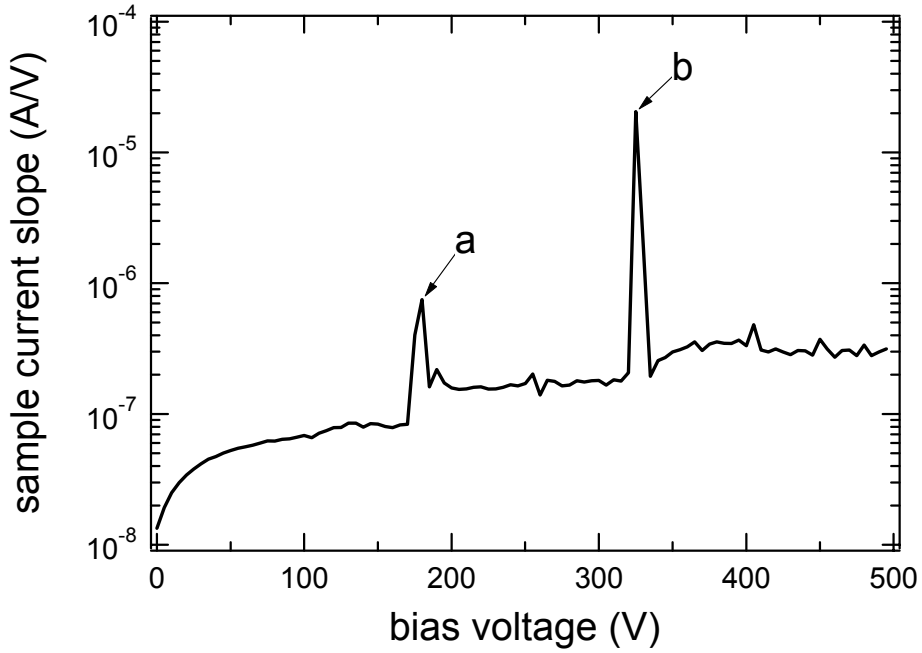

FIG. 4.1. (a) Semi-log plots of the I-V profile and (b) first derivative plot for a typical sample (1.27-cm conductor diameter Cu-Teflon™). The I-V profile exhibits current jumps attributed to a) preliminary snapover, b) primary snapover, and d) Paschen discharge. The derivative plot shows the effective conductivity of the system and peaks corresponding to the snapover jumps.

consistently for most runs at voltages ranging from 220 V to 350 V. Due to their regularity and magnitude, these current jumps became the primary focus of this study. As discussed in Section 2.3, it has been proposed that these current jumps are related to the SE emissions of the sample insulators, although a clear distinction between the roles played by SE emission and gas discharge could not be made in this study, and it is possible that both mechanisms were occurring simultaneously (e.g. through SE stimulated ionization). However, as will be discussed further, gas discharges occurring at higher voltages were distinct from the primary snapovers. Results for primary snapover are listed in Table 4.1 for the samples studied. Included in the table are sample material types, sample numbers corresponding to the sample key of Fig. 3.1, snapover onset voltages, current jump magnitudes (the absolute change in the current after and before the jump), current jump ratios (the fractional change in the current, that is the ratio after to before the jump), the number of runs performed on the sample that are included in the sample statistics, and the percent occurrence of primary snapover for the number of runs performed.

iii) Gas Discharge: The third major category of current jumps (~ 0.1 mA to 5 mA for 1.27-cm diameter conductors) appeared in a sporadic fashion from one run to the next and had onset voltages ranging anywhere from 350 V to 600 V. These larger current jumps were attributed to gas discharges in the near vicinity of the sample conductor arising from materials out-gassed from the sample and then immediately ionized by the high density of electrons near the sample surface. Current jumps of this magnitude and onset voltage range were identified by Stillwell *et al.* (1985) as the vapor-enhanced current collection mode (see Section 1.2). These gas discharges may have resulted from the ionization of

TABLE 4.1. Primary snapover inception voltages and collection currents. Results are for untreated samples at relatively low-to-medium Argon pressures of 60-80 μTorr, electron number densities of n_e=1-3·10^5 cm^{-3}, and electron temperatures T_e=1-3 eV ramped at 10 V/s. First runs were excluded from the statistics. Standard deviations are shown in parentheses.

Sample Type (Diam. Conductor-Dielectric)	Sample No. (see Fig. 3.1)	Onset Voltage (V)	Magnitude of Current Jump (μA)	Current Jump Ratio	No. of Runs	Occurrence Percentage
1.3 cm Cu-Teflon™	2	274 (38)	89 (66)	5 (2)	16	100%
1.3 cm Cu-Teflon™	6	278 (27)	12 (8)	1.6 (0.4)	6	100%
1.3 cm Al-Teflon™	3	219 (35)	18 (19)	3 (1)	11	100%
1.3 cm Al-Teflon™	11	--	--	--	3	0%
1.3 cm Cu-Kapton™	1	263 (27)	108 (63)	6 (4)	16	88%
1.3 cm Cu-Kapton™	5	224 (14)	51 (15)	3.0 (0.6	4	100%
1.3 cm Cu-SiO_2	18	259 (11)	94 (12)	10.6 (0.8)	9	100%
0.32 cm Cu-Teflon™	4	225 (54)	2. (2)	19 (23)	26	85%
0.64 cm Cu-Teflon™	8	262 (36)	10 (11)	12 (13)	27	89%
2.5 cm Cu-Teflon™	12	198 (8)	68 (35)	3.0 (1.0)	8	100%
5.1 cm Cu-Teflon™	16	226 (27)	215 (148)	1.9 (0.5)	21	100%
1.3 cm Hemispherical Al Alloy (Al 2017-T4)--Teflon™	17	271 (11)	140 (60)	5 (2)	9	100%

out-gassed sample materials resulting from local sample heating or electron stimulated desorption. Results are listed in Table 4.2 for the samples studied. The column headings are the same as those described for Table 4.1 for primary snapover.

iv) Paschen Discharge: The fourth major category of current jumps (~2 mA to >10 mA for 1.27-cm diameter conductors) also appeared intermittently with onset voltages ranging from ~500 V to 1000 V. These larger current jumps were attributed to breakdown of the background argon gas at high voltages (Vayner *et al.,* 2000).

These four categories are labeled (by letter) on I-V curves in Figs. 4.1 and 4.2 (a) as a) preliminary snapover, b) primary snapover (or just snapover), c) gas discharge, and d) Paschen discharge. This lettering scheme is used in figures throughout the rest of the thesis to identify the different types of current jumps. Of these four categories, preliminary and primary snapovers were assumed to be the same modes identified by Stillwell *et al.* (1985) as surface-enhanced current collection modes, while the gas and Paschen discharges were assumed to be the same as the vapor-enhanced modes (see Section 1.2).

Although these four categories provided a general framework, ambiguities in classification did occur. For example, the onset voltage of the primary snapover and preliminary snapover current jumps could "drift" from run to run and in some cases "fuse" together. Alternately, the primary snapover onset could drift to higher voltages from one run to the next (up to 350 V to 400 V at higher pressures), and take on properties similar to gas discharge (large collection currents and the "hook" shaped current jump). It was not always clear whether a SE or gas discharge induced current jump was occurring, or whether both mechanisms were occurring simultaneously and, if so, how they were interrelated. Because of the occasional confusion involved in classification: i) all major current jumps (>10 FA) below 350 V

TABLE. 4.2. Gas discharge inception voltages and collection currents. Results are for untreated samples at relatively low-to-medium Argon pressures of 60-80 μTorr, electron number densities of n_e=1-3·10^5 cm^{-3}, and electron temperatures T_e=1-3 eV ramped at 10 V/s. First runs were excluded from the statistics. Standard deviations are shown in parentheses.

Sample Type (Diam. Conductor-Dielectric)	Sample No. (see Fig. 3.1)	Gas Discharge Onset Voltage (V)	Magnitude of Current Jump (mA)	Current Jump Ratio	No. of Runs	Occurrence Percentage
1.3 cm Cu-Teflon™	2	461 (38)	0.7 (0.5)	9 (6)	16	44%
1.3 cm Cu-Teflon™	6	458 (39)	1.1 (0.2)	24 (2)	6	33%
1.3 cm Al-Teflon™	3	386 (46)	0.4 (0.2)	14 (7)	11	73%
1.3 cm Al-Teflon™	11	323 (56)	0.27 (0.05)	25 (5)	3	100%
1.3 cm Cu-Kapton™	1	414 (44)	1.0 (0.4)	11 (4)	16	44%
1.3 cm Cu-Kapton™	5	457 (48)	1.5 (0.4)	12.1 (0.7)	4	75%
1.3 cm Cu-SiO_2	18	510 (60)	5.7 (0.7)	16 (15)	9	89%
0.32 cm Cu-Teflon™	4	454 (81)	0.3 (0.2)	101 (32)	26	23%
0.64 cm Cu-Teflon™	8	393 (48)	0.2 (0.1)	38 (17)	18	61%
2.5 cm Cu-Teflon™	12	472 (28)	1.9 (0.4)	9.9 (2.1)	8	75%
5.1 cm Cu-Teflon™	16	477 (86)	4.1 (3.5)	4.7 (3.7)	21	57%
1.3 cm Hemispherical Al Alloy (Al 2017-T4)--Teflon™	17	485	4.1	21	9	11%

(a)

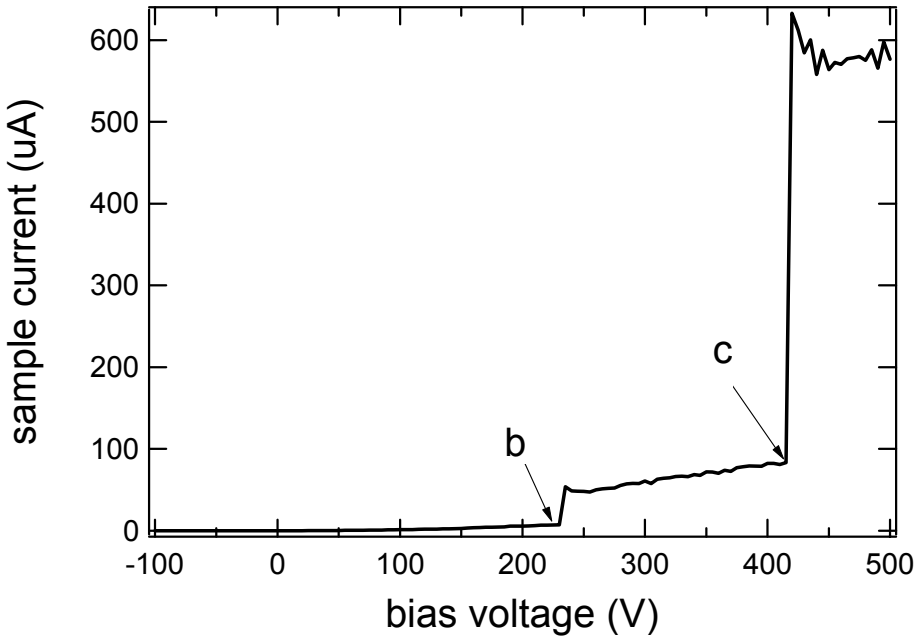

(b)

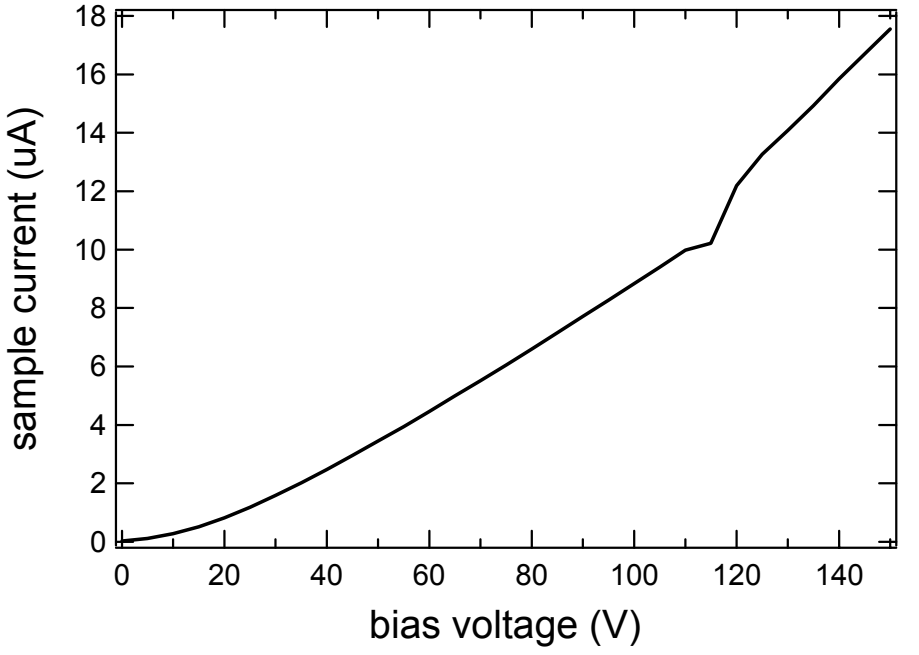

FIG. 4.2. Linear plot I-V profiles for typical samples. Shown are (a) current jumps attributed to b) primary snapover and c) gas discharge and (b) a typical small current anomaly at an onset voltage of ~ 120 V. Both I-V plots are for 1.27-cm diameter Cu-Kapton™ samples. Note the characteristic hook shape of the gas discharge current jump profile in graph (a).

were categorized as primary snapover unless a clear distinction could be made with the preliminary snapover and ii) any large magnitude current jumps occurring over ~350 V were identified as either gas discharge or Paschen discharge.

For the same samples or similar material type samples, the onset voltages of the preliminary and primary snapovers (when they occurred) were reproducible to within approximately ± 20 V holding all other parameters fixed. The current jump magnitudes were also reproducible to within an order of magnitude. Variations in the onset voltages were a concern in studying the dependence of snapover on insulator type since differences in insulator first crossover energies also differ by roughly ± 20 eV. Finally, following preliminary and primary snapover the slope of the I-V curve (or the effective conductivity of the sample/plasma system) would generally increase.

The onset voltages of gas discharge and Paschen discharge were not nearly as reproducible as preliminary and primary snapover, and could vary by as much as ± 100 V for similar sample types or the same samples on different runs (later, this is illustrated nicely in Fig. 4.12). Also, the current jump magnitudes for the discharge current jumps could vary by as much as two orders of magnitude. As already explained, immediately following a gas discharge or Paschen discharge current jump, the I-V curve exhibited a hook shaped decline in the collected current before roughly linear behavior on the applied voltage was reestablished. The observed diversities in snapover and discharge characteristics (such as variations in the onset voltage and current jump magnitudes) for identical or similar samples on different runs could have resulted from the adsorption of surface contaminants, changes in surrounding plasma conditions, and material surface modifications from previous snapover events.

In addition to these four major current jump categories, many smaller magnitude current jumps were observed throughout the voltage range of 80 V to 1000 V. Most of these jumps

occurred irregularly, and were attributed to random gas discharges. However, of particular interest were very small current anomalies occurring in the voltage range of 100-150 V (see Fig. 4.2 (b)). Upon closer examination of the I-V curves at voltages under 150 V it was noticed that numerous small current jumps and abrupt changes in current slope with magnitudes < 1 μA occurred (especially for Kapton™ insulator samples). Even though the current jump magnitudes of these anomalies were relatively insignificant compared with higher voltage snapovers, the low inception voltage of these anomalies corresponded closer in magnitude to the associated first crossover energies of the insulators. These current jumps may have resulted directly from transitions of the nearby insulator's total electron yields, σ, from a value below to a value exceeding one, while a major current jump transition did not occur.

4.2 Comparisons of Measured Current Collection with Plasma Probe Theory

From the plasma electron number density and energy, measured with a Langmuir probe at the beginning of each experiment, the relevant parameters such as the Debye length, λ_D, the mean electron thermal speed, u_e, and the random electron current density, J_e, were all estimated using Eqs. (2.1), (2.2), and (2.3). At background pressures of 73 FTorr, the measured electron energy and number density values were found to vary from 1.1 to 3.5 eV and $1.2 \cdot 10^{11}$ to $3.3 \cdot 10^{11}$ m^{-3}, respectively. With these uncertainties, the calculated Debye length, mean electron speed, and random electron current density were also found to vary between the following extremes:

Plasma Debye length (Eq. (2.3)):	1.4 to 4.0 cm
Mean electron velocity (Eq. (2.1)):	$7.0 \cdot 10^5$ to $1.3 \cdot 10^6$ m/s
Random electron current density (Eq. (2.2)):	0.0034 to 0.017 A/m^2.

From these calculated values, it was found that the plasma Debye lengths were roughly the same dimensions as the sample conductors (0.32- to 5.08-cm diameter conductors were used).

Consequently, the plasma regime at low voltages (thin (r_s<<r) or thick (r_s>>r) sheath), and thus the current collecting behavior, could not be easily determined for our samples, but it was expected that the measured current to the samples would lie somewhere between the thick-sheath and thin-sheath approximations for planar and spherical probes.

From the measured number densities and energies taken at 73 FTorr, the calculated random electron current densities as shown above were used as the lower and upper limits in subsequent modeling of the sample current. With the random electron current density, the current as a function of applied voltage was calculated for 5.08-cm, 2.54-cm, 1.27-cm, 0.635-cm, and 0.318-cm diameter conductor plasma probes using Parker and Whipple's planar probe current collection model (Eq. (2.10)). Additionally, both the thin- and thick-sheath current to a hemispherical probe were calculated using Eqs. (2.7) through (2.9) (by dividing the spherical probe current collection by two). Then, the modeled current collection was plotted along with the average (over approximately 10 consecutive runs) measured collected current for 5.08-cm, 2.54-cm, 1.27-cm, 0.635-cm, and 0.318-cm diameter conductor Cu-Teflon™, Al-Teflon™, Cu-Kapton™, and Cu-SiO_2 planar conductor samples, and also for the 1.27-cm diameter hemispherical Al-Teflon™ sample. Results for the calculated current regimes along with the average measured currents are shown in Figs. 4.3 through 4.5.

For the planar sample I-V curves shown in Figs. 4.3 through 4.5 (a), the average measured current data are represented by lines while the upper and lower limits for planar probe theory predictions (including uncertainties derived from uncertainties in the measured number density and random current density given above) are represented by the shaded region. Notice in Figs. 4.3 through 4.5 that since the I-V curves are averaged over multiple cycles, the snapover

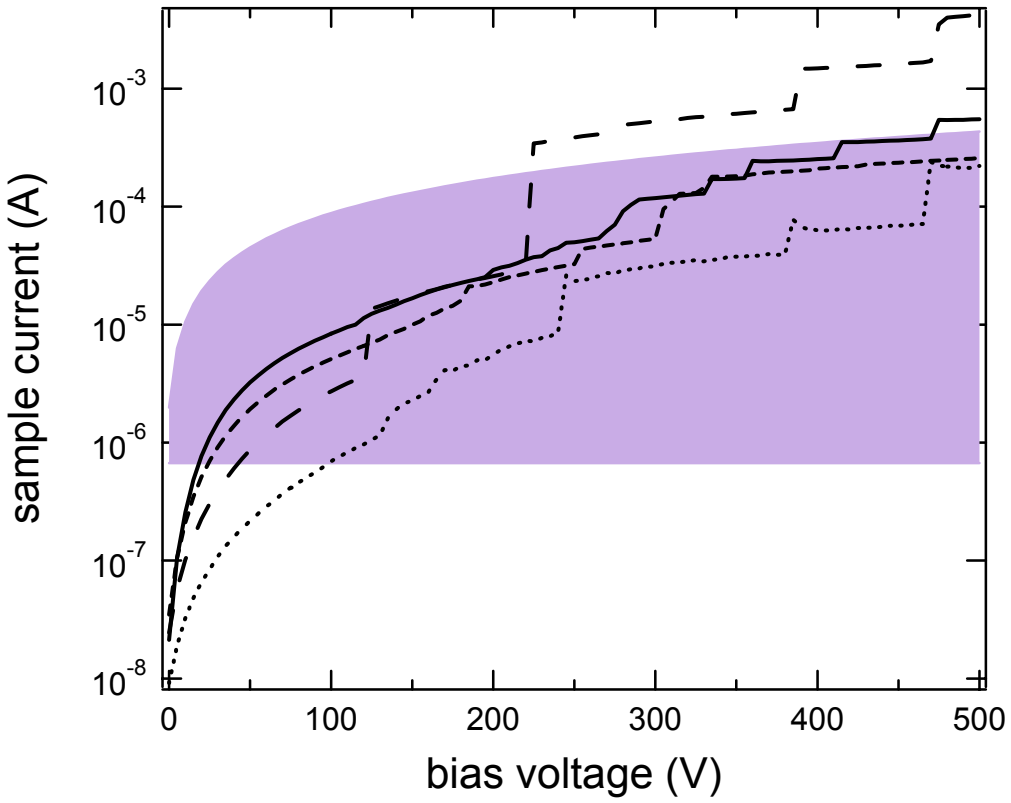

FIG. 4.3. Semi-log plot of the average measured and modeled currents for 1.27-cm diameter samples at similar pressures. The sample materials and corresponding pressures are as follows: Cu-Kapton™ 71 uTorr (solid line), Cu-Teflon™ 73 uTorr (short dashes), Cu-SiO_2 73 uTorr (long dashes), and Al-Teflon™ 66 uTorr (dots). Also plotted are the thin-sheath to thick-sheath current collection regimes (shaded region) for planar probes. Below ~100 V the measured currents fell below the model's predictions.

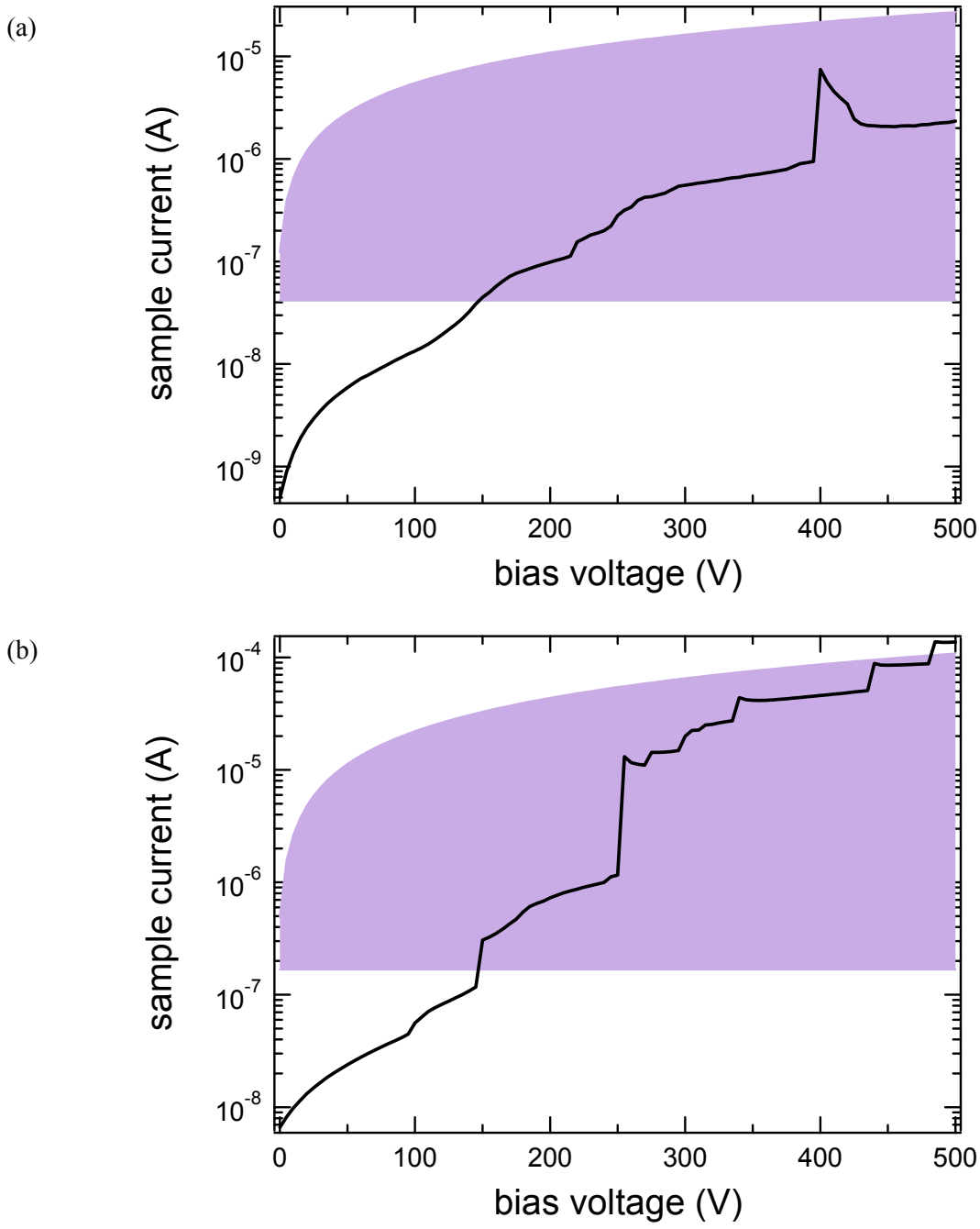

FIG. 4.4. Semi-log plots of the average measured and modeled current for the (a) 0.32-cm and (b) 0.64-cm diameter Cu-Teflon™ samples. Also plotted are the thin-sheath to thick-sheath limits (shaded region) for planar probe current collection. Below ~ 150 V the measured current fell below the model's predictions.

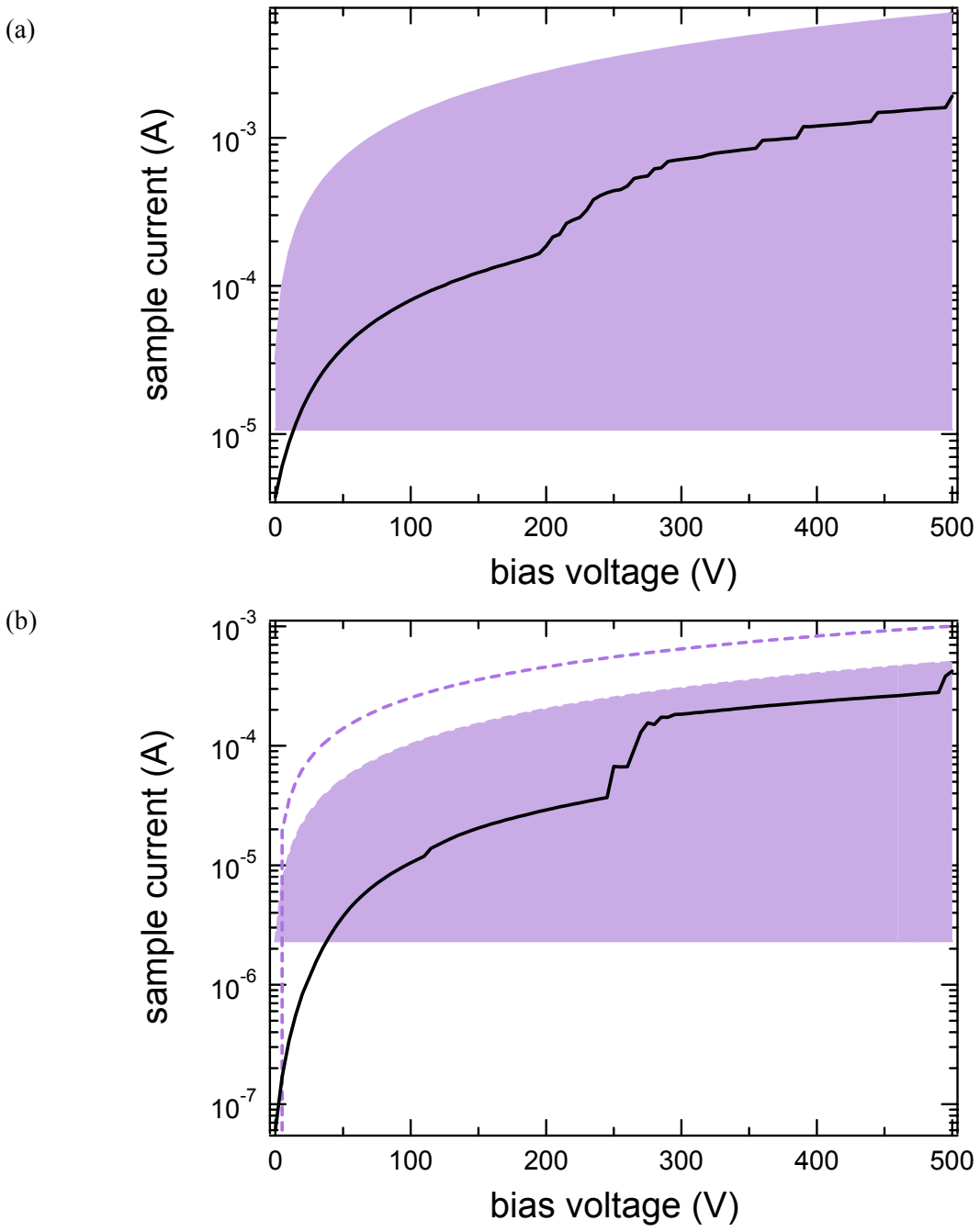

FIG. 4.5. Semi-log plots for the average measured and modeled currents for the (a) 5.1-cm diameter Cu-Teflon™ and the (b) 1.3-cm diameter hemispherical Al-Teflon™ samples. Also shown are the thin-sheath to thick-sheath limits for planar and hemispherical probe current collection (the upper dashed line represents the thick-sheath approximation for a hemispherical probe calculated from Eq. (2.9)). Below ~50 V the measured current fell below the model's predictions.

and gas-discharge current transitions are not abrupt as they are in the single cycle I-V curves of Figs. 4.1 and 4.2 due to variations in the snapover and gas discharge onset voltages and currents. Also, error bars in the averaged measured I-V curves have been omitted. At low voltages (< 150 V before snapover) the standard deviations of the averaged I-V curves were found to be insignificant (usually 1% of the averaged current). However, at high voltages (> 250 V) the standard deviations could be on the order of the current jump magnitudes as a result of variations in snapover and gas discharge onset voltages. Consequently, displaying error bars at high voltages visually obscured the average sample I-V curve behavior.

In Figs. 4.3 through 4.5 (a), the lower limit of the shaded region represents the thin-sheath or infinite plane limit for planar current collection that is attained by letting the parameter b62 in Eq. (2.10). For this limit, the current is not dependent on applied voltage, and in fact immediately saturates to a value $2 \cdot J_e$. For the planar models, the upper portion of the shaded region is attained by letting b60 in Eq. (2.10), and represents the thick-sheath extreme for planar probe current collection. Similar interpretations apply for the hemispherical graph (Fig. 4.5 (b)), where the spherical thin-sheath saturation current is equal to the random electron current density, J_e from Eq. (2.7) (plotted is the spherical probe current collection divided by two for a hemispherical probe). Also shown in the hemispherical plot are two different upper estimates for the hemispherical thick-sheath regime as calculated from Eqs. (2.8) and (2.9). As an aside, note that results for the planar 2.54-cm diameter conductor sample are not shown in any of the following figures since the calculated current far exceeded the measured current. In other analysis studies involving current as a function of conductor diameter, it was found that the data set for the 2.54-cm diameter conductor sample was extremely inconsistent. Data for this sample were taken prior to my arrival at NASA GRC, and it is possible that a wrong feed-through was connected in measuring this data set. Consequently, data from this sample were excluded in the analysis.

For all planar and hemispherical samples, it was observed that the calculated random current densities from Eq. (2.2) and Eqs. (2.6) through (2.10) gave estimates for the sample current that were too high by one to two orders of magnitude for lower voltages before snapover (below 150 V for all samples regardless of material type and conductor size and shape) as shown in Figs. 4.3 through 4.5. After voltages of 50 to 150 V (depending on the sample) the measured averaged currents rose into the probe model current collection regime. Finally, after primary snapover (occurring at voltages of ~250 V) the current collection to most of the samples further approached the upper thick-sheath limit. Furthermore, the 1.27-cm diameter conductor Cu-SiO_2 sample exhibited current collection that exceeded the model's predictions by as much as an order of magnitude.

It was not clear why the theoretical current for both planar and hemispherical conductor samples exceeded the measured planar and hemispherical current at low voltages, but a similar effect has been reported in previous snapover studies with the interpretation that the insulator charges slightly negative, and causes repulsion in the near vicinity of the conductor before snapover (refer to Sections 1.2 and 2.3). Negative insulator charging can act to repel additional plasma electron current until the insulator has snapped-over and acquires a positive charge gradient. For example, as explained in more detail in Section 1.2, Grier and McKinzie (1972) reported that the measured current through holes in numerous insulators was initially suppressed as compared to the planar probe model until a current jump occurred at ~1000 V. After the current jump, the measured current exceeded the calculated current. Additionally, Thiemann and Schunk (1990a) found in their computational study that the perpendicular sheath dimensions were diminished by one order of magnitude (compared to probe theory predictions) as a consequence of insulator negative charging. This reduction of the plasma sheath before snapover acts to suppress the electron current. An alternative explanation for the lack of agreement between

plasma probe theory and the measured sample current at low voltages is that the probe model from Eq. (2.10) is oversimplified, and does not adequately describe the plasma conditions that existed during our experiments.

Although previous experiments and computational modeling have offered some support for the observed discrepancies between calculated and measured I-V curves, it still seems peculiar that the models for spherical (Eq. (2.8)) and planar (Eq. (2.10)) probe currents do not agree with the measured currents at applied biases of zero volts for each sample. Particularly, the models predict that the samples should collect current density of J_e (for spherical probes) and $2 \cdot J_e$ (for planar probes) at zero volts. Clearly, from Figs. 4.3 through 4.5 this was not the case. Hence, the modeling of the measured currents was performed once again with the random current densities from Eqs. (2.8) through (2.10) set to match the measured currents at zero volts (that is, the y-intercepts of the calculated and measured I-V curves were set equal to each other). After adjusting the initial random current densities, it was found that all measured sample currents at low voltages generally fit within the two approximation limits as shown in Figs. 4.6 through 4.8 (the exceptions were for 1.27-cm diameter Cu-Kapton™, Cu-Teflon™, and Cu-SiO_2 samples where the sample current exceeded the model at nearly all voltages). However, at higher voltages (above ~100 V for the planar samples and ~50 V for the hemispherical sample) the measured collected currents began to exceed the modeled currents. Finally, at applied biases of 500 V some measured currents exceeded the modeled currents by as much as two or three orders of magnitude.

For planar probes, it was found that smaller probes collected less current density than larger probes. Fig. 4.9 shows average measured current densities for Cu-Teflon™ samples of

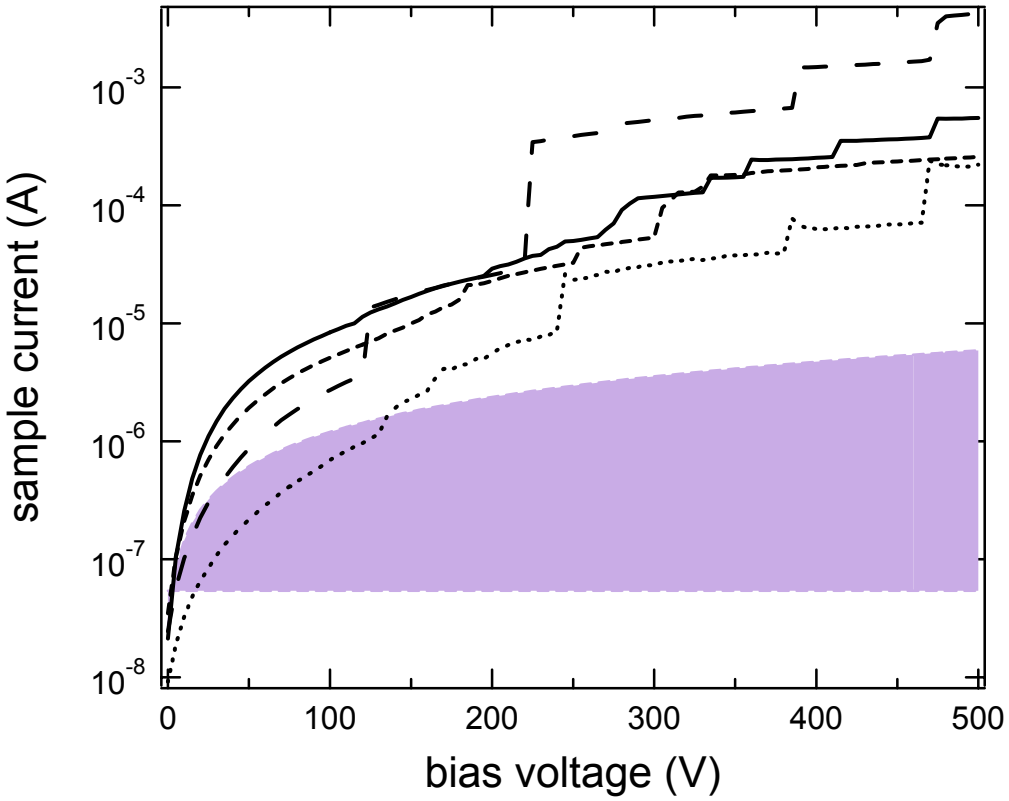

FIG. 4.6. Semi-log plot of the average measured and adjusted modeled current for 1.27-cm diameter samples at similar pressures. The sample materials and corresponding pressures are as follows: Cu-Kapton™ 71 uTorr (solid line), Cu-Teflon™ 73 uTorr (short dashes), Cu-SiO_2 73 uTorr (long dashes), and Al-Teflon™ 66 uTorr (dots). Also plotted are the thin-sheath to thick-sheath current regimes (shaded region) for planar probe current collection. After adjusting the initial modeled random electron current to match the measured sample current at bias voltage V=0, the measured current overshot the modeled current after ~150 V for all samples, and exceeded the modeled current by as much as two to three orders of magnitude at 500 V.

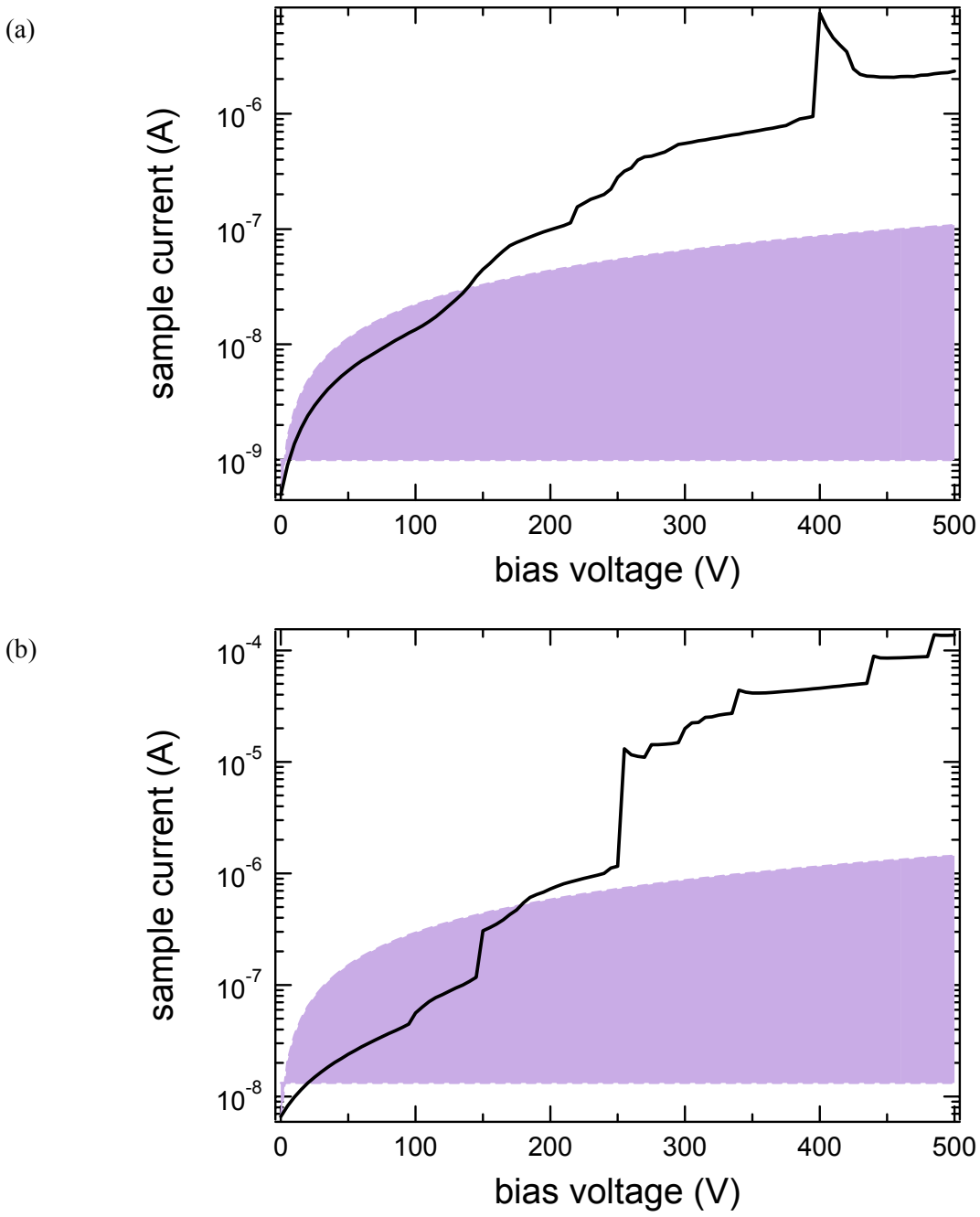

FIG. 4.7. Semi-log plots of the average measured and adjusted modeled currents for the (a) 0.32-cm diameter and (b) 0.64-cm diameter Cu-Teflon™ samples. Also plotted are the thin-sheath to thick-sheath limits (shaded region) for planar probe current collection. After adjusting the initial modeled random electron currents to match the measured sample currents at bias voltage V=0, the planar probe model gave a much better overall fit to the measured sample current at low voltages and showed enhanced measured current above ~ 200 V. At 500 V the measured current exceeded the modeled current by as much as two orders of magnitude.

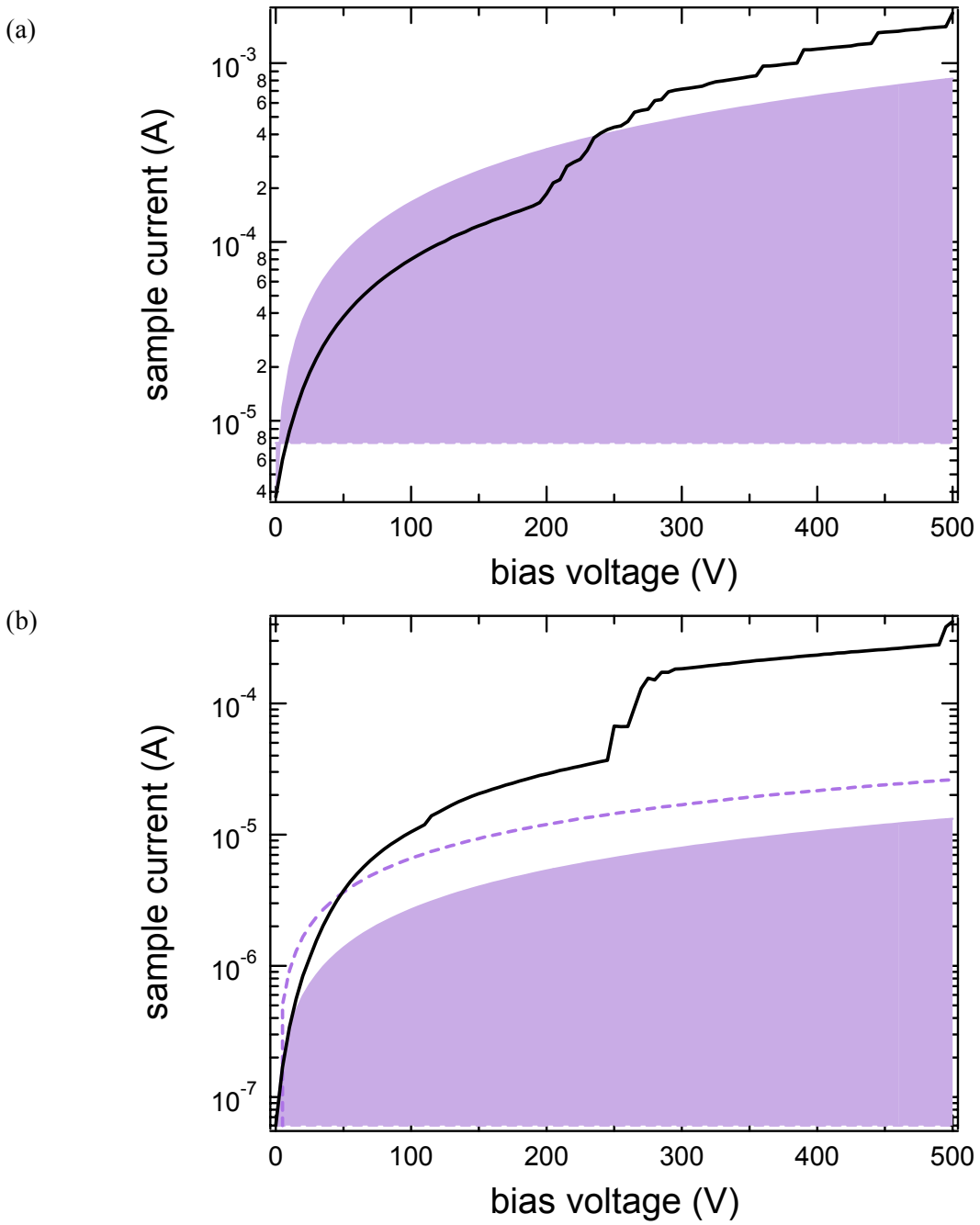

FIG. 4.8. Semi-log plots for the average measured and adjusted modeled currents for the (a) 5.1-cm diameter Cu-Teflon™ and the (b) 1.30-cm diameter hemispherical Al-Teflon™ samples. Also shown are the thin-sheath to thick-sheath limits for planar and hemispherical probe current collection (the upper dashed line represents the thick-sheath approximation for a hemispherical probe calculated from Eq. (2.9)). After adjusting the initial modeled random electron currents at V=0, the probe models gave much better overall fits to the measured sample currents at low voltages and showed that the enhanced measured current at ~ 250 V (plane) and ~ 25 V (hemisphere) exceeded the modeled current.

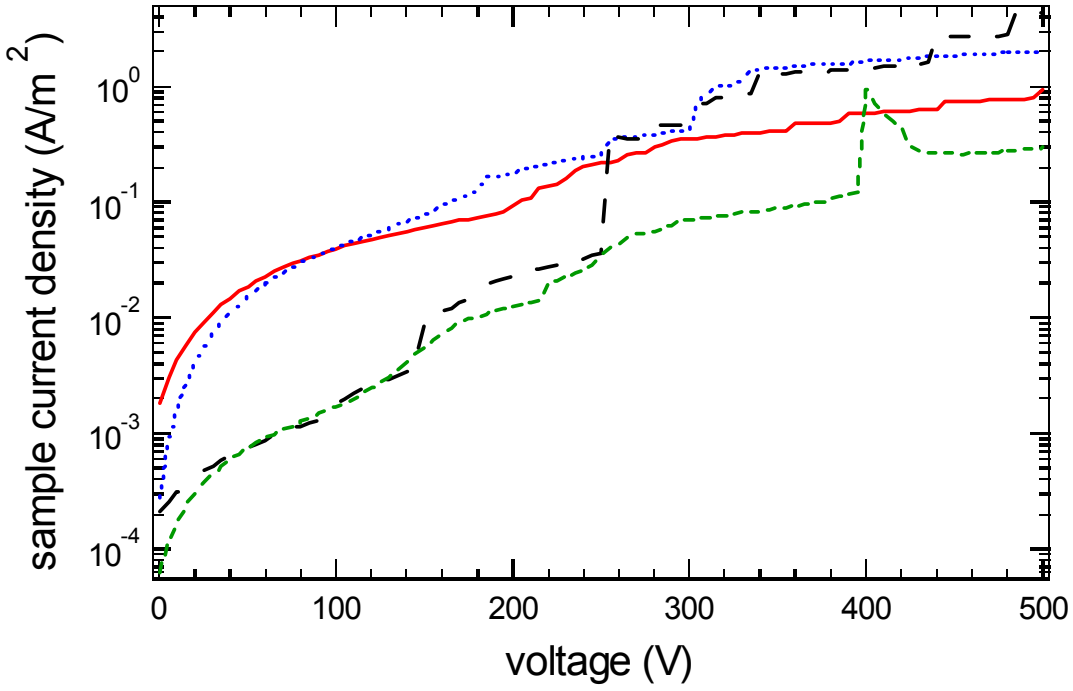

FIG. 4.9. Average measured current densities for Cu-Teflon™ samples of different conductor sizes. Samples with larger diameter conductors (1.27 cm (dotted) and 5.08 cm (solid line)) collected substantially larger current densities than smaller diameter conductors (0.317 cm (short dashes) and 0.635 cm (long dashes)) at low voltages before snapover. After primary snapover (at voltages ~ 250 V), conductor diameter did not have as strong of an effect on collected current.

different conductor sizes under similar plasma conditions. As shown, the current densities (conductor areas have been divided out) to smaller conductor samples (0.318- and 0.635-cm diameter conductors) were substantially less than the current density for the larger conductor samples (5.08- and 1.27-cm diameter conductors) at low voltages (before snapover) holding all other conditions fixed. One would expect the current density to smaller samples to exceed the current density to larger samples since planar probe theory predicts that for the thick-sheath limit ($r_s>>r$) (more applicable to smaller samples than to larger samples) the current density is regulated more strongly by the applied voltage whereas for the thin-sheath limit ($r_s<<r$) the current saturates. In fact, it appears that an abrupt current density transition occurred somewhere between the 0.635-cm and 1.27-cm diameter conductor samples as shown in Fig. 4.9. Also, at voltages exceeding ~250 V (corresponding to the primary snapover transition) the size of the conductor did not influence the collected current as strongly (see Fig. 4.9). For example, the 0.635-cm diameter conductor sample began to collect as much or more average current then the 1.27-cm and 5.08-cm diameter conductor samples. This behavior will be discussed further in Section 4.12.

In order to further examine the modeled planar probe current density behavior from Eq. (2.10), the parameter b was calculated as a function of sample diameter. From planar probe theory (refer to Section 2.1), it was expected that smaller conductor samples should exhibit smaller b values (approaching zero) than larger conductor samples. This in turn would cause greater current density to be collected by the smaller samples as can be seen from Eq. (2.10). In order to fit to the parameter b, Eq. (2.10) was rewritten in terms of the mean electron temperature and number density (from Eq. (2.2)), which provides an equation that is linear in applied voltage:

$$J_{p\ln} = ne\left(\frac{\kappa T}{2\pi m_e}\right)^{1/2}\left[1+\frac{b^2}{4}\right]+\frac{ne^2}{\kappa T}\left(\frac{\kappa T}{2\pi m_e}\right)^{1/2}\left[1-\frac{b^2}{4}\right]V \qquad (4.1)$$

where the first term is the y-intercept and the second term is the slope term multiplied by the applied voltage. From Eq. (4.1) a simple linear fit was performed on the measured data from 0 to 75 V along with a 95 % confidence interval for each sample size as shown in Fig. 4.10. From this it was found that to within the specified 95% confidence interval, the calculated slopes were accurate to within one or two decimal places. However, the y-intercept values showed greater uncertainties, and consequently were excluded in the calculations for the parameter b.

Along with the fitted slope values, the measured electron energies and number densities (incorporating experimental uncertainties) at 75 FTorr were used to calculate b values for Cu-Teflon™ samples of different conductor diameters (uncertainties from the fitted slopes and from the measured electron energies and number densities were carried through the calculation using numerical quadrature). Results for the fitted parameter b along with estimated uncertainties are plotted as a function of conductor diameter in Fig. 4.11. Several key points should be brought forth concerning the relationship between the parameter b and the conductor diameters at low voltages. First, all b values for the Cu-Teflon™ samples were below the upper end limit, b=2. However, the b values were very close to this upper limit, suggesting current collection in the planar thin-sheath regime ($r>>r_s$) for all samples, where overall current is suppressed and the current density saturates. However, calculated values for the Debye length indicated that for all samples, the plasma sheath dimensions were on the order of the sample conductors. Therefore, the thin-sheath or infinite plane limit should not have dominated the current collection for the

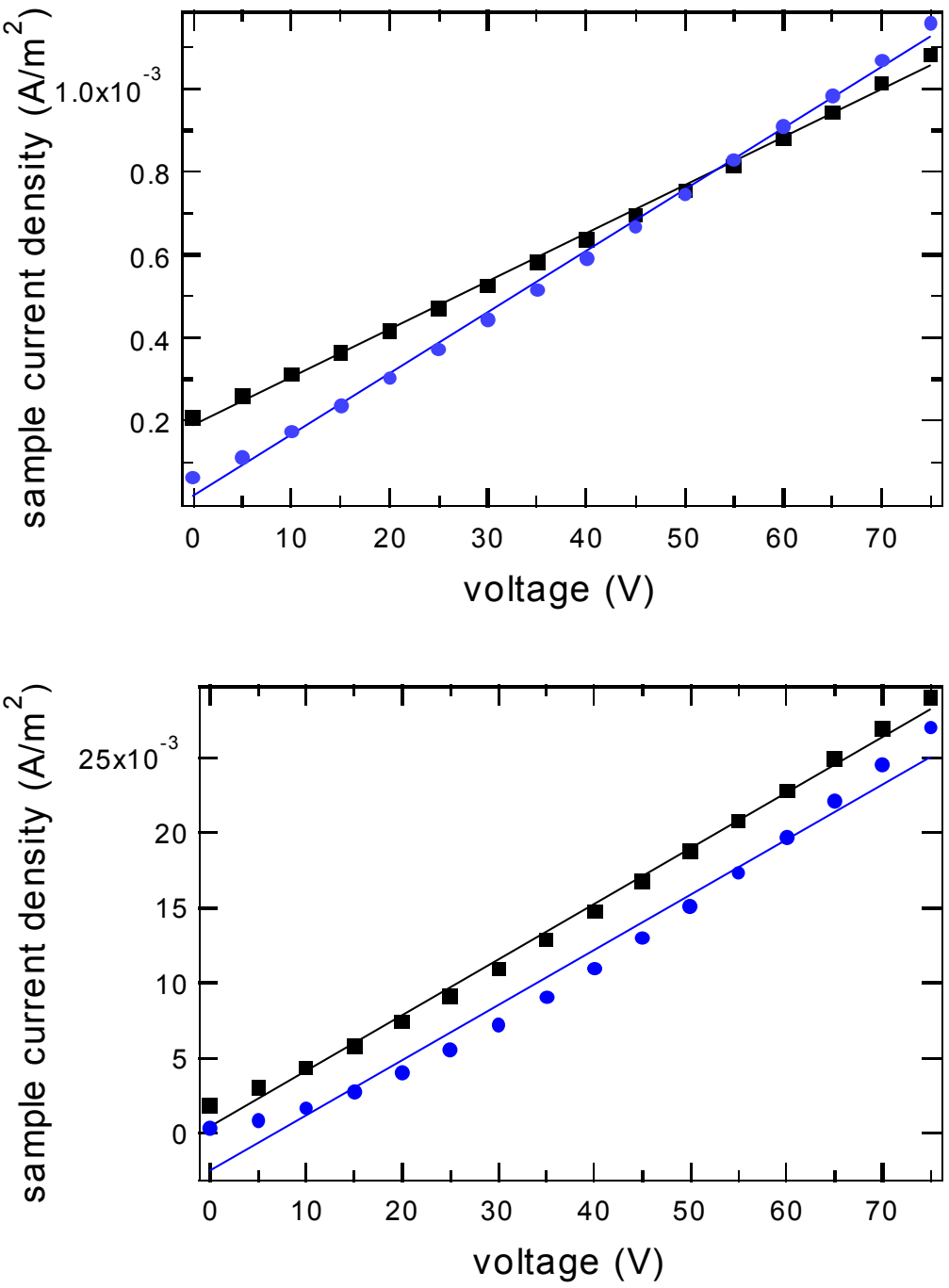

FIG. 4.10. Linear fits to measured current densities for Cu-Teflon™ samples. Shown are (top) small conductor samples (0.635-cm ( ) and 0.317-cm( ) conductor diameters) and (bottom) larger conductor samples (5.08-cm ( ) and 1.27-cm( ) conductor diameters). The planar probe parameter, b, from Eq. (4.1) was calculated from the slopes of the linear fits.

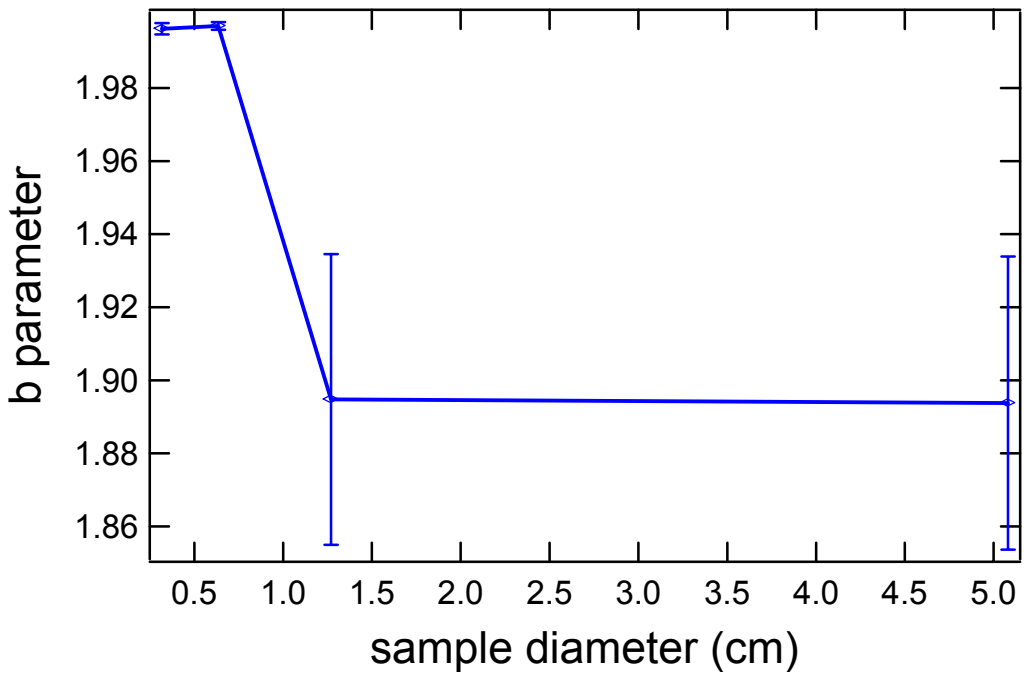

FIG. 4.11. Fit to planar probe parameter, b, for samples of different conductor diameter. Smaller conductor samples (0.32 and 0.64 diameters) showed larger b values with small uncertainties. Larger conductor samples (1.27 and 5.08 diameters) showed smaller b values with large uncertainties.

samples so strongly. In other words, according to this fit the samples exhibited abnormally low I-V slopes before snapover as compared to the corresponding modeled conductor probe current.

A second point to note is the abrupt transition in calculated b values (and errors) between larger conductor samples to smaller conductor samples (specifically between the 1.27- and 0.635-cm diameter conductor samples). This transition was in the opposite direction as predicted by the planar probe model. From Fig. 4.11 it is seen that the larger conductor samples displayed smaller b values than the smaller conductor samples. The model predicts that smaller conductor samples should exhibit smaller b parameters (since they are better modeled with a thick-sheath approximation), and larger samples should exhibit larger b parameters (since they are better modeled with a thin-sheath approximation). As mentioned before, it was not clear whether the

suppressed current density (in comparison the theoretical current density) resulted from flaws in the overly simplified plasma current model used, or was in fact caused by surrounding insulator current suppression as reported in previous snapover investigations (see Section 1.2). In hindsight, an isolated planer conductor sample should have been included in this study so that its I-V curve characteristics could have been directly compared with that of a conductor in the presence of an insulator.

Finally, from Figs. 4.3 and 4.6 note that holding all other parameters fixed, the Cu-Kapton™ sample collected higher overall current than any other 1.27-cm diameter conductor sample of different insulator material type before snapover, and the Cu-SiO_2 sample collected significantly more current than other samples after snapover. A dependence of current collection on material type (even before snapover) was present at all measured pressures in a consistent manner. This observation will be addressed further in Section 4.9. Finally, although it cannot be seen clearly in the average I-V curves of Figs. 4.3 through 4.8, small current jumps and changes in current slope were observed at voltages from 100 to 150 V. The origin of these small current anomalies was unknown (refer to Section 4.1).

4.3 Snapover Behavior in First Ramping Cycles

The I-V curves resulting from the initial ramping cycle performed on each sample exhibited anomalous current behavior that was not displayed in subsequent runs; hence these first runs were excluded from the sample statistics used to determine the importance of the other parameters explored in our investigation. Two different types of current jumps, a low-voltage snapover and a high-voltage gas discharge, were noted to occur frequently for most samples. At background argon pressures of 60-80 FTorr, irrespective of conductor or dielectric material type, initial ramping cycles exhibited an abnormal low-voltage snapover at 122±22 V with a 75%

occurrence rate and an initial gas discharge at an average voltage of 475±28 V with an 83% occurrence rate.

After this initial cycle, the surface of the sample was in some way altered and more consistent current jump behavior was observed in subsequent cycles. The abnormal behavior of samples on first runs was attributed to liberation of materials such as oil and water initially adsorbed to the sample surface or trapped in the conductor/insulator junction. At high voltages and low pressures, either surface heating or electron-induced desorption allowed surface neutrals to escape, only to be quickly ionized by the high density of electrons near the dielectric surface. Electrons freed during the ionization were immediately drawn to the positive conductor creating the anomalous hook-shaped current jump in the gas discharge I-V curve profiles. Representative plots of first and subsequent I-V profiles for a Al-Teflon™ sample are shown in Fig. 4.12.

4.4 The Effects of Multiple Runs on Snapover

The effects of multiple snapovers and gas discharges on a sample were studied using a set of 43 consecutive runs, on a 1.27-cm diameter Cu-Teflon™ sample. These ramping cycles ran from 100 V to 800 V (1000 V for the last eight runs) at 10 V/s with chamber background pressures of 210-230 FTorr. Two current jumps were observed consistently for all 43 runs the first occurring from 196±27 V–attributed to primary snapover–and the second at 437±78 V–attributed to gas discharge. A third, very large, current jump–attributed to Paschen discharge–occurred intermittently at 818±110 V.

The Paschen discharge seemed to also affect the surface of the sample, and consequently the behavior of subsequent lower-voltage current jumps. Fig. 4.13 shows the response of the onset voltage and collection current of the primary snapover and gas discharge jumps to the

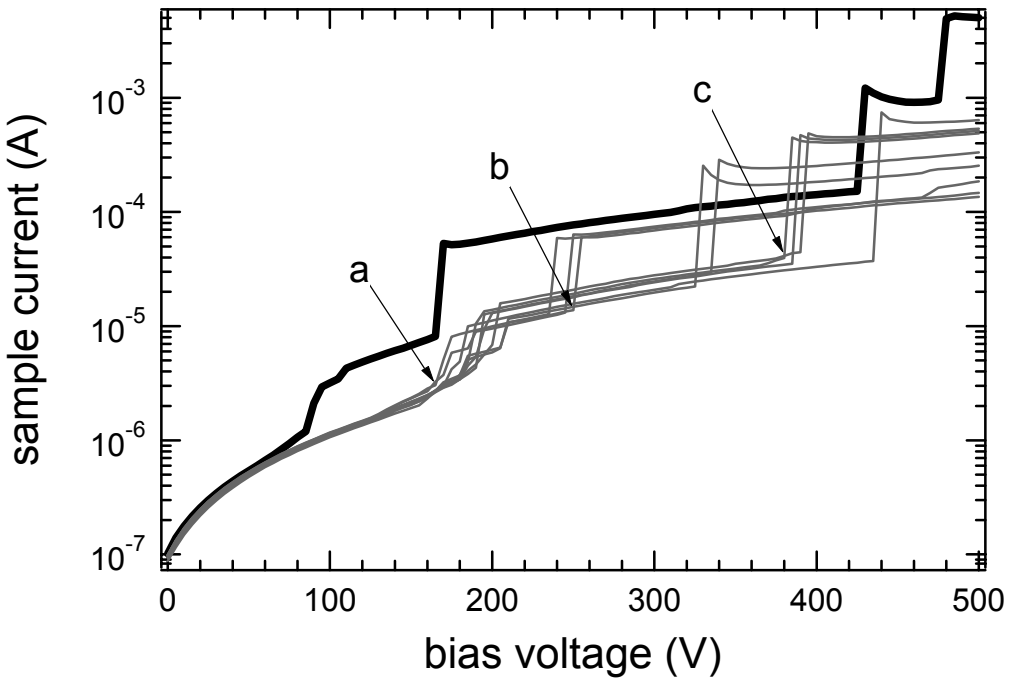

FIG. 4.12. Semi-log plot of nine consecutive ramping cycles for an Al-Teflon™ sample. Multiple ramping cycles on all samples revealed that first run I-V curves (dark curve) typically displayed current jumps and overall current collection behavior that was not reproducible during later runs (light curves). Current jumps labeled a), b), and c) are attributed to preliminary snapover, primary snapover, and gas discharge respectively.

Paschen discharge (bars) for consecutive ramping cycles. The primary snapover onset voltage and current jump magnitude were not significantly affected by the Paschen discharge for the first 34 runs after the initial cycle. However, the collection current and onset voltage of the gas discharge jump often increased substantially in subsequent cycles immediately following a Paschen discharge. For the last eight runs, the sample was ramped up to 1000 V to induce more frequent Paschen discharges. For these last seven runs the onset voltage and current collection of the gas discharges steadily drifted to higher values, as it did for the primary snapovers to a lesser extent.

This behavior suggests that the higher energy, more intense Paschen discharge jump modified the surface, perhaps through thermal- or electron-induced desorption, and that the gas

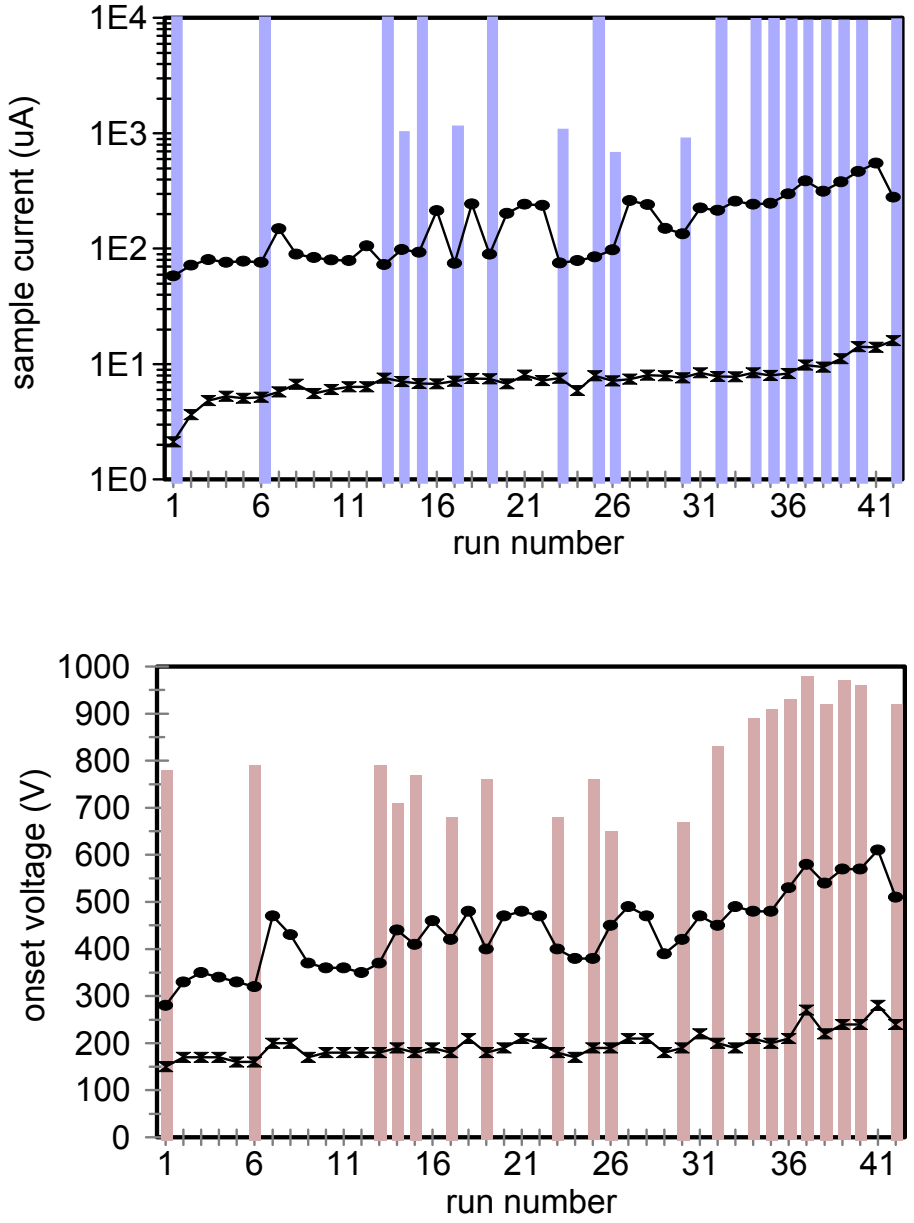

FIG. 4.13. Collection current and onset voltage response to multiple runs. Shown are the responses to high-voltage discharge (either gas discharge or Paschen discharge) of (top) sample current and (bottom) onset voltage for primary snapover (x) and gas discharge(•). Vertical bars indicate the current magnitudes and onset voltages, respectively, for the high-voltage Paschen discharge that occurred during a given run for a 1.27-cm diameter Cu-Teflon™ sample.

discharge jump was sensitive to the surface modifications while the snapover jump was less sensitive.

4.5 Hysteresis

As shown in Fig. 4.14, current jumps in the voltage range of 100 V to 700 V exhibited hysteresis. As a general rule, for a given ramping cycle the return I-V curve would retrace the forward I-V curve, falling rapidly with the major forward current jump, but then it would not respond as dramatically to any smaller lower voltage snapovers. Also, although the reverse I-V curve dropped at voltages corresponding to the forward I-V curve snapovers and gas discharges, it did so more smoothly without the discontinuous current jumps (but rather with steep declines).

In an attempt to identify a correlation between the snapover inception voltages and dielectric first crossover energies, the sample I-V curve behavior was examined for full ramping cycles–beginning at zero volts, ramping to the maximum voltage, and then returning to zero volts with the same ramping rate. Special attention was given to voltages at which sample current in the reverse bias direction dropped significantly (or voltages at which the sample "un-snapped over"). Also of interest were voltages at which the forward-bias and reverse-bias I-V curves converged. Voltage regimes in the I-V curves were identified where the step-down bias curve converged roughly to the same current as the forward-bias curve, and were quantified by:

$$I_{up} - I_{down} = \gamma \tag{4.2}$$

where γ was an arbitrary threshold of convergence for the forward and reverse current difference.

It was suggested by Mandell (2000) that the reverse-bias I-V curve may fall substantially

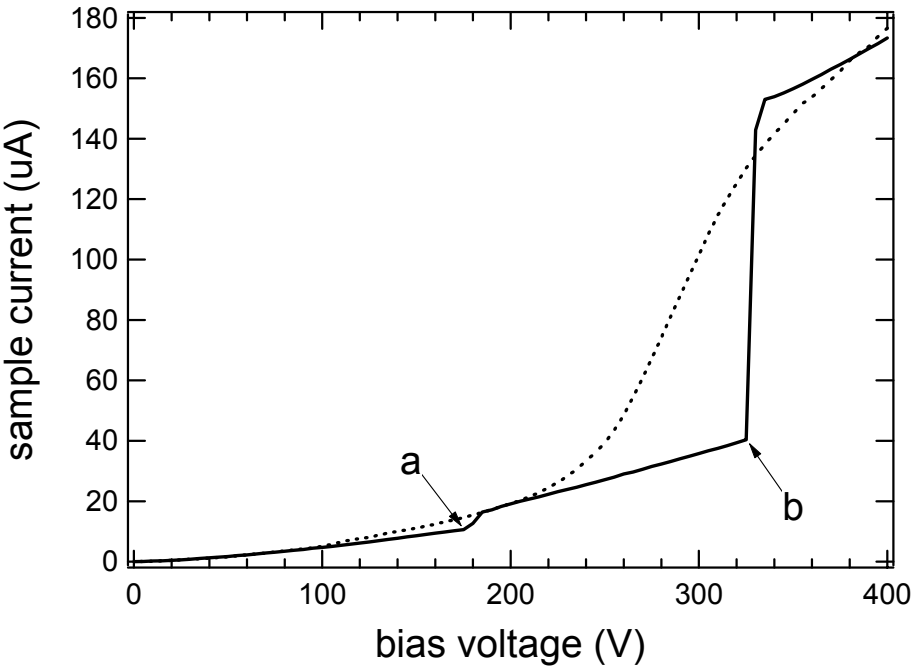

FIG. 4.14. Snapover I-V curve hysteresis. Shown is the I-V profile hysteresis behavior of a typical sample (1.27-cm diameter Cu-Teflon™) for a full cycle of increasing (solid curve) and decreasing (dotted curve) voltages. Current jumps labeled a) and b) were attributed to preliminary snapover and primary snapover, respectively.

at voltages more representative of the dielectric first crossover energy. He reasoned that this would occur if the onset of snapover in the forward-bias direction was delayed due to a potential energy barrier due, for example, to a surface charge migration activation energy barrier. If this were the case, this same potential barrier might not affect current collection transitions as energy was removed from the system in the reverse-bias direction. In effect, this in some ways is analogous to the latent heat in a first-order phase transition that can result, for example, in super cooling of a liquid but not "super heating" of a solid. The idea of a phase transition energy between two current collection modes was also proposed by Hastings and Chang (1989).

From 0 to 500 V, two major voltage regimes were identified where the forward and reverse currents converged. These voltage regimes were more or less consistent for all sample

types. As shown in Fig. 4.15 (a), the forward and reverse curves converged at 250 ±25 V to $|\gamma|$ <20 μA for all samples irrespective of material type. Also, all samples (irrespective of sample type) converged at 110 ±10 V to $|\gamma|$ <2 μA as shown more clearly in Fig. 4.15 (b).

It is interesting to note that for all samples, not only did the forward and reverse bias curves converge at voltages corresponding to the primary snapover voltages (250 ±25 V), but there also was a convergence at much lower voltages corresponding more closely to the insulator (or diffusion pump oil) first crossover energies at 110 ±10 V. This converging behavior may have corresponded to the numerous current anomalies observed at lower voltages as mentioned in Section 4.1. Although these current anomalies were insignificant in magnitude compared to higher voltage current jumps (preliminary snapover, primary snapover, and gas-discharge), the bias voltages at which they occurred corresponded more closely to the first crossover energies of the sample insulators. This may indicate that at voltages of ~110 V portions of the insulator immediately adjacent to the conductor were being bombarded by electrons sufficient in energy to allow the insulator to surpass its first crossover energy and produce electron yields in excess of one. However, at these voltages not enough energy was available for the system to initiate an insulator charge cascade and rapid sheath expansion perhaps due to an activation energy required for surface charge migration. This would explain why significant snapovers did not occur at these lower voltages. However, this local charging would likely cause minor fluctuations in the immediate plasma potentials which, in turn, could account for the divergence of the current difference readings shown in Fig. 4.15 (b) after the point of convergence at ~110 V.

It should be mentioned that the order in which the current convergence occurred for different sample types was not clear for either of the convergence regimes (as seen in Fig. 4.15) and was not sensitive to dielectric type as would be expected if the convergence were in fact a

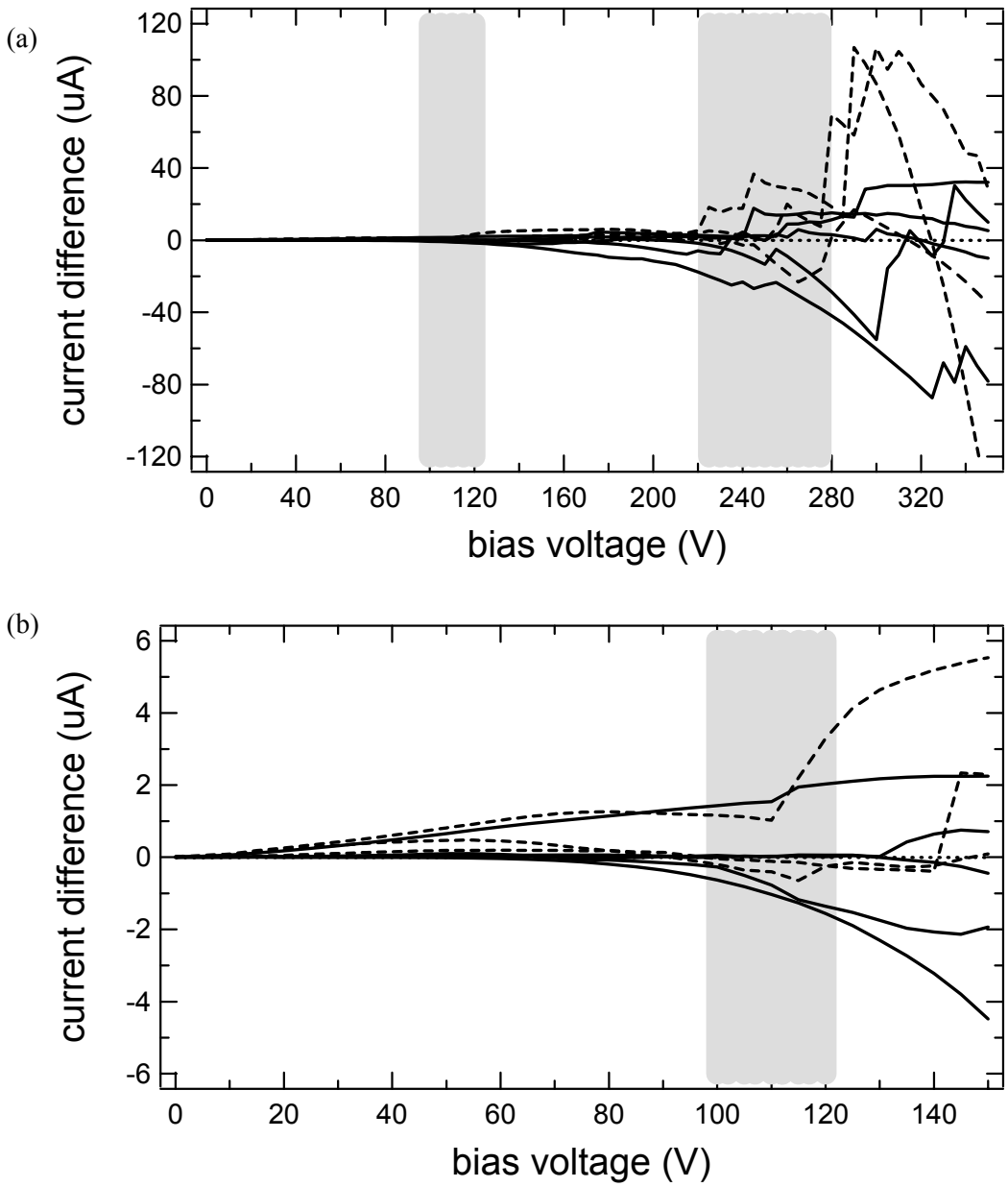

FIG. 4.15. Forward and reverse bias difference convergence. Current collection differences, between forward and reverse-bias curves showed a regime of convergence for all samples at (a) ~250 V and at ~ 110 V (shaded regions) and (b) a detailed view of the convergence at ~ 110 V. The 250 V voltage convergence corresponded to the primary snapover of the sample. Solid lines are Teflon insulator samples. Dashed lines are Kapton insulator samples. The dotted line is a SiO_2 insulator sample.

signature of the dielectric first crossover energies. However, as will be discussed further in Section 4.7, significant diffusion pump oil contamination may have veiled unique sample insulator influence on snapover inception.

Continuing the analysis of the snapover I-V curve hysteresis behavior, it was observed that the reverse bias I-V curves exhibited smoother behavior than the forward bias I-V curves. Exploiting this continuous curve behavior, first and second derivatives were taken of the averaged (averaged over nine ramping cycles) reverse bias curves for 1.27-cm diameter Cu-Teflon™, Cu-Kapton™, and Al-Teflon™ sample types. This was done in an attempt to look for I-V curve slope changes (changes in the effective conductivity of the system) and I-V curve inflections (rates of change in the effective conductivity) as a function of applied voltage. As expected, the first derivative curves showed steep rises in the slopes at voltages corresponding to primary snapovers (or more correctly, voltages corresponding to an "un-snapover" in the reverse bias direction). This can be seen in Fig. 4.16 by the dramatic change in slope values starting at ~250 V for numerous sample types.

Interesting behavior was observed in the second derivative plots both at voltages corresponding to primary snapover and at much lower voltages. As with the hysteresis convergence studies presented above (Fig. 4.15), there appeared to be some abnormal current behavior at voltages of ~100 V for Cu-Teflon™, Cu-Kapton™, and Al-Teflon™ samples. Specifically, the second derivatives of the averaged reverse I-V curves showed little variation about the zero value until about 75 to 100 V as shown in Fig. 4.17 for 1.27-cm conductor diameter Cu-Teflon™ samples. Then the fluctuations in the second derivative curves (and the corresponding uncertainties) grew substantially. Similar behavior was observed for Cu-Kapton™ and Al-Teflon™ samples. Although the physical interpretation of this behavior is not entirely

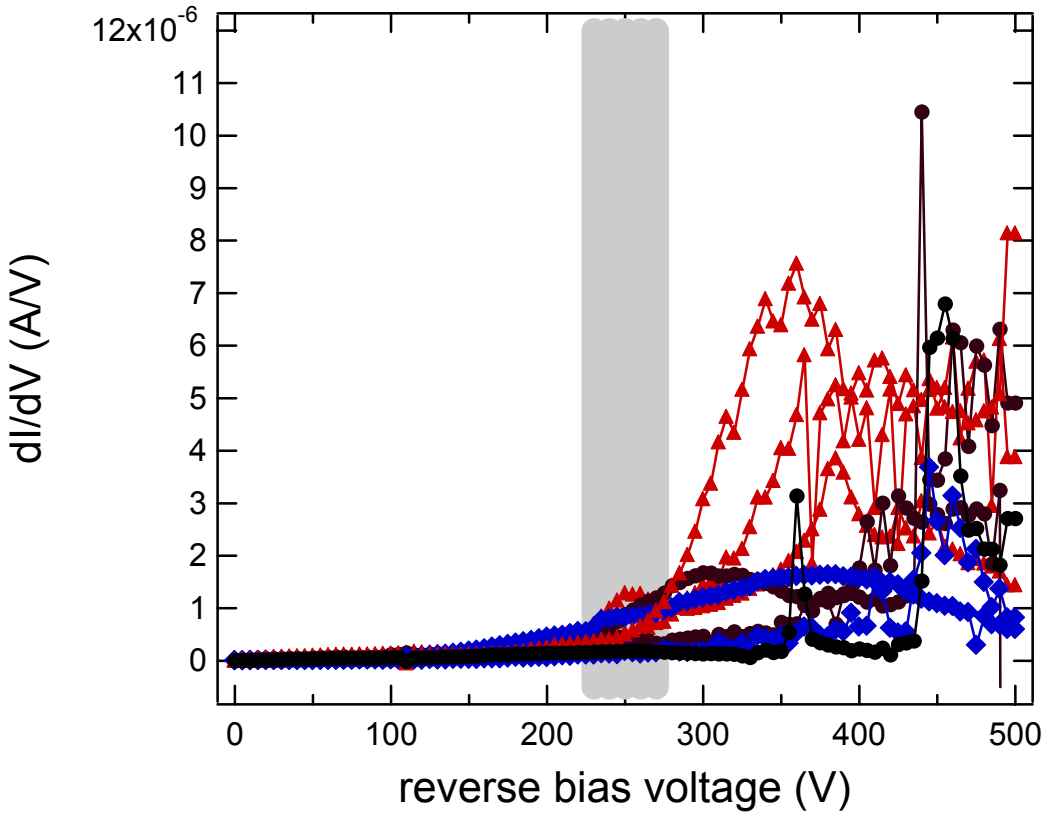

FIG. 4.16. Average first derivatives of reverse bias I-V curves. Shown are 1.27-cm diameter Cu-Teflon™ ( ), Cu-Kapton™ (•), and Al-Teflon™ (—), all of which showed a dramatic increase at voltages corresponding to primary snapover (~ 250 V).

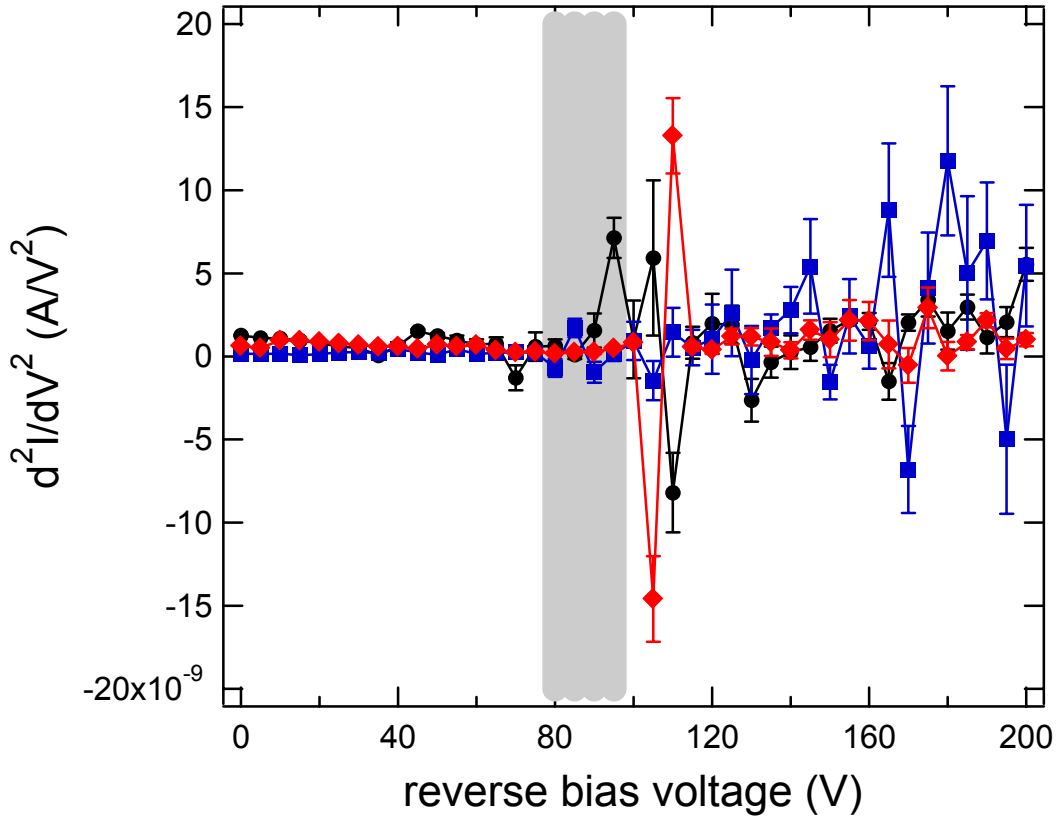

FIG. 4.17. Average second derivatives of reverse bias I-V curves. Shown are 1.27-cm diameter Cu-Teflon™ samples at different pressures, 66 FTorr ( ), 73 FTorr ( ), and 80 FTorr (—). At voltages of 75 to 100 V the second derivative curve (along with the uncertainties) began to fluctuate.

clear, it is again interesting that changes associated with the I-V curves of the samples occur at voltages closer to the associated insulator first crossover energies. As with the hysteresis behavior discussed before, a similar interpretation holds that the immediate insulator charges positively, but that not enough energy exists to initiate a charging cascade. However, changes in the local insulator potential may affect the surrounding plasma potentials, accounting for the fluctuations in the collected current and its second derivative curve as shown in Fig. 4.17.

4.6 The Effects of Ramping Rate–Voltage Step and Time Delay

The applied samples bias voltages used in the experiments were referenced to chamber ground. However, in studying snapover it is not the potential with respect to chamber ground that is relevant in comparing the snapover inception voltage with the insulator SE emission energies. Instead, it is the potential of the sample with respect to the far-field shielded plasma that is relevant. In order to obtain this potential, two correction terms to the measured applied bias were considered: a quasi-static bias between chamber ground and the far-field plasma in the vicinity of the sample array; and the potential lag due to the response time for the plasma sheath to adjust to changing sample potentials (both conductor and insulator potentials). The value of the plasma potential (near the sample array) with respect to chamber ground was determined using a Langmuir probe at the beginning of each series of cycles. Its value varied from -3 V to +25 V depending on the experiment. Also, the response time for the plasma sheath adjacent to a conductor has been shown in computer models to be very short < 100 ms (Thiemann and Schunk, 1990a). This alone should have caused no significant voltage offset on time scales related to our ramping rate.

Although the plasma response time to changing conductor biases has been shown to be very short, surrounding insulator charging effects (facilitated for example by a finite insulator

surface resistivity leading to leakage currents between the insulator and the conductor) may have prolonged the total time for the sample/plasma system to reach current equilibrium. This time lag associated with the sample/plasma equilibrium in response to the sample bias ramping rate (usually 10 V/s) may have resulted in an accumulative voltage difference between the effective sample/plasma potential in comparison with the sample/chamber ground potential. This would occur if the sample/plasma current equilibrium time for a given applied voltage step was significantly greater than the ramping rate time interval. Under these conditions, although the conductor bias would increase at the same rate as the applied voltage, the surrounding insulator charge gradient (and resulting plasma sheath responses) would not completely evolve before the next bias step was applied. As a result, the snapover inception voltage (measured with respect to chamber ground) could have been delayed, and this may have contributed to the observation that the snapover inception voltages exceeded the associated insulator first crossover energies by over 200 V.

One can imagine that the sample/plasma current equilibrium time would depend on the applied voltage step. To illustrate this, before snapover experiments were performed, samples were switched instantaneously from 0 to 500 V, 0 to 600 V, and 0 to 700 V. As can be seen in Fig. 4.18, upon switching to these high voltages, it took between 10 to 60 s for the sample to attain equilibrium (depending on the applied voltage step size). Unfortunately, the equilibrium times of smaller voltage steps more representative of those used throughout the snapover experiments (usually 5 V) were not measured, and in hindsight may have differed substantially from equilibrium times of these high voltage steps. For example, gas discharges and snapovers may have somehow manifested their effects in current equilibrium times for the large applied voltage steps of 500 V, 600 V, and 700 V, whereas small voltage steps of ~5 V may not have been

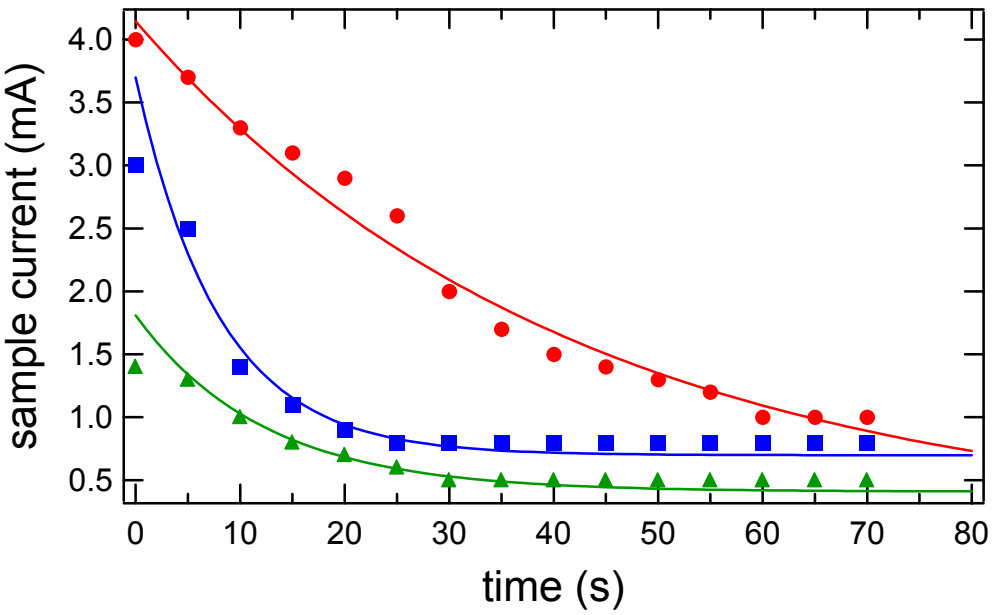

FIG. 4.18. Current equilibrium curves for high applied-voltage steps. Shown are temporal current measurements upon switching the sample bias on to 700 ( ), 600 V( ), and 500 V(•). For these large sample bias voltages, the current equilibrium times ranged from 10 to 60 s.

affected by such mechanisms (especially at accumulated biases less than the snapover or gas-discharge inception voltages).

From these high-voltage steps, an upper bound of 10 to 15 s was estimated for the response time of sample/plasma equilibrium at low-voltage steps, and analysis of Vayner *et al.* (1999) suggested that the effective plasma sheath to sample potential may have lagged behind the applied bias by . 50 V. The exact value of this effective voltage lag should depend sensitively on ramping rate. Consequently, the primary snapover onset voltage response to ramping rate (voltage step and time delay) was measured for multiple runs on a 1.27-cm diameter Cu-Teflon ™ sample at a pressures of 66 FTorr. Data shown in Fig. 4.19 indicates that there was no statistically significant dependance on ramping rate of the primary snapover current jump, onset voltage, current jump magnitude, or current ratio. In addition, Fig. 4.20 shows an increase of <15

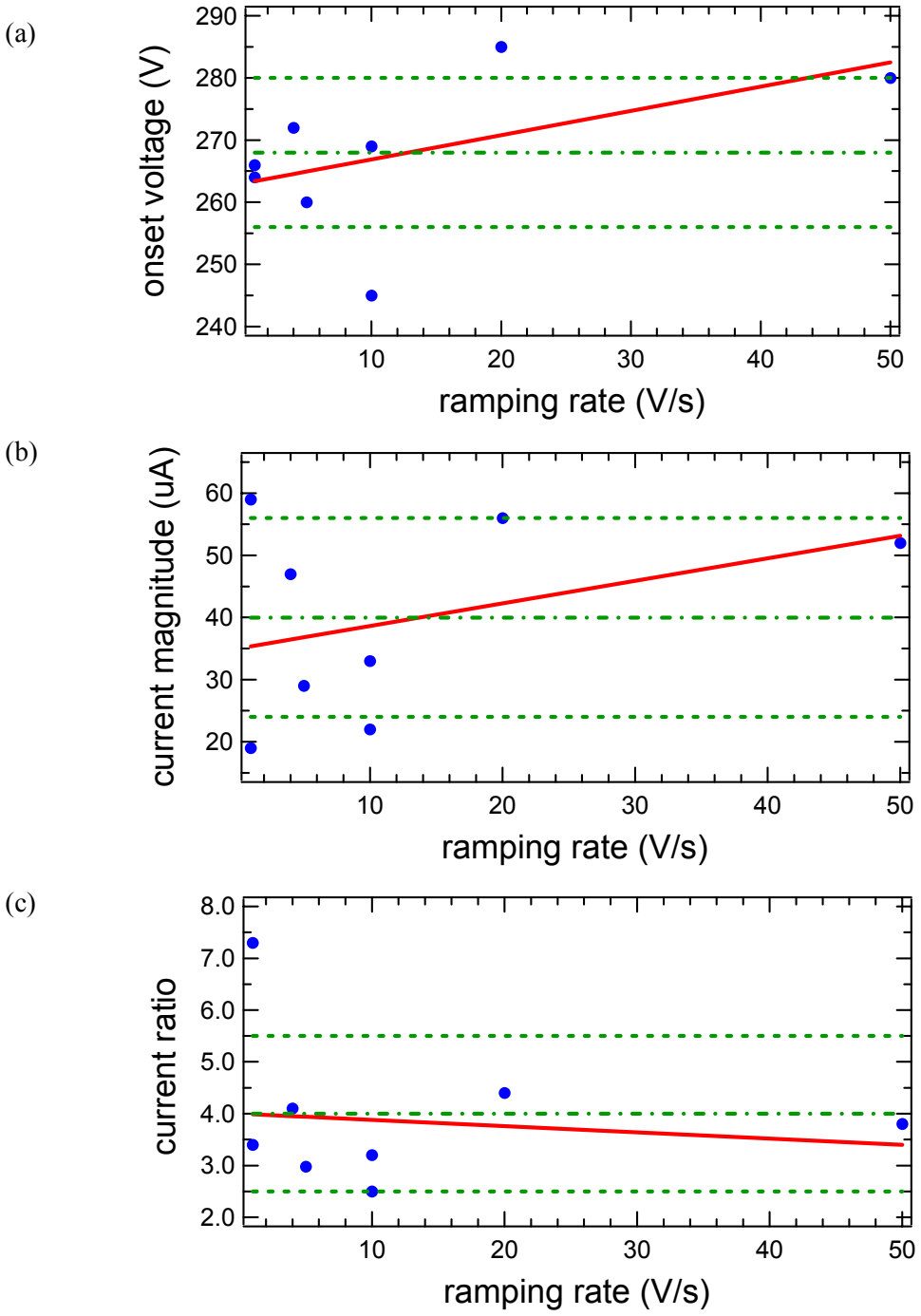

FIG. 4.19. Dependence of snapover (a) onset voltage, (b) magnitude of current jump, and (c) current jump ratio on ramping rate for a typical sample (1.27-cm diameter Cu-Teflon™). Symbols show data, while dash-dotted and dashed lines indicate the average value and limits of uncertainty to within ±σ (standard deviation), respectively. Solid lines are linear fits to the data. In all cases, there is no statistically significant dependance on ramping rate, that is, the slopes are zero to within the uncertainty of the slopes.

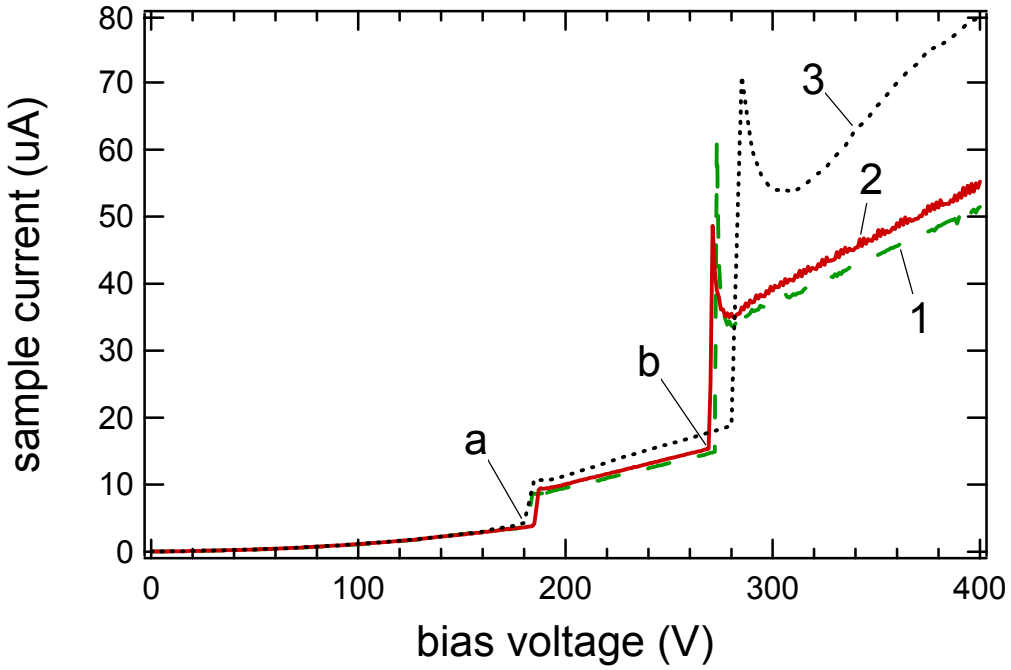

FIG. 4.20. Sequential snapover I-V plots showing the effect of ramping rate. This shows the effect of ramping rate for (1) 4 V/s, (2) 10 V/s and (3) 50 V/s. Current jumps at a) and b) are attributed to preliminary snapover and primary snapover, respectively. Measurements were made on a 1.27-cm diameter Cu-Teflon™ at a pressure of 70 FTorr.

V in the primary snapover onset voltage in three sequential cycles when the ramping rate was increased from 1 V/s to 50 V/s. Thus, the offset potential due to relaxation rate for the small voltage steps used may have been substantially less than the value suggested by Vayner *et al.* (1999). Further evidence of this conjecture came from stepping the sample bias by increments of 10 V, 25 V, and 100 V while manually recording collection current stabilization times. Of these, only voltage steps of 100 V produced relaxation times / 0.5 s.

Taken together, modeling indicates the measured bias with respect to chamber ground may be between ~15 V and 50 V higher than the actual sample/plasma effective potential, but direct measurements suggest a smaller voltage offset of . 15 V for 10 V/s ramping rates.

4.7 Dependence on Surface Contamination

Surface contamination presented a serious limitation to our experiments. After approximately 10 cycles, samples would develop a visible yellow ring around the conductor, identified as diffusion pump oil originating from the vacuum system of the plasma chamber. Later, it was reported that during the experiments, a faulty pump valve may have caused excess diffusion pump oil contamination of the samples (Galofaro *et al.*, 2000). We estimated the deposition rate of diffusion pump oil as ~30 nm/cycle by noticing that after roughly 10 cycles the diffusion pump oil layer became visible, and that a visible layer corresponded to roughly half the wavelength of visible light (Hansen, 1999). By contrast, the maximum escape depth of SE for diffusion pump oil is 20-30 nm, for incident energies less than 1000 V, as determined by Goto and Ishikawa (1968) from measurements of SE yields of diffusion pump oil on a conductor substrate. In their study, after roughly 20-30 nm of diffusion pump oil deposition, the substrate SE contributions became negligible, and subsequent SE yields for greater film thicknesses were all the same (namely, diffusion pump oil SE yields). The SE emission properties of diffusion

pump oil are listed in Table 2.1. Since SE emission of low-energy electrons is very surface sensitive, even monolayers of contamination can significantly affect emissions (Davies and Dennison, 1997; Chang *et al.,* 2000; Dennison *et al.*, 2001). At Utah State University, we are pursuing work along these lines to look at changes in the SE, BSE, and total yields curves for monolayers of diffusion pump oil contamination.

The effects of chamber contamination on our data were undeniable. This impeached the verisimilitude of our studies of the dependence of snapover on sample materials, since all samples were covered (to some extent) with diffusion pump oil. Additionally, diffusion pump oil may have influenced sample out-gassing and ionization processes involved in higher-voltage current jumps.

4.8 Dependence on Plasma Parameters

At the beginning of each experiment the background gas (argon) pressure was set, and plasma electron densities and energies were measured with a Langmuir probe. Then, for each measurement sequence, the background pressure was checked to verify that the plasma conditions had not changed substantially. In carefully watching the background pressure on a regular basis, it was found that from one run to the next the measured pressure would only vary by no more than ±3%. Although the plasma electron densities were not measured between each sample sequence, in comparing measured density values for the same pressure on different dates, it was found that the number densities could vary by a factor of two for any given pressure.

The overall average current to the samples was found to clearly depend on plasma pressure at low voltages before the onset of snapover. Shown in Fig. 4.21 are the averaged current versus voltage graphs for 1.27-cm conductor diameter Cu-Teflon™, Al-Teflon™, and

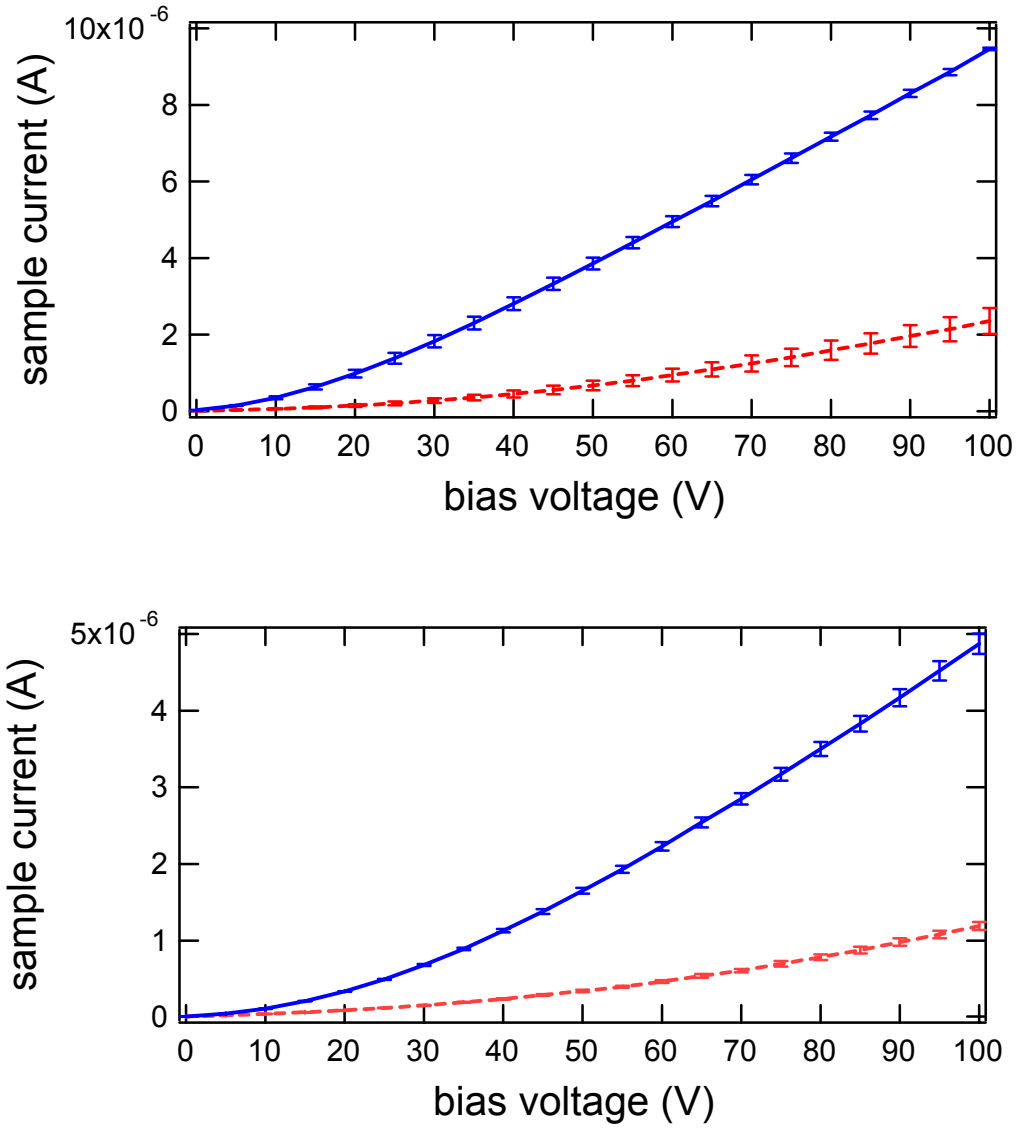

FIG. 4.21. Current collection dependence on pressure before snapover. Shown are the I-V curves (with standard deviations as error bars) for Cu-Kapton™ (top) and Cu-Teflon™ (bottom) at 66 FTorr (dashed) and 80 FTorr (solid) from 0-100 V bias voltage. The collected current for all samples showed a clear dependence on background pressure before snapover occurred.

Cu-Kapton™ samples at 66 and 80 FTorr plotted up to 150 V. The overall current for the 80-FTorr measurements exceeded the current for the 66-FTorr measurements over this voltage range. However, after snapover, it was observed that the current at low plasma pressures could match or exceed the current of higher pressures as shown in Fig. 4.22. This indicates that before snapover the current collection mechanism was very sensitive to plasma pressures or electron number densities. After snapover, the collected current was not as strongly governed by surrounding plasma charge densities, but instead was dominated by sample material effects.

For Cu-Teflon™, Al-Teflon™, and Cu-Kapton™, changes in the background gas pressure (from 66 to 80 FTorr) or equivalently plasma density (from 1 to $4 \cdot 10^{11}$ m^{-3}) did not have any clear effect on the average pre-snapover (~ 200 V) and primary snapover (~ 275 V) onset voltages or current jump magnitudes. Additionally, the average onset voltages (~ 450 V) of the gas-discharge did not seem to be affected by changes in pressure. However, the gas-discharge average current jump magnitudes showed clear increases with increasing plasma pressure (from 66 to 80 FTorr) for all the Cu-Teflon™ (58% increase), Al-Teflon™ (34% increase), and Cu-Kapton™ (63% increase) samples. Increases in pressure did not have a noticeable effect on the frequency of occurrence of pre-snapover, primary snapover, or gas-discharge current jumps for Cu-Teflon™, Al-Teflon™, and Cu-Kapton™ samples. However, it was found that at high pressures of roughly 1.5 to $3.0 \cdot 10^{-4}$ Torr Paschen discharges could be regularly excited at high voltages (> 600 V) whereas at low pressures they could not.

As reported by Vayner *et al.* (2000), gas species (either argon or xenon as the background gas) had no discernable effects on snapover or gas-discharge onset voltage and current jump magnitudes. Finally, no systematic study of the effect of plasma temperature was performed.

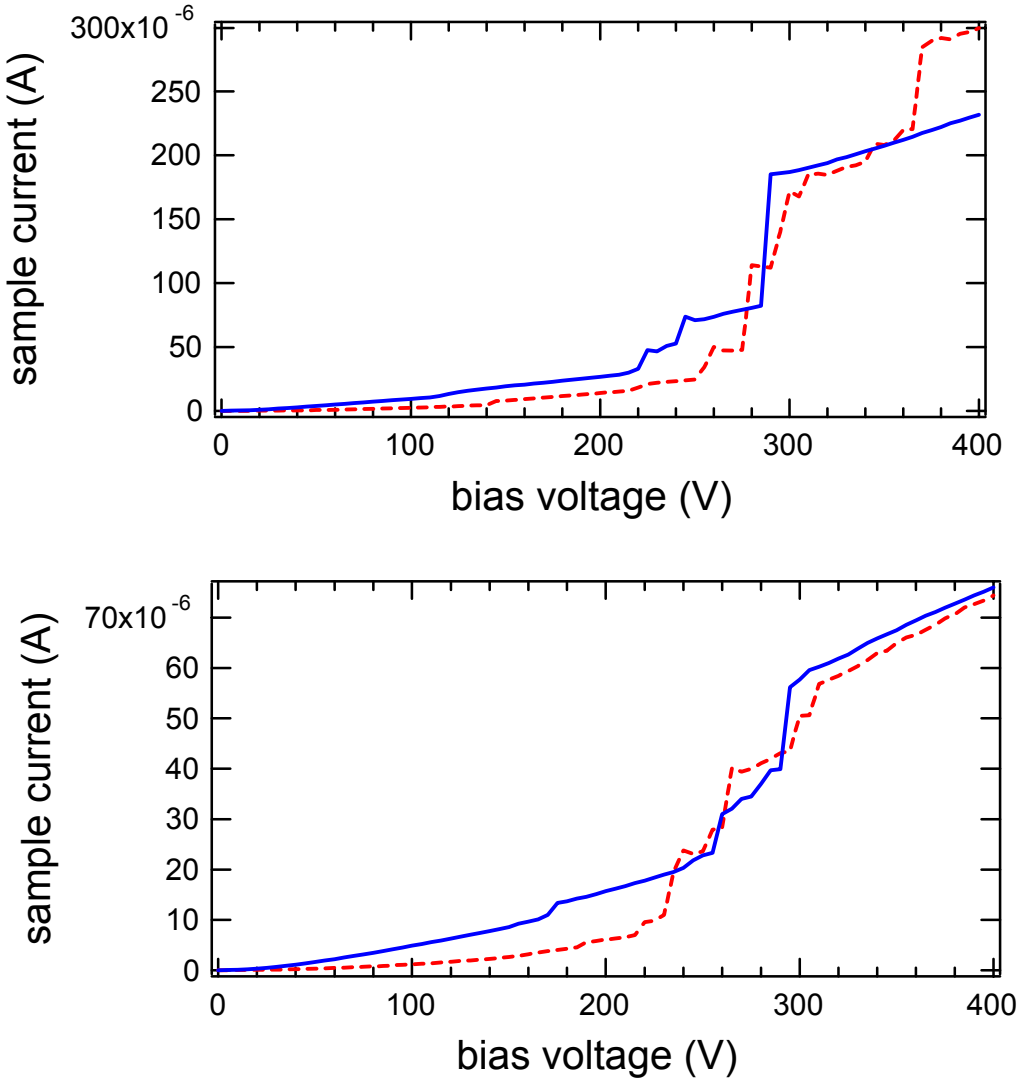

FIG. 4.22. Current collection dependence on pressure after snapover. Shown are the average I-V curves for (top) Cu-Kapton™ and (bottom) Cu-Teflon™ at 66 FTorr (dashes) and 80 FTorr (solid) from 0-400 V. After snapover occurred, the background gas pressure did not have as strong of an effect on collected current.

4.9 General Current Collection Dependence on Sample Materials

In Section 4.2, it was explained that the I-V profiles of the samples exhibited some material dependence at low voltages before the onset of snapovers irrespective of pressure. Shown in Figs. 4.23 and Fig. 4.24 (a) are averaged I-V profiles (for nine consecutive runs) for 1.27 cm diameter conductor samples of Cu-Kapton™, Cu-Teflon™, Al-Teflon™, and Cu-SiO_2, at 66 μTorr, 80 μTorr, and 71-73 μTorr, respectively. Clearly, at low voltages (before snapover) and at all measured pressures, the Cu-Kapton™ sample collected more current than either of the Teflon™ samples or the SiO_2 sample holding all other parameters fixed. Additionally, from Fig. 4.23 it can be seen that the Cu-Teflon™ sample collected more current than the Al-Teflon™ sample at both 66 FTorr and 80 FTorr.

These material effects on sample I-V curve behavior became apparent after only a few volts of applied bias (as opposed to voltages corresponding to the insulator or conductor first crossover energies). It was suggested by Ferguson (2001a) that this behavior may be explained by differences in insulator surface conductivities that arise from adsorption of conducting materials. For example, Kapton™ is especially prone to H_2O adsorption that can possibly increase the surface conductivity and lead to leakage currents across the surface to the conductor (since the insulators tend to maintain a slightly negative charge before snapover). Additionally, a finite insulator surface conductivity would allow the near insulator to approach the applied conductor bias, causing the sheath around the conductor to grow slightly. This could expose more of the sample to the plasma, and hence act to enhance the collected current even before any snapover current jump had occurred. It is likely that a similar argument of surface adsorption can be used to explain why the Cu-Teflon™ samples collected more current than the Al-Teflon™ samples. For example, while aluminum forms an insulating oxide layer, copper forms a

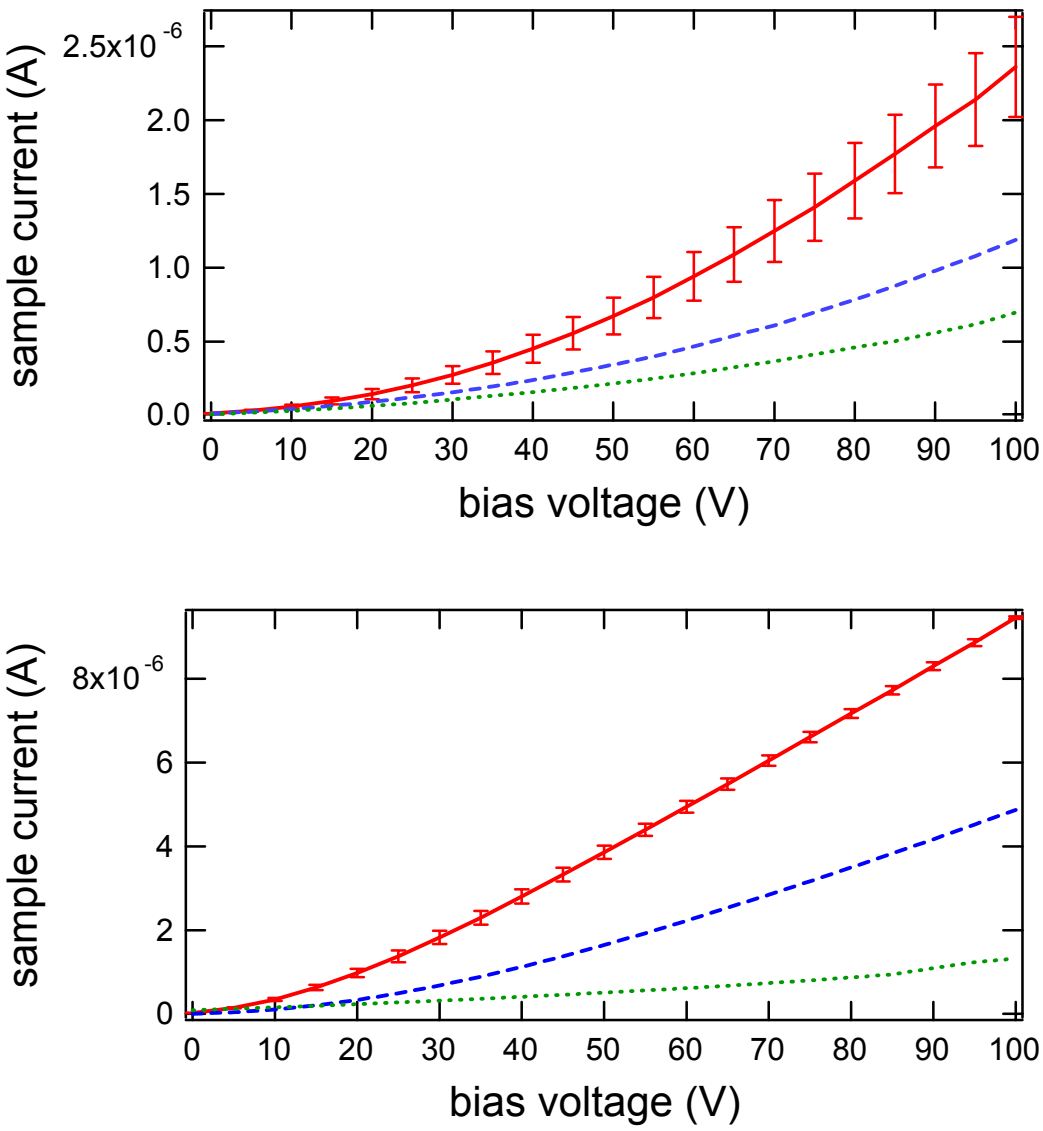

FIG. 4.23. Material dependence of current collection before snapover at (top) 66 FTorr and (bottom) 80 FTorr. Shown are averaged I-V profiles for 1.27-cm diameter samples: Cu-Kapton™(solid line), Cu-Teflon™(short dashes), and Al-Teflon™(dots). Even before snapover occurred, the current collected to samples showed material dependence for any given pressure with Cu-Kapton™ samples exhibiting higher overall current than Cu-Teflon™, and Al-Teflon™. Standard deviations are shown as error bars on the Cu-Kapton™ but are omitted for other samples for visual clarity. Errors for the other samples were comparable to the Cu-Kapton™ errors at low voltages.

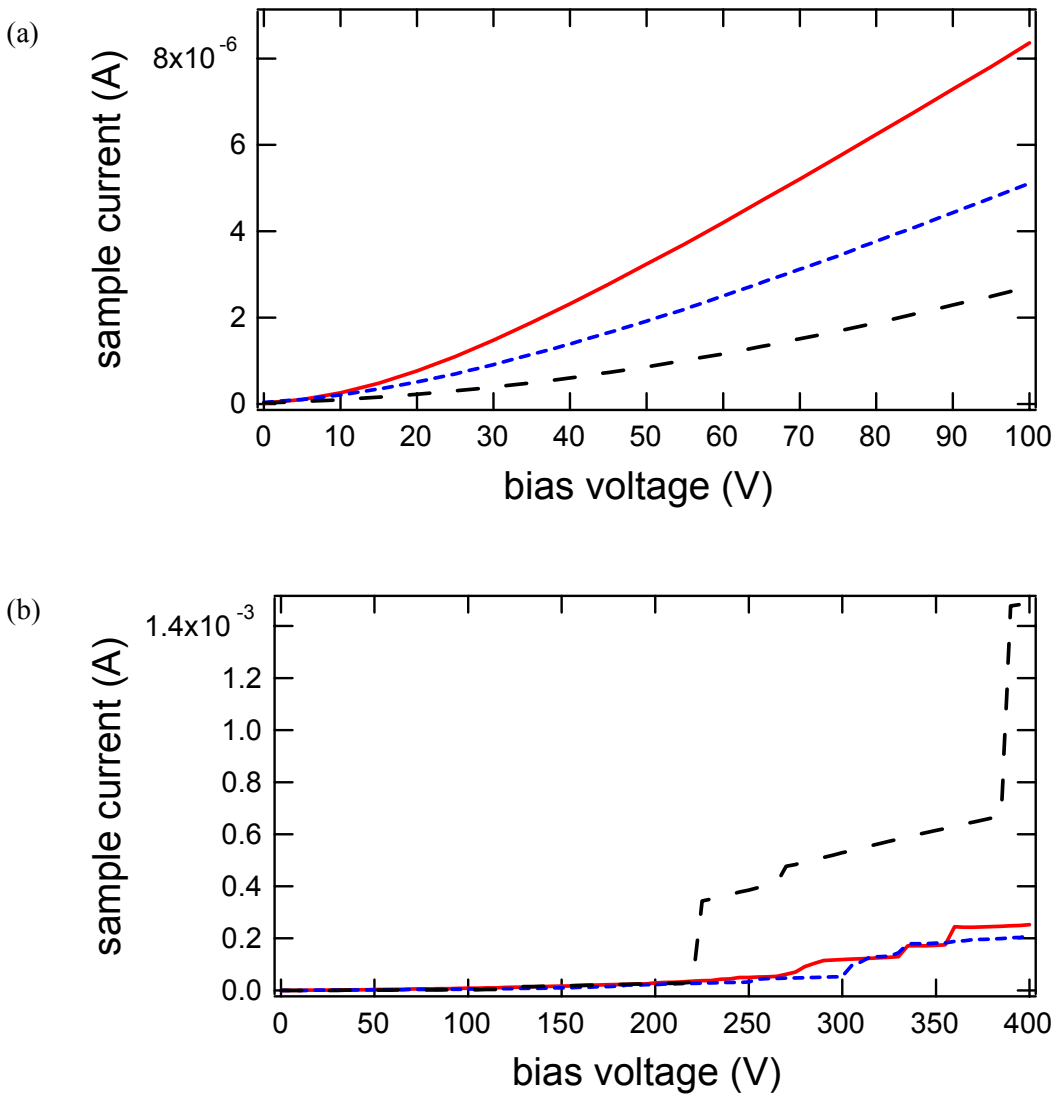

FIG. 4.24. Material dependence of current collection at 71-73 FTorr. Shown are average I-V profiles at 71-73 FTorr for 1.27-cm diameter samples: Cu-Kapton™(solid line), Cu-Teflon™ (short dashes), and Cu-SiO_2 (long dashes). (a) Before snapover Cu-Kapton™ insulator samples collected more current than Cu-Teflon™ and Cu-SiO_2 samples. (b) However, after primary snapover the Cu-SiO_2 sample collected significantly more current than the Kapton™ or Teflon™ samples.

conducting oxide layer that may facilitate electron current collection at the conductor/insulator interface. Alternatively, the different insulators and conductor materials may have a varied propensity for condensation of diffusion pump oil or water, and thus a variability in surface conductivities.

As shown in Fig. 4.24 (b) and 4.25, the Cu-Kapton™ sample continued to collect two to five times more overall current than Cu-Teflon™ and Al-Teflon™ samples at high voltages (after snapover and gas discharge) at all pressures. However, although the current to the Cu-Kapton™ sample initially exceeded the Cu-SiO_2 sample current as shown in Fig. 4.24 (a), after ~225 V (corresponding roughly to primary snapover) the current collected by the Cu-SiO_2 sample exceeded both the Cu-Kapton™ and Cu-Teflon™ sample currents by more than a factor five as shown in Fig. 4.24 (b). This may have resulted from the higher maximum electron yields of SiO_2 (see Table 2.1), or from the relatively smooth surface of SiO_2 as compared to the Teflon™ and Kapton™ surfaces.

4.10 Dependence on Sample Dielectric Type

To determine the importance of sample dielectric and conductor (also see Sections 4.11 below) materials on snapover, multiple biasing cycles were performed at a constant ramping rate of 10 V/s under similar plasma conditions of 66-80 μTorr argon pressure, electron number densities of n_e=1-3·10^5 cm^{-3}, and electron energies of E_e=1-3 eV.

The measured primary snapover onset voltages for samples with 1.27-cm diameter copper conductors and different dielectrics (see samples 1, 2, 5, 6, and 18 in Table 4.1) are, in increasing order, Kapton™ (247±23 eV), SiO_2 (259±11 eV), and Teflon™ (275±34 eV). The measured gas discharge onset voltages (see Table 4.2) are, in increasing order, Kapton™ (433±50 eV), Teflon™

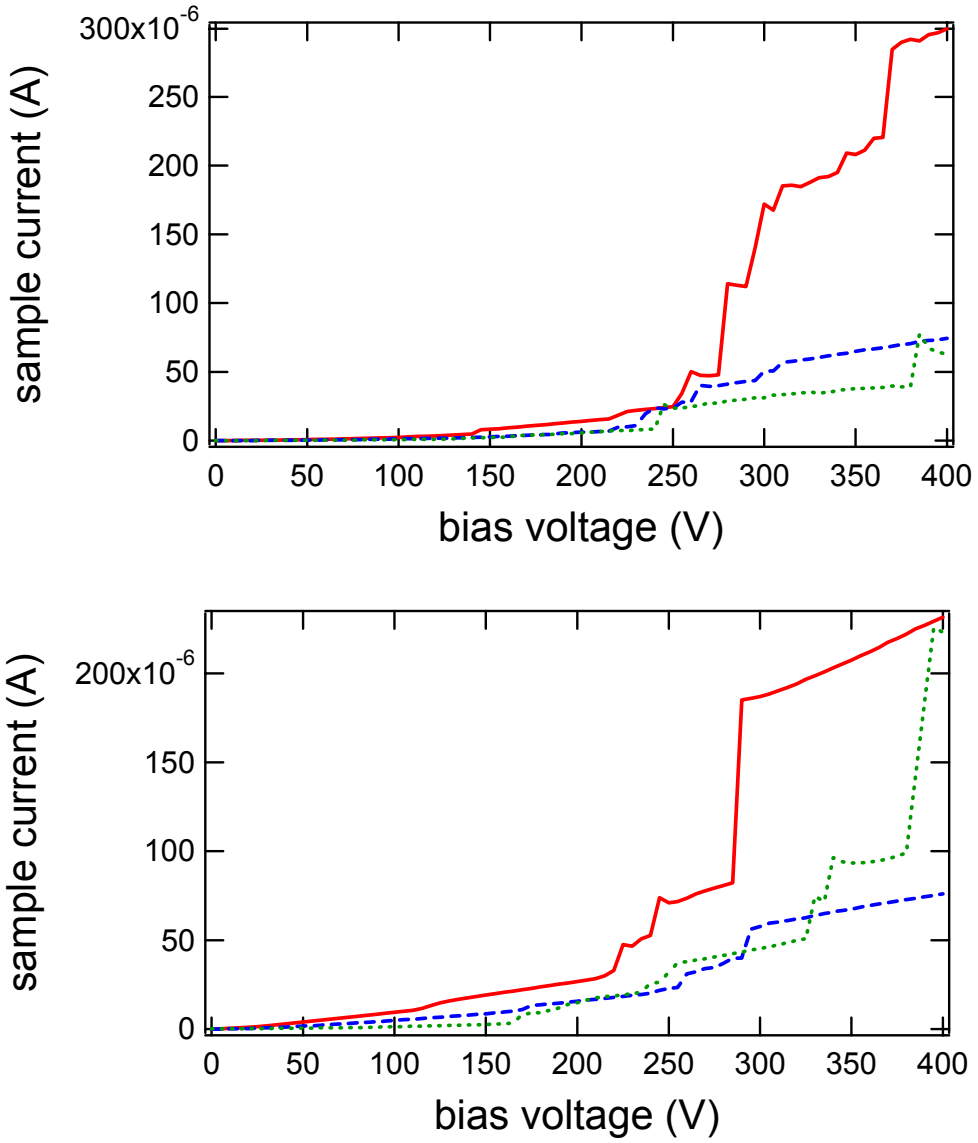

FIG. 4.25. Material dependence of current collection after snapover at (top) 66 FTorr and (bottom) 80 FTorr. Shown are average I-V profiles for 1.27-cm diameter samples: Cu-Kapton™(solid line), Cu-Teflon™ (short dashes), and Al-Teflon™(dots). Before and after primary snapover Cu-Kapton™ insulator samples collected more current than Cu-Teflon™ and Al-Teflon™ samples regardless of background pressure. However, at ~375 V (bottom graph) a gas discharge event raised the average current of the Al-Teflon™ to a value nearly equal to the Cu-Kapton™.

(460±33 eV), and SiO_2 (510±60 eV). In contrast, literature values for the first crossover energies (see Table 2.1), in increasing order, are SiO_2 (40-45 eV) (Mueller, 1945; Krainsky *et al.*, 1981), Teflon™ (50 to 69 eV) (Willis and Skinner, 1973; Krainsky *et al.*, 1981), and Kapton™ (30 to 75 eV) (Willis and Skinner, 1973; Krainsky *et al.*, 1981).

These results suggest that measured primary snapover and gas discharge onset voltage were not directly dependant on the dielectric first crossover energy. Specifically:

i) Snapover inception voltage varied significantly from one run to the next (as compared to differences in insulator first crossover energies) for identical or same sample types in similar plasma conditions. Also, measured variations in the primary snapover or gas discharge onset voltages were not statistically different from one another, suggesting that either perturbations in the local plasma or evolving material surface conditions (contamination or damage) dominated snapover inception rather than insulator material effects.

ii) The order of increasing primary snapover or gas discharge onset voltage were not consistent with the order of increases in insulator first crossover energies. Again, this may have been due to random variations in inception voltages due to plasma variations and sample surface conditions. Additionally, extensive diffusion pump oil surface contamination could have made samples of different insulator type behave similarly. However, as explained in Section 2.3, the values of crossover energies for insulators reported in the literature also have large uncertainties, making it difficult to evaluate their effect on snapover inception (see Table 2.1).

iii) The primary snapover onset voltage values were / 180 V higher than the first crossover energies of any of the dielectrics or of diffusion pump oil (see Table 2.1). Even after corrections for the offset voltage due to finite sample/plasma equilibrium time (discussed

further in Section 4.6), the measured onset voltages were still more than 100 V above the first crossover energies.

Likewise (see Tables 4.1 and 4.2), variations due to different dielectric materials in the current jump magnitude (absolute change in current before to current after jump) and current jump ratio (fractional change of current before and after jump) for both primary snapover and gas discharge were comparable to their uncertainties and showed no significant dependence on dielectric type. However, as discussed in Section 4.9 the overall averaged current collection to a sample (before and after snapover) did depend on insulator type with Kapton™ insulator samples collecting up to five times the current of Teflon™ samples before snapover, and SiO_2 samples collecting more than five times the current of all other insulator samples at high voltages. Finally, as was the case for onset voltage dependence on first crossover energies, the extensive contamination of the samples by diffusion pump oil (discussed in Section 4.7) may have masked current jump magnitude dependence on dielectric SE emission properties.

4.11 Dependence on Sample Conductor Type

Comparison of results in Tables 4.1 and 4.2 for 1.27-cm conductor diameter Cu-Teflon™ samples (samples 2 and 6) with 1.27-cm conductor diameter Al-Teflon™ samples (samples 3 and 11) suggested statistically significant differences in snapover and gas discharge onset voltages and currents due to conductor type. Aluminum conductor samples exhibited lower onset voltages (primary snapover: 219±35 V; gas discharge: 386±46 V and 323±56 V for samples 3 and 11, respectively) than samples with copper conductors (primary snapover: 274±38 V and 278±27 V for samples 2 and 6, respectively; gas discharge: 461±38 V and 458±39 V for samples 2 and 6, respectively). Aluminum conductor samples also exhibited lower current jump magnitudes (primary snapover: 18±19 FA; gas discharge: 0.4±0.2 mA and 0.27±0.05 mA for samples 3 and

11, respectively) than samples with copper conductors (primary snapover: 89±66 FA and 12±8 FA for samples 2 and 6, respectively; gas discharge: 0.7±0.5 mA and 1.1±0.2 mA for samples 2 and 6, respectively). Results for the current jump ratio were inconclusive. Additionally, as discussed in Section 4.9, copper conductor samples exhibited higher overall collected current than aluminum conductor samples at low voltages before snapover, but relatively the same overall current at high voltages after snapover and gas discharge. One might interpret this as evidence that the conductor type dependence is restricted to before snapover, and in some way may influence the snapover transition (since current jump magnitudes and inception voltages were influenced by conductor type), but after snapover has occurred and the insulator charges positively, conductor effects become insignificant.

Dependence of snapover and gas discharge onset voltages and current collection on conductor type was not expected based on the discussions of snapover in Sections 1.2 and 2.3. These trends may reflect differences in surface oxide conductivity and contaminant desorption properties for the metals. As a possible example, aluminum has an insulating oxide film of Al_2O_3 that may have led to surface charging and accumulation of charged or polarizable contaminants, while the oxide of copper formed in a vacuum is conducting (Moore *et al.,* 1989). Differences in the surface roughness of the aluminum versus copper conductors could also have affected SE emission and snapover directly (see Section 4.14 below) or affected the adsorption/desorption of contaminants.

4.12 Dependence on Sample Conductor Size

The effects of conductor size on snapover and gas discharge current collection were tested using four Cu-Teflon™ sample sizes (comprised of five samples, numbers 4, 8, 2, 6, and 16) with different conductor diameters (0.32 cm, 0.64 cm, 1.27 cm, and 5.1 cm), respectively. The effects

of conductor size on current collection at low voltages before snapover were discussed briefly in Section 4.2, and it was found that the overall current density increased as a function of conductor diameter (see Fig. 4.9), especially at low voltages before snapover. The nature of collected current dependence on conductor size before snapover was determined to follow a clear power law relationship, $I \propto d^n$ with $n=+3.3\pm0.5$ as shown in Fig. 4.26 (the current was taken at 50 V for 10 runs and then averaged). This power law relationship does not follow Eq. (2.10), where before snapover one would expect the current to be roughly proportional to the conductor area (or the diameter squared). However, if it can be assumed that the plasma sheath diameter scales linearly with the conductor diameter, then this measured power law relationship implies that the collected current varies more or less with the volume of the sheath.

In addition to measuring the conductor size dependence before snapover, the measured current immediately following primary snapover and gas discharge current jumps was averaged for 10 runs. These results are also presented in Fig. 4.26, and again a power law dependence of $I \propto d^n$ was observed with $n=+1.7\pm0.4$ (after primary snapover) and $n=+0.6\pm0.4$ (after gas discharge). In comparison, Stillwell *et al.* (1985) reported that current collection following lower voltage surface-enhanced current jumps (interpreted as being the same as primary snapovers in our experiments) was strongly dependent on hole size and was less than proportional to conductor area (in agreement with our results). Additionally, they reported that after higher voltage vapor-enhanced current jumps (interpreted as being the same as gas discharge in our experiments) the size of the conductor did not affect the amount of current collected. Our analysis suggested a weak dependence of current on conductor size following gas discharge; note, however, that the

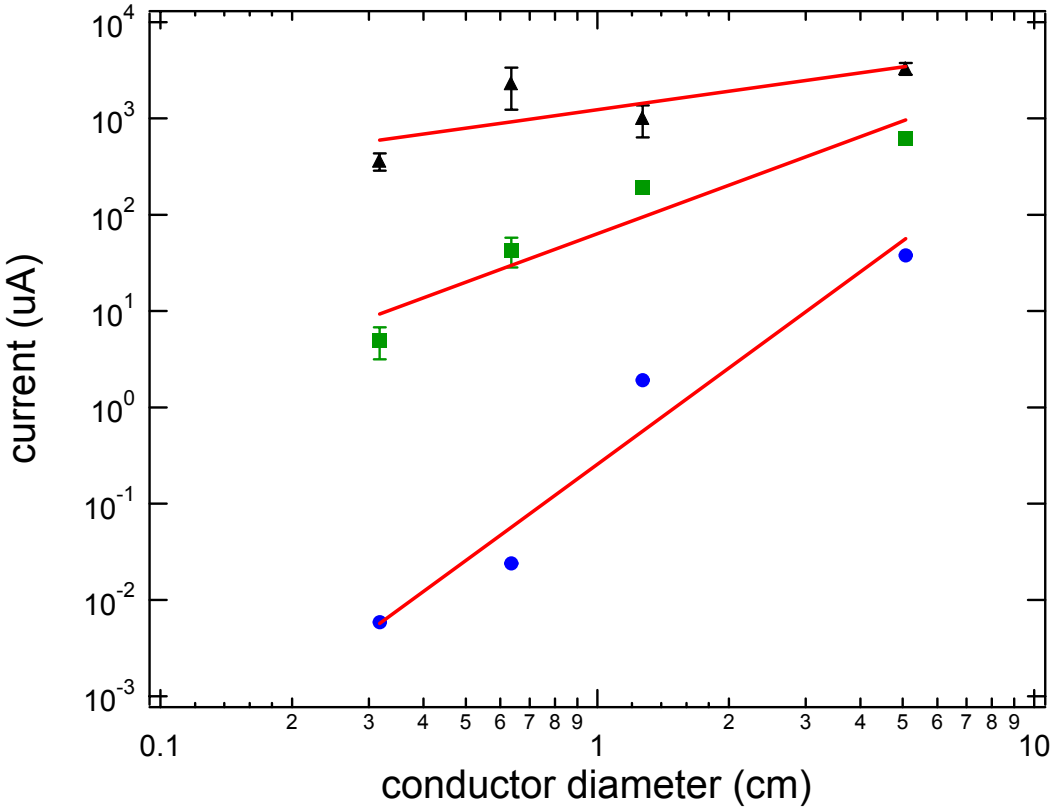

FIG. 4.26. Effect of conductor size on measured current. The currents shown are before snapover ( ) (at 50 V), immediately after snapover ( ), and immediately after gas discharge (•) for Cu-Teflon™ samples of different diameters. Solid lines are power law fits to data demonstrating statistically significant dependance of current in each current collection mode. Error bars are ± standard deviations of the mean of the averaged data for ten runs.

power coefficient displays greater uncertainty (66%) than the coefficients before or after primary snapover.

From these observations it might be argued that before primary snapover, the plasma sheath is roughly spherical with a diameter that varies approximately linearly with the conductor diameter so that the number of electrons within the plasma sheath scales roughly as the conductor diameter cubed (assuming a constant electron density). It then follows that the current below primary snapover is proportional to the total number of available electrons within the plasma sheath. Furthermore, it might also be argued that the current collection above the primary snapover is nearly proportional ($n=+1.7\pm0.4$) to the conductor/insulator current collection area (perhaps slightly less than proportional if the radial dimension of the insulator charge gradient does not scale quite linearly with conductor diameter). Finally, perhaps the current above the gas discharge current jump is proportional to the ionized particle transport distance that scales just less than linearly ($n=+0.6\pm0.4$) with the conductor diameter. An alternative explanation for the nearly linear relationship between the current and conductor diameter above gas discharge may be that the current scales just less than proportional to the conductor/insulator interface length (or the circumference of the conductor).

It is interesting that although the magnitude of the collected current increases after each current mode transition (as displayed in the I-V curves), the current dependence on conductor size diminishes after each transition as shown in Fig. 4.26. This indicates that once a sample has snapped over, the plasma sheath expansion and area of insulator charging becomes less dependent on conductor size while more strongly dependent on applied voltage as seen from the increase in I-V curve slopes (Figs. 4.1 and 4.2). Thus, the slope of the I-V curves (that is, the effective conductivity) increases with each current jump, but shows no dependence on conductor size (within statistical uncertainty). After snapover, a new current equilibrium is established where

any electron that enters the expanded sheath region must be accompanied by an electron that is collected to the conductor (due to charge conservation), regardless of the conductor size. Additionally, during gas discharge, any electrons liberated in a material ionization event will eventually be absorbed by a conductor (regardless of the conductor size) since the potential of the conductor will greatly exceed the kinetic energy of the ionized electrons. Thus, after a current jump, the I-V curve behavior (the absolute current, current jump magnitude, ratio, and I-V curve slope) is fully dominated by the most recent current transition, and the dependence of collected current on the conductor size diminishes.

As presented in Fig. 4.27, the relationships between snapover onset voltage, size of the current jump magnitudes, and current jump ratios on conductor size were also measured. For both snapover and gas discharge, no statistically significant correlation was found between the onset voltage and conductor diameter (see Fig. 4.27 (a)). However, both the current jump magnitude, ΔI, and current jump ratio, I_f/I_b, showed clear power law relationships to conductor diameter (see Figs. 4.27 (b) and (c)). For primary snapover, the current jump magnitude scaled somewhat less than the conductor area, or $\Delta I \sim d^n$ where $n=+1.6\pm0.3$ (within the uncertainty, this is the same power law relationship as was found for the absolute current dependence on conductor diameter after snapover). Also, the current jump magnitude of the gas-discharge was approximately linearly proportional to diameter, or $\Delta I \sim d^n$ where $n=+1.1\pm0.2$ (within the uncertainty this is also the same power law relationship as was found for the absolute current dependence on conductor diameter after gas discharge). The current jump ratios for both primary snapover and gas discharge were approximately inversely proportional to conductor diameter, or $I_f/I_b \sim d^n$ where $n=-0.87\pm0.09$ for primary snapover and $n=-1.1\pm0.1$ for gas discharge.

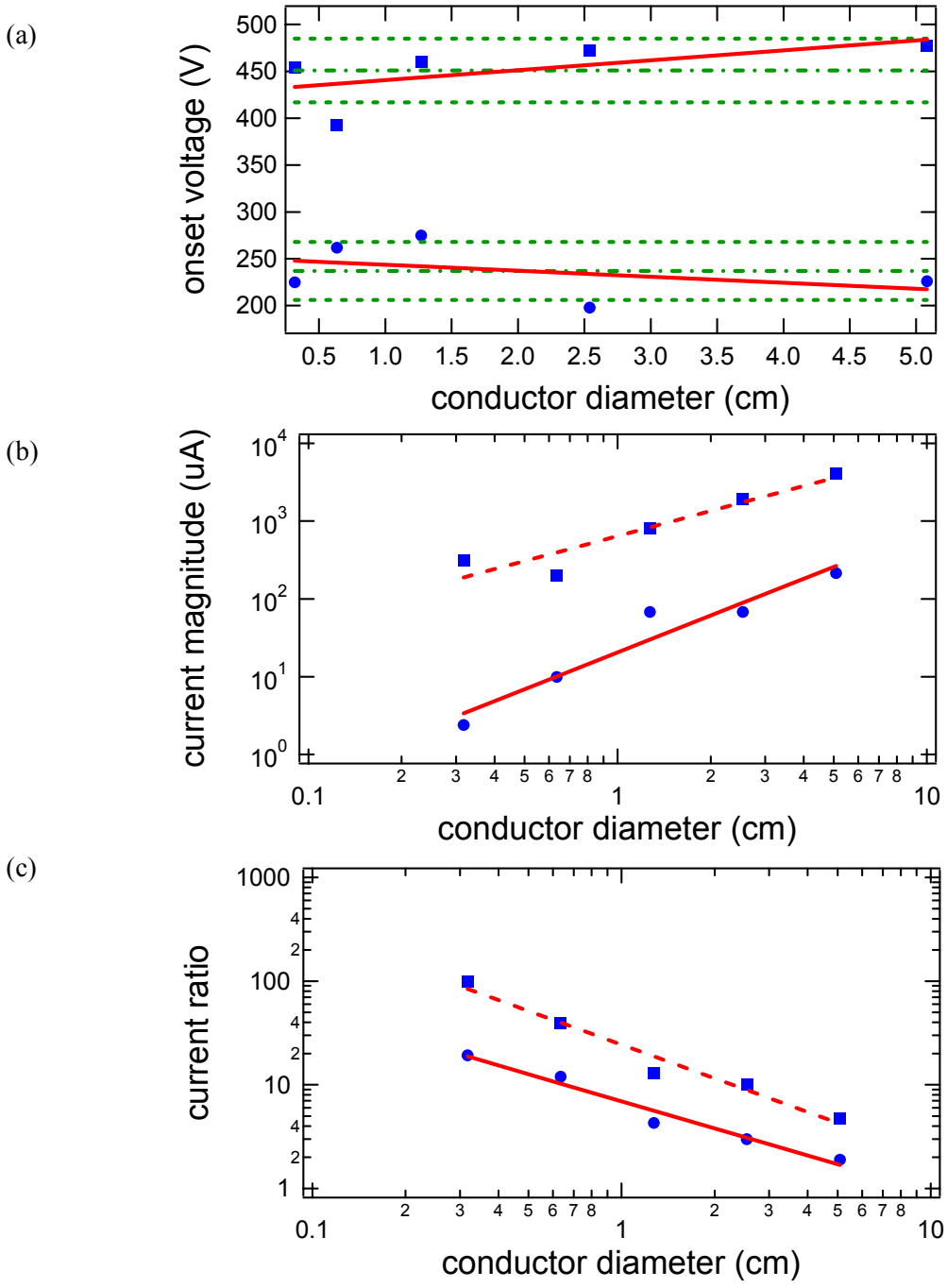

FIG. 4.27. Dependence of snapover and gas discharge onset voltages, current jump magnitudes, and current jump ratios on conductor size. Shown are the primary snapover current jumps (●) and gas discharges (■) for Cu-Teflon™ samples. (a) Dash-dotted and dashed lines indicate the average values and limits of uncertainty to within ±σ (standard deviation), respectively. Solid lines are linear fits to the data. There is no statistically significant dependence on onset voltage. (b) and (c) Shown are power law fits to the data demonstrating statistically significant dependence on current jump magnitude and current ratio.

In summary, these results show that snapover and gas discharge current jump magnitudes followed roughly the same power law dependence on conductor diameter as the absolute current measurements immediately following their respective current jumps. These two measurements are related because in the calculation of the current jump magnitudes (I_f-I_b), the current after snapover or gas discharge, I_f, is always much greater than the current before, I_b, (by one to three orders of magnitude) so that the power coefficient for I_f always dominates the current jump magnitude dependence on conductor diameter. The inverse relationship between the current jump ratios and conductor diameter can also be explained in terms of the absolute current measurements. Since the power law coefficient immediately before snapover or gas discharge is greater than the power law coefficient immediately after the current jump (by one), the ratio of the two quantities, I_f/I_b, goes roughly as $d^n/d^{(n+1)}$ with conductor diameter. Thus, for both snapover and gas discharge the ratio displays an inverse relationship on conductor diameter. A summary of the dependence of I-V curve characteristics on conductor size is presented in Table 4.3.

4.13 Dependence on Sample Conductor Shape

The effects of conductor shape on snapover and gas discharge current jumps were tested using a 1.27-cm diameter aluminum alloy hemisphere (sample 17) and 1.27-cm diameter aluminum alloy disks (samples 3 and 11) on Teflon™. The onset voltage for the hemispherical conductor was 52 V higher for primary snapover and 99-162 V higher for the gas discharge than the planar conductor. This result for primary snapover contradicts the analysis of Hastings and Chang that predicts that the planar geometry should have a larger snapover voltage than a hemispherical geometry (Hastings and Chang, 1989).

The overall current to the hemispherical conductor exceeded the current to the disk by

TABLE 4.3. Dependence of snapover and gas discharge characteristics on conductor diameter.

I-V curve characteristics	Before primary snapover	Across primary snapover	After primary snapover	Across gas discharge	After gas discharge
Current	$I \sim d^3$ ($n=3.3\pm0.5$)	–	$I \sim d^2$ ($n=1.7\pm0.4$)	–	$I \sim d^1$ ($n=0.6\pm0.4$)
Magnitude of current jump	–	$\Delta I \sim d^2$ ($n=1.6\pm0.3$)	–	$\Delta I \sim d^1$ ($n=1.1\pm0.2$)	–
Current jump ratio	–	$I_f/I_b \sim d^{-1}$ ($n=-0.9\pm0.1$)	–	$I_f/I_b \sim d^{-1}$ ($n=-1.1\pm0.1$)	–
I-V curve slope (effective conductivity)	$\Delta I/\Delta V \sim d^3$ ($n=2.7\pm0.6$)	–	$\Delta I/\Delta V \sim d^3$ ($n=2.8\pm1.0$)	–	–
Onset voltage	–	no dependence	–	no dependence	–

roughly an order of magnitude over the whole voltage range. According to area effects only (and assuming similar current densities) the hemispherical conductor sample should have only collected twice the current (since it had twice the exposed area) as the planar conductor sample. Perhaps the additional current to the hemispherical conductor before snapover resulted from having more of the conductor area standing away from the surrounding insulator plate, thus reducing the effects of insulator current suppression before snapover. After snapover, the increased current could have resulted from a more efficient capture of plasma electrons since the protruding hemispherical conductor geometry would more effectively intercept those electrons that would otherwise (for planar geometries) fly over the conductor region.

The current jump magnitudes for the hemisphere were eight times larger for the primary snapovers and 11 times larger for the gas discharges than the same diameter disk conductor. However, the current jump ratios did not show large variations with conductor shape. The large differences in current jump magnitude between planar and spherical geometries just reflect the differences in the overall enhanced current to the hemispherical sample throughout the I-V curves. However, for the current jump ratios, the overall increased current contribution before and after the current jumps divides out in the fraction such that this quantity is relatively the same for both planar and hemispherical geometries.

4.14 The Effects of Sample Surface Treatments

To further test the secondary electron model of snapover and also to explore methods of inhibiting current jumps and stave off the onset of snapover, the insulator surfaces of several Teflon™ samples were treated and tested through repeated cycling. Fig. 4.28 compares typical I-V curves of the treated samples to an untreated 1.27-cm conductor diameter Cu-Teflon™ sample

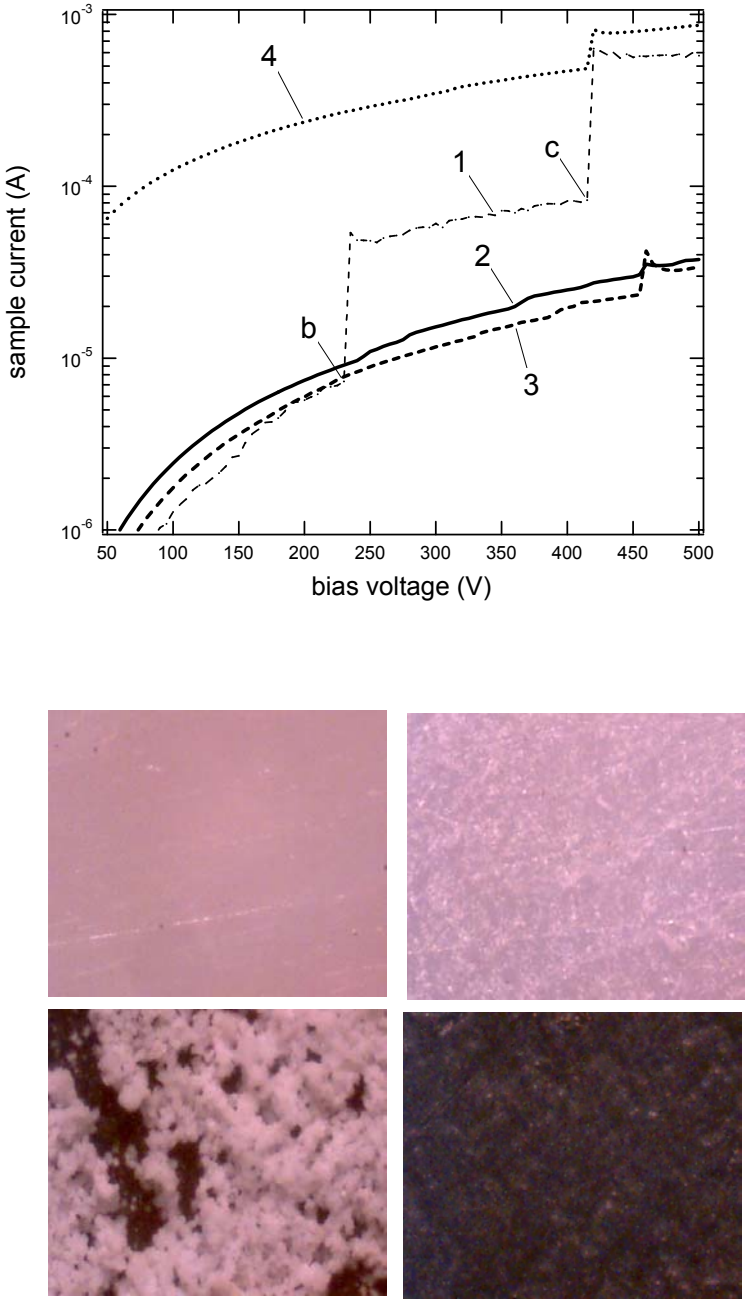

FIG. 4.28. I-V curves and optical micrographs for treated samples. (top) Current-voltage profiles showing the effects of surface modification on the b) primary snapover and c) gas discharge current jumps. Profiles shown are for: (1) an untreated 1.27-cm diam. Cu-Teflon™; (2) a 1.27-cm diam. Al-Teflon™ sample roughened with 70-μm grit sandpaper; (3) a 1.27-cm diam. Al-Teflon™ sample with the dielectric coated with a thin film of ~50-μm-sized cubic crystals of MgO; and (4) a 1.27-cm diam. Cu-Teflon™ sample with the dielectric coated with a thin film of colloidal microcrystalline graphite (Aerodag^{TM}). (bottom) Optical micrographs of these four samples (in order from left to right) are of ~900 μm x 500 μm areas.

acquired under similar plasma environments and with consistent ramping rates. Fig. 4.28 also shows optical micrographs of the surfaces.

For a 1.27-cm conductor diameter Al-Teflon™ sample, the insulator was roughened using 70-Fm and 100-Fm grit sandpaper. By doing so, snapover current jumps were greatly reduced or eliminated. In addition, gas discharge current jumps were typically reduced by more than an order of magnitude. In some cases both snapover and gas discharge current jumps almost completely disappeared. Reduction in snapover is consistent with the fact that roughening can reduce SE-induced current collection by recapturing SE's on adjacent surfaces before they can be transported to the conductor and initiate a charging cascade. However, the observation that both snapover and gas discharge current jumps were suppressed suggests that surface modification had other effects on the processes. Previous experimental studies have reported varied results for roughened surfaces (Stillwell *et al.*, 1985; Krauss, 1989), although Stillwell *et al.* (1985) reported similar findings that roughening decreases both snapover and gas discharge collection currents.

For a 1.27-cm conductor diameter Al-Teflon™, the sample insulator was coated with a thin film of ~50-µm sized nearly-cubic crystals of MgO suspended in alcohol. The results were very similar to those for roughened surfaces, with snapover nearly fully suppressed and gas discharge current jumps delayed and greatly reduced in magnitude. Since thin film MgO has a maximum SE yield two to eight times that of Teflon™, it is reasonable to expect SE-enhanced current jumps to increase rather than to be suppressed. However, the MgO microcrystals can be considered an alternate way to roughen the surface on approximately the same scale as the sandpaper, leading to diminished current collection similar to the roughened samples described above.

Finally, a thin film of Aerodag™ (colloidal microcrystalline graphite in isopropyl alcohol

with a polymer based binder) was applied around the conductors of two 1.27-cm conductor diameter Cu-Teflon™ samples in annulus rings with outer diameters of 2.3 cm and 4.3 cm. In doing so, the overall current flow to the conductor was increased by almost two orders of magnitude. The enhanced collection current resulted from the conducting properties of the graphite, and the absence of any visible gap between the Aerodag™ coating and the conductor. In effect, the conductor size of the samples was increased, resulting in a corresponding increase in the sample collection currents (see Section 4.12 above) due to an increased conductor area. The collected current to the Aerodag™-treated samples, along with an untreated Cu-Teflon™ sample compared to the calculated probe current to a 1.27-cm diameter planar probe, is shown in Fig. 4.29. As shown, the current to the treated samples increased with increasing Aerodag™ diameter, and was either modeled best by the thick-sheath limit (for the 2.3-cm OD region) or exceeded the thick-sheath model (for the 4.3-cm OD region). This result simply illustrates that the conducting properties of the graphite film enhanced the overall collected current to the samples as compared to the planar probe model for untreated samples.

Because of the large overall current increases due to the Aerodag™ conductivity on the semi-logarithm plots of Figs. 4.28 and 4.29, snapover and gas discharge current jumps on the Aerodag™ samples appear to be suppressed. However, closer inspection on a linear plot revealed that the current jumps were still present with magnitudes similar to those of untreated surfaces while the onset voltages remained relatively unaffected. However, based on the results of Section 4.12 one would expect the current jump magnitudes to scale with the conductor diameters as $\sim d^2$ for primary snapover and $\sim d^1$ for gas discharge. So, by increasing the conductor diameters by factors of roughly two and three (as was done by applying the Aerodag™ films) the current jump magnitudes should have increased by factors of roughly four and nine for primary snapover and

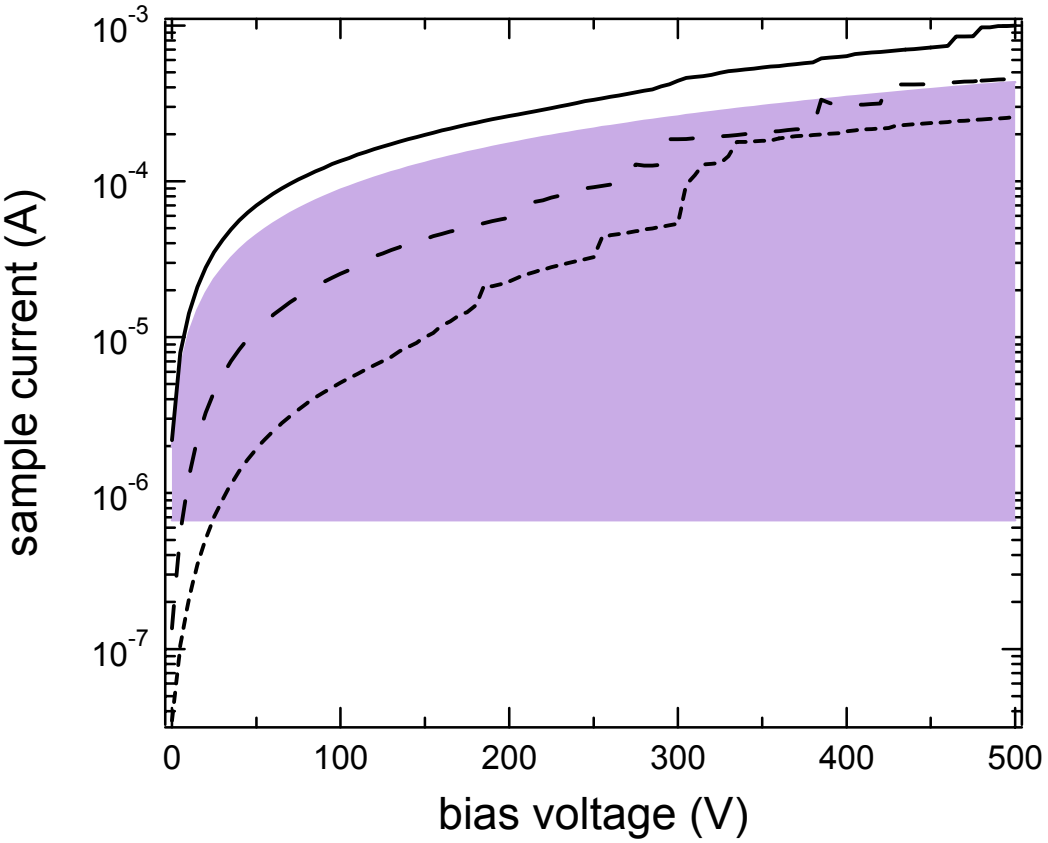

FIG. 4.29. Collected current to Aerodag™ treated Cu-Teflon™ samples. The 2.3-cm OD (long dashes) and 4.3-cm OD (solid) samples are compared to planar probe modeled current (shaded region) to a 1.27-cm diameter conductor probe without Aerodag™ (see Eq. (2.10)), and also to the average measured current to untreated 1.27-cm diameter Cu-Teflon™ samples (short dashes). The 2.3-cm OD treated sample was best modeled by the thick-sheath limit while the 4.3-cm OD treated sample exceeded planar probe model predictions.

two and three for gas discharge. Since this behavior was not observed, it seems that the Aerodag™ film acted to suppress the magnitudes of snapover and gas-discharge current jumps even though it increased the overall collected current to the sample. Graphite does not have a first crossover energy since δ_{max} <1; therefore, the SE model predicts a significant decrease in the collection currents after snapover (if snapover is to occur at all). The observed behavior that snapover and gas discharge occurred with current jump magnitudes similar to the untreated Teflon™ sample may have resulted from the diminished SE yields of the graphite films.

4.15 Optical Spectra of the Gas-Discharge Glow

During the normal snapover runs, at times a faint glow was observed to accompany the gas-discharge phenomenon. However, it was difficult to capture the optical glow on video or with a spectrometer since it did not always occur regularly under normal plasma conditions. In an attempt to increase the frequency of the glow phenomenon, the background Argon gas pressure was increased beyond 10^{-4} Torr. In doing so, it was observed that high-voltage current jumps occurred regularly between voltages of 600 V and 1000 V, and were accompanied by an intense blue-violet glow that was captured both on video and by a spectrometer (setup is outlined in Chapter 3). Spectral measurements of the optical glow revealed Argon, but no lines of other species were observed in part due to the low resolution of the spectrometer (see Fig. 4.30). This observation is consistent with the classification of such high-voltage current jumps being Paschen discharge of the background gas (see Section 4.1).

Any glow accompanying lower-voltage (between 200 V to 500 V) snapovers and gas discharges was too faint to analyze with the spectrometer, although previous studies have reported a faint white glow accompanying snapovers at inception voltages of ~250 V (Ferguson *et al.,* 1998). Gas discharge occurring at voltages of 350 V to 600 V was believed to be caused by the

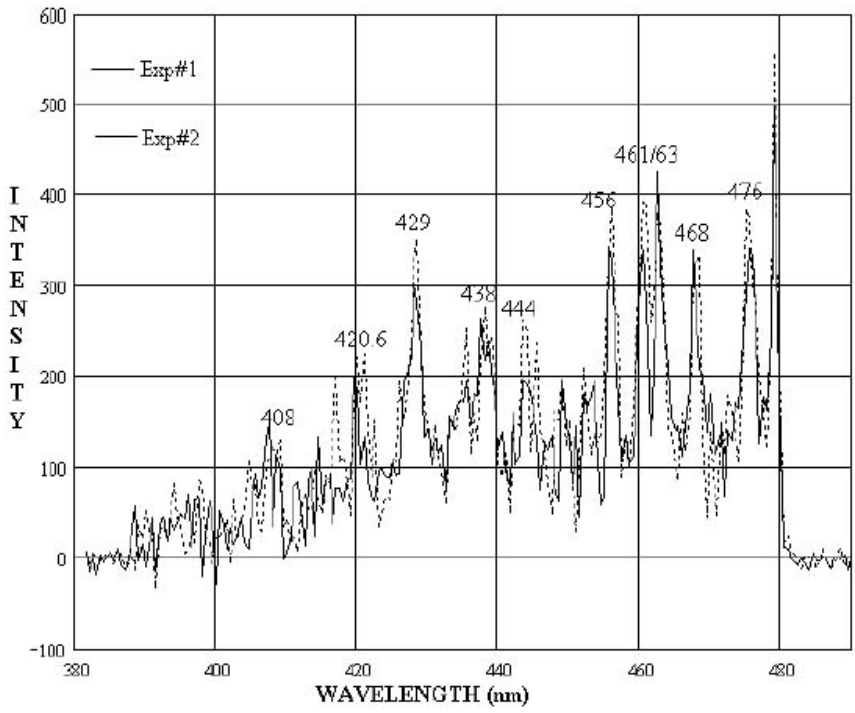

FIG. 4.30. Optical spectrum of the gas-discharge glow. Current jumps from 600 V to 1000 V showed Argon lines (420.6, 429, 438, 444, 456, 461). No other material lines could be clearly identified (figure adapted from Vayner *et al.*, 1999; see the Appendix).

out-gassing and subsequent ionization of materials originating from the sample. It was hoped that atomic or molecular emission and ionization signatures of the out-gassed materials would be evident in the spectra. However, due to the low intensity of the glow for the gas-discharge events, no spectra could be recorded. Further details of the glow discharges are found elsewhere (Vayner *et al.,* 1999, 2000; Galofaro *et al.,* 2000).

CHAPTER 5

PROPOSED FUTURE WORK

5.1 Future Snapover Experimental Work

In continuation of this work, a series of experimental investigations are proposed, some of which will be conducted by our group, to provide better statistical results, and additional information not obtained in the first experimental investigation. Many of the original experiments should be repeated, and other studies should be performed both to improve the previous investigation and to provide additional information on the snapover phenomenon. Suggestions for improvements and additional experiments include:

i) Reduce plasma chamber diffusion pump oil contamination on samples so that insulator dependence on snapover can be studied unambiguously (see Section 4.7). During the original experiment a valve on the plasma chamber was malfunctioning, causing excessive diffusion pump oil contamination (Galofaro *et al.*, 2000). Cleaner samples can be obtained in future experiments if the chamber is operating properly.

ii) To further monitor diffusion pump oil and other contamination effects, perform a "time in chamber" study on snapover inception voltages and current collection.

iii) Systematically study sample relaxation times for various voltage step sizes to accurately determine sample/plasma voltage lag dependence on ramping rates. Also, measure the equilibrium times for small voltage steps. In our current study, only the equilibrium times for large voltage steps (500 V, 600 V, and 700 V) were measured and could not be compared directly to voltage steps used in the I-V curve measurements (see Fig. 4.18). While performing these measurements, it would also be beneficial to measure equilibrium times immediately following snapover and gas discharge by modifying the sample bias

ramping program such that a large current jump would stop the ramping process (and maintain the sample at a constant voltage) but continue to measure sample current with time. By comparing the equilibrium times after snapover and gas discharge to equilibrium times before (but at comparable bias voltages), the temporal effects of these major current jumps on sample equilibrium could be determined. Finally, it would be beneficial to completely shut off the sample bias at various places on the I-V curve to measure snapover and gas discharge effects on sample discharging rates. Influences of snapover on solar array discharging rates have become a recent concern on the International Space Station since snapped-over solar arrays may hold a significant positive charge for extended lengths of time and may present electrical safety hazards to astronauts who come in contact with the arrays (Ferguson, 2001b).

iv) Use small bias voltage steps (perhaps 1 V) with relatively long time delays (0.5 to 1 s) when ramping samples so that measured uncertainties in snapover onset voltage are less than errors displayed in dielectric first crossover energies reported in the literature (10-20 eV). This would ensure that any uncertainty in correlating snapover inception voltages to first crossover energies does not arise from measurement resolution, but instead results from plasma perturbation effects or changing sample characteristics.

v) Perform ramping cycles on an isolated conductor disk (with no surrounding dielectric) for comparison with conductor/insulator sample current collection and planar probe theory so that insulator effects on snapover can be identified in I-V curve behavior (instead of being speculated from plasma probe theory as was done in this investigation).

vi) Gather more data of both insulator and conductor influences on snapover inception voltage and current collection to supplement data already taken. Specifically, experiments need to be repeated to test snapover onset voltage and current jump

magnitude on insulator and conductor type and conductor shape and size. Other insulators (such as isomica for comparison with Stillwell *et al.*, 1985) should be included to once again try to establish a dependence on insulator type. Also, different conductors should be used since both primary snapover and gas discharge onset voltages and current jump magnitudes showed some statistical dependence on conductor type (see Section 4.11). Insulator and conductor types should be chosen by the diversity of their SE characteristics.

vii) Include reduced conductor-sized samples (0.1 to 5 mm) so that experimental results can be directly compared with results reported by Stillwell *et al.* (1985), and also to simplify associated plasma physics by having the plasma sheath Debye length (~ 1-3 cm) much greater than the conductor probe dimensions. In principle, this would restrict plasma current collection to the thick-sheath regime. Also, by including smaller conductor-sized samples, the current power law relationship on conductor diameter discussed in Section 4.12 could be tested for smaller conductor sizes.

viii) Use insulator plates of different areas to explore the "area effect" as described by Grier and McKinzie (1972). By systematically increasing the area of the surrounding insulator, it may be possible to experimentally determine the extent of the insulator participating in snapover if the collected current approaches an asymptotic limit as a function of increasing insulator area.

ix) Perform identical studies with xenon background gas for comparison with argon. Lower voltage snapovers should not respond to such a change, but Paschen discharge and its characteristic glow should be. This would allow one to further determine the nature of high-voltage current jumps.

x) Continue to systematically explore sample surface treatments such as roughening and

coatings to find ways to mitigate parasitic currents to spacecraft by: using Aquadag™ (as opposed to Aerodag™) without a polymer binder to see if snapover will be triggered even though Aquadag™ has no first crossover energy; obtaining microimages of samples before and after multiple snapover cycles to obtain information on snapover induced surface damage, diffusion pump oil deposition, surface roughness, and applied coating thickness and topology; and systematically roughening surfaces on the order of 1 μm to 100 μm to determine optimal topology dimensions for reducing snapover current collection.

xi) Increase sensitivity of optical spectroscope setup to obtain stronger spectral lines of snapover and gas discharge glow, and determine the ion species contributions to each of these.

xii) Monitor insulator temperature simultaneously while measuring I-V curve behavior by implanting a thermocouple just beneath the insulator surface. This may yield information about the involvement of electron-stimulated insulator surface heating and any resulting gas desorption in I-V curve current jumps.

xiii) Monitor insulator charging and/or surface voltage in the vicinity of the conductor using a noncontacting capacitively coupled surface voltage probe (Stevens, 1979). This would allow the mapping of the area of the insulator participating in snapover, and also the monitoring of how insulator charging at various voltages affects sample/plasma current equilibrium times (see Section 4.6).

xiv) In addition to measuring insulator charging it would be extremely beneficial to simultaneously measure the surrounding plasma potentials along with sample I-V curves. Probe potential measurements could be made using an emissive probe following a similar technique used by Carruth (1987) and Gabriel *et al.* (1983) where a loop of

tungsten/rhenium wire is heated to incandescence and allowed to electrically float so that it reaches the surrounding plasma potential by thermal emission of electrons. By combining simultaneous measurements of the insulator potential, plasma potential, and sample I-V profile, the relevant physical mechanisms of snapover (sudden insulator charging, plasma sheath expansion, and anomalous currents) could be monitored, and the temporal sequence of these events could be used to improve present models. This would also provide a way to observe the dynamics of the insulator and sheath potentials during the low voltage snapovers and higher-voltage gas discharges.

5.2 Future Snapover Analysis

In addition to performing these experimental studies on snapover, further analysis of snapover data will include:

i) A model for dielectric charging under plasma electron bombardment and surface electron emission, in order to predict effects on snapover inception voltage. Dielectric charging estimates will be facilitated by experimental measurement of the charged insulator in the vicinity of the sample conductor. This model will include a review of previous work on "flashover" of insulators (dielectric breakdown of insulator/conductor systems in a vacuum) and of electron "hopping" conductivity for SE transport across insulator surfaces.

ii) Perform a more in-depth study of probe theory for planar geometries (both in the thick sheath and thin sheath limits) and plasma sheath response to changing dielectric surface charge. This may cast light on the discrepancies that occurred in using a Maxwellian velocity, collision-free, fully ionized plasma model for the planar sample conductor current.

iii) Perform PIC code simulations of the sample/plasma system to better understand plasma dynamics and resulting surface and plasma electron current involved in snapover and gas discharge. Both plasma dynamics and surface currents are coupled in a way that appears too complicated to calculate analytically. Such work may be accomplished in collaboration with R.W. Schunk at Utah State University based on his previous work with H. Thiemann (Thiemann and Schunk, 1990a, 1990b, 1994).

iv) Study models for incident and secondary electron effects on sample surface heating, neutral molecule desorption, and surrounding gas and neutral molecule ionizations in the vicinity of the sample. This may provide a model of gas-discharge snapovers that occurred at higher voltage.

5.3 Future Secondary Electron Emission Study of Insulators

In this study, it was found that reported first crossover energies for SE emission varied by as much as ±20 eV from one investigation to the next as different experimental methods were used to obtain these values. Consequently, to obtain self consistent SE yield values, measurements on multiple insulators must be made while maintaining an identical experimental setup for each insulator measurement. In doing so, systematic errors will remain constant, and relative insulator SE yield values can be directly compared to one another. Hopefully, this will provide the necessary precision in dielectric first crossover energies to test possible snapover inception voltage correlations. These studies will be conducted at Utah State University where the following tasks will be completed:

i) Conduct a systematic study of the total, secondary, and backscattered electron yield behavior as a function of incident electron beam energy for insulators used in spacecraft construction (Kapton™, Teflon™, SiO_2, etc.). In the process, obtain first crossover

energies of these insulators using consistent experimental methods so that yield values for different insulators can be directly compared to one another in a self consistent manner.

ii) Study the SE yield properties as a function of incident electron energy for other materials used in the snapover investigation such as MgO, diffusion pump oil, and Aquadag™.

iii) Monitor the degree of dielectric charging under electron beam bombardment at various incident electron energies and currents by comparing SE yield measurements at different pulsing and discharging rates and by using capacitive measurement techniques to estimate the charge accumulated on the insulator surfaces.

5.4 Peripheral Experimental Snapover Studies

If time permits, the following snapover studies will also be performed:

i) Vary sample temperature to induce surface contaminant desorption and study resulting gas discharge inception voltages and current collection magnitudes.

ii) Construct samples similar in geometry to solar arrays (thin linear conductor strips) to simulate parasitic current collection on spacecraft. Also, apply surface treatments to these geometries to study mitigation strategies for parasitic currents.

iii) Construct samples similar in geometry to spacecraft tethers (long conductor ribbons with insulator (Teflon™) strips running lengthwise) to simulate possible snapover-related effects on spacecraft tether technology.

iv) Use insulator plates of different thicknesses to study sample charging dependence, as well as possible influences this might have on snapover onset voltages and current collection.

v) Devise an ultra-high-vacuum (UHV) snapover simulation experiment where samples are biased (as in the plasma chamber) to collect electrons emanating from a low-energy

electron flood gun (< 50 eV). Although an UHV experiment would not realistically simulate plasma environment conditions, it would offer the advantage of testing the snapover phenomenon in the absence of surface contamination and background gas, and only in the presence of an electron current density. As a result, ionization processes in the total current collection could be eliminated and snapover dependence on insulator material driven currents could studied exclusively. An UHV chamber along with low-energy electron sources already exists at USU for these measurements.

CHAPTER 6

SUMMARY AND CONCLUSIONS

To summarize, snapover occurs when a conductor that is surrounded by an insulator is biased above some critical positive voltage with respect to the surrounding plasma. During snapover, the current drawn to the conductor suddenly increases at a positive threshold voltage. Snapover can occur on high-powered spacecraft solar array interconnects or on other exposed conductor surfaces that operate at high voltages. When snapover occurs, the parasitic current collected by the conductor increases substantially beyond the normal plasma electron current. Measurements of the surrounding plasma sheath and insulator potentials have shown that after snapover, large areas of the surrounding insulator charge positively to voltages just under the applied conductor voltage, and that the sheath area expands over large portions of the insulator, which allows greater interaction between the conductor/insulator system and plasma. Since the snapover phenomenon only occurs in the presence of insulators and since the insulator charges substantially positive after snapover occurs, researchers have been led to speculate that electron emissions from the insulator itself are in some way responsible for the enhanced parasitic current of snapover. Additionally, at higher voltages (> 300 V) it has been speculated that desorption, vaporization, and ionization processes on the insulator in the near vicinity of the conductor can further lead to sudden increases in the current collection.

Numerous computational and theoretical investigations have been performed on snapover, and have combined the dynamics of plasma electron and ion currents about a positively biased conductor that is surrounded by an insulator. Additionally, these models have simulated the emission and collection of secondary electrons from the insulator. In general, these models have shown that in the presence of secondary electrons, an anomalous current jump can occur at

voltages that are strongly dependent on the insulator SE first crossover energies. Additionally, they have simulated experimental measurements of sheath and insulator potentials before and after snapover. For example, they have shown that before snapover, the sheath is approximately spherical about the biased conductor and that the majority of the insulator surface is at a near zero (slightly negative) potential. They also show (in agreement with experiment) that after snapover, the insulator charges positively to a voltage just under the applied voltage, and that the sheath expands over a large area of the insulator. However, these models fail to predict threshold voltages in agreement with experiment (predicted voltages are typically too low by $ 100 V). Additionally, they fail to predict multiple current jumps that are seen in experiments (see Section 1.2 for more details).

The purpose of this investigation was to test the fundamental parameters of the snapover phenomenon, both to add to the already existent snapover data (most experimental data were taken more than 20 years ago), and to perform additional studies specifically aimed to test the secondary electron model. In our study, it was found that more than one current jump was observed over the range of +100 V to 1000 V; these jumps tended to grow in current jump magnitude with higher onset voltages. Based on previous interpretations, it was assumed that the lower voltage (~180 to 300 V) current jumps were dominated primarily by the SE mechanism and charging of the insulator, while higher voltage (> 300 V) current jumps were in fact dominated by gas-discharge processes (still intimately related to the presence of insulator SE's perhaps through secondary electron stimulated desorption).

However, the exact role of insulator SE emission in the multiple snapovers is still not clear. For example, during our measurements the inception of primary snapover would often drift to higher voltages and increase in current jump magnitude until it was indistinguishable from gas discharge. Additionally, much smaller current anomalies (current jumps and I-V curve slope

increases) were observed at lower voltages (100 to 150 V) more representative of the insulator SE first crossover energies. Future experimental investigations should be undertaken to reveal the true nature of SE involvement (see Chapter 5). For example, one method that could be used to test if a current jump was dominated by the insulator SE mechanism (as set forth by computational and theoretical models) would be to measure the sheath and insulator potential profiles while simultaneously measuring the I-V curve profiles to identify which current jump (see Section 5.1) is associated with rapid sheath expansion and insulator charging. To date, although plasma and insulator potentials have been measured separately well before and well after snapover, no experiment of the above type has been performed.

In an attempt to formulate a rough organization scheme to be used as a reference throughout this study, the multiple current jumps were classified into four major categories based on the value of onset voltage, magnitude of current jump, I-V curve behavior, dependence on conductor size, and optical emission as follows: a) preliminary snapover (~ 150 to 220 V onset voltage), b) primary snapover (also referred to as just snapover in this investigation, or as surface-enhanced mode by Stillwell *et al.* (1985) (~ 220 to 350 V onset voltage), c) gas discharge (or vapor-enhanced mode) (~ 350 to 600 V onset voltage), and d) Paschen discharge (600 to 1000 V onset voltage). In general, the preliminary snapover and primary snapover onset voltages were reproducible to within ± 20 V, and occurred consistently (primary snapover occurred more consistently than preliminary snapover) from one ramping cycle to the next. The gas-discharge and Paschen discharge onset voltages were not as reproducible, displaying an uncertainty of roughly ± 100 V. Additionally, they did not occur consistently from one ramping cycle to the next. The current typically increased by one to two orders of magnitude for preliminary and primary snapover, while the current could increase by as much as three orders of magnitude for gas discharge and Paschen-discharge current jumps.

Studies were focused mostly on the primary snapover phenomenon since it occurred most regularly for all samples, and was believed to be heavily influenced by SE emission from the insulator. This assumption was based both on previous interpretations and on the following observations: i) primary snapover occurred consistently for all sample types from one run to the next with a more or less regular threshold voltage; ii) the current to the samples after primary snapover was sustainable (roughly linear I-V curve behavior) indicating that a new quasi-steady state current equilibrium had been attained. In contrast, gas-discharge I-V curve current jumps were followed by a pronounced hook-shaped decline and subsequent recovery in the collected current, more representative of a burst of electrons released during out-gassing and ionization. On some runs, primary snapovers also exhibited this hook-shaped signature, but to a lesser extent.

Our parametric investigation of snapover yielded the following results:

i) Current collected to the conductor at low voltages (. 100 V) was substantially less than the predicted current to planar conductor probes as given by Parker and Whipple (1967), and modeled by Eq. (2.10). Similar findings have been reported in other experimental investigations, where it has been assumed that the insulator somehow suppresses plasma current collection to the conductor perhaps through a slightly negative charge induced on the surface by the surrounding plasma (Grier and McKinzie, 1972). Unfortunately, conductor samples (without the surrounding insulator) were not included in our experiments for comparison. After snapover and gas discharge, the measured current increased to (or exceeded) theoretical predictions.

ii) The I-V curve current jump behavior on first ramping cycles was notably different from subsequent ramping cycles. Particularly, many low-voltage (but small in current magnitude) snapovers occurred in addition to higher voltage (350 V to 500 V) gas-discharge current jumps (large in current magnitude). Although low-voltage snapovers

and gas discharges were observed on later runs, the first runs almost always displayed this behavior. The origin of these current jumps was interpreted as being excess contaminants (left over from vacuum break) that were desorbed and ionized during the initial gas discharge.

iii) Multiple cycles on a sample revealed that high-voltage Paschen discharge altered primary snapover and gas-discharge behavior (and thus appeared to have altered sample surface conditions) on ramping cycle runs immediately following these high-voltage current jumps.

iv) Hysteresis was observed in the I-V curve profiles. Generally, the current collected during reverse bias would follow the forward bias I-V curve back down, but without the discontinuous jumps in current at snapover and gas discharge voltages (as seen in the forward bias direction). A study of convergence of the average forward and reverse bias I-V curves (for a series of consecutive ramping cycles) was performed by taking the difference of the two curves. It was found that the two curves converged at voltages roughly corresponding to primary snapover (this behavior was expected), and also at a lower voltage of ~110 V (this was not expected). It should be noted that this lower voltage corresponded more closely to the insulator first crossover energies, which generally ranged from 30 V to 80 V (depending on the SE yield study). This convergence at ~110 V may have been associated with the small anomalies that sometimes occurred in this voltage range (see Fig. 4.2 (b)).

v) In taking the average first and second derivatives of the reverse bias curves it was found that the first derivative values increased substantially at voltages corresponding to primary snapover (due to the steep rise in collection current, or the increased I-V curve slopes during snapover). Additionally, at ~100 V the average second derivative curves

(and associated errors) fluctuated dramatically as compared to values prior to this voltage. As with the hysteresis convergence study, the curious behavior at ~100 V may have been associated with the small current anomalies that occurred in this voltage range.

vi) Ramping rates (1 V/s to 50 V/s) did not significantly alter the onset voltages of primary snapover. This indicated that the sample/plasma equilibrium time was significantly smaller than the time delay (usually 0.5 s) between the small voltage steps (usually 5 V) used in our study (even though instantaneous large voltage steps of 500 V, 600 V, and 700 V showed equilibrium times ranging from 10 s to 60 s). Consequently, the large discrepancies between primary snapover onset voltages and the corresponding insulator first crossover energies could not be reconciled by arguing that the sample/plasma system had not reached a current equilibrium state (Vayner *et al.*, 1999). In future investigations, this conjecture will be tested by monitoring the current equilibrium times for small voltage steps (see Section 5.1).

vii) Diffusion pump oil contamination introduced a problem in studying the insulator dependence of snapover. Between each vacuum break visible diffusion pump oil contamination was observed on the samples possibly due to a defective pump valve (Galofaro *et al.*, 2000). Although the diffusion pump oil did not completely mask insulator effects (since an insulator dependence before and after snapover was observed in the collected current as explained in Sections 4.9 and 4.10), it was suspected that the diffusion pump oil film thickness (estimated to be > 30 nm) was on the order of the mean SE escape depth for diffusion pump oil (20-30 nm) (Goto and Ishikawa, 1968). If this were the case, the snapover dependence on insulator type could not be correctly determined. Hopefully in future experiments the extent of diffusion pump oil contamination will be limited by properly functioning equipment.

viii) The I-V curves showed a clear plasma pressure dependence (current collection increased with increasing plasma pressure) prior to snapover. However, after snapover the overall average sample current at low pressures (66 FTorr) was comparable to the sample current at higher pressures (80 FTorr). This may be an indication that before snapover, the effective plasma current impedance (regulated primarily by the surrounding sheath dimensions) was strongly influenced by the surrounding background gas pressure. However, after snapover the local sheath expanded and surface contributions to the overall effective impedance dominated the current collection process.

ix) A clear snapover or gas-discharge onset voltage dependence on insulator type could not be established. The variations in snapover and gas-discharge inception voltages for a given sample insulator type exceeded the differences in average inception voltages between samples of different insulator types. This could have resulted from both diffusion pump oil contamination on insulator surfaces (so that all SE emission originated from diffusion pump oil) or local plasma conditions (such as perturbations) having a dominant effect on snapover inception. Also, the order of average snapover inception voltages did not correspond to the order of first crossover energies of the insulator materials. However, the reliability of reported insulator first crossover energy values is in question since insulator SE yield data vary substantially from one study to the next. Also, the primary snapover inception voltages were typically / 180 V higher than the corresponding insulator first crossover energies. Although there may have been some effective sample-plasma voltage lag (with respect to the applied conductor voltage) due to a finite sample/plasma equilibrium time, ramping rate studies showed that this lag was probably not significant for the small voltage steps used in our investigations (see Section 4.6). Consequently, one must conclude that primary snapover was not directly triggered

simply by reaching the insulator first crossover energy (or the associated applied conductor voltage), but that a more complicated condition for snapover inception existed. This condition involved a positive charge gradient originating from the conductor perimeter and emanating across the immediate insulator surface (facilitated by adsorbate finite conductivity effects). However, this expanding gradient would have to compete with the plasma/insulator equilibrium condition on the rest of the insulator outside of the conductor sheath region, where the insulator is maintained at a slightly negative voltage by the surrounding plasma. This competition could suppress the conductor sheath expansion and insulator charging, and potentially delay snapover to higher voltages.

x) Although it was observed that neither the current jump magnitude nor current jump ratio showed any definite dependence on sample insulator type, the overall current collection to a sample did show some dependence on the insulator. Before snapover, Kapton™ samples collected more current than either Teflon™ or SiO_2 samples (see Section 4.9). This was attributed to surface contaminants (such as H_2O) that readily adsorb onto the surface of Kapton™, and acted to increase the surface conductivity of the insulator. After voltages of ~ 250 V (corresponding to primary snapover onset voltages) the SiO_2 insulator sample collected significantly more current than either the Kapton™ and Teflon™ samples (see Section 4.9). This may have resulted either from the higher SE maximum yields of SiO_2 (in comparison to Kapton™ or Teflon™), or from the smoothness of the glass surface in comparison to the Kapton™ or Teflon™ surfaces.

xi) The data suggested that both primary snapover and gas-discharge inception voltages and current jump magnitudes may have displayed some dependence on conductor type–aluminum conductor samples exhibited lower inception voltages and current jump magnitudes than copper samples. Additionally, the overall current collected to the copper

samples was higher than the aluminum samples at lower voltages, before snapover. This dependence on conductor type was not expected, and may reflect differences in conductor oxide conductivity and desorption properties. For example, the insulating oxide layer of aluminum (Al_2O_3) may have experienced surface charging that could have affected both local sheath dynamics and polarizable contaminants. Further testing needs to be performed to confirm such conductor dependence. Results for the current jump ratio were inconclusive.

xii) For Cu-Teflon™ samples of different conductor diameters, conductor size did not seem to significantly alter primary snapover or gas-discharge onset voltages. However, the overall current as well as the current jump magnitudes and ratios for primary snapover and gas discharge showed a clear power law dependence on conductor size. Before snapover (at 50 V), the current to the sample scaled roughly as the conductor diameter cubed. If, at low voltages, the sheath diameter scaled linearly with the conductor diameter, then this result would imply that before snapover, the collected current varied with the plasma sheath volume or alternatively with the number of electrons within the sheath (assuming constant electron density) (see Section 4.12). Immediately following primary snapover the current scaled just less than proportional to the conductor area. This result could be interpreted as the current is proportional to the conductor/insulator collecting area, where the extent of the charged insulator participating in charge collection does not scale quite linearly with conductor diameter. Finally, immediately following gas discharge the current scaled less than proportional than the conductor diameter. From this, it could be interpreted that the current after gas discharge is proportional to the ionized particle transport distance across the charged portion of the insulator (where the radial extent of the charging scales less than proportional to the

conductor diameter). Alternatively, it could be interpreted that the current above gas discharge scales just less than linearly to the conductor/insulator interface (or circumference of the conductor). In general, these results showed that the dependence on conductor size diminished after each current collection transition (see Section 4.12). Finally, for primary snapover, the current jump magnitude scaled roughly as the diameter squared (or scaled roughly linearly with conductor area). For gas discharge, the current jump magnitude scaled roughly linearly with conductor diameter. Thus, the diameter-dependent trends for the current jump magnitudes seemed to correspond to the trends for the overall sample current after the corresponding current jump since the current after the jump dominated the difference calculation, I_f-I_b. For both primary snapover and gas discharge, the current jump ratios were roughly inversely proportional to conductor diameter. This inverse relationship for both snapover and gas discharge resulted since the current (as a function of diameter) power law coefficient before the respective current jump always exceeded the coefficient after the current jump by one.

xiii) The snapover average onset voltage of a hemispherical conductor was higher (by 52 V) than a planar conductor of similar material (both aluminum conductors surrounded by Teflon^{TM}), in contradiction to the prediction of Hastings and Chang (1989) based on their SE model. The hemispherical conductor probe collected roughly an order of magnitude more overall current than the planar probe over the entire bias voltage range. According to area effects only (and assuming similar current densities) the hemispherical conductor sample should have only collected twice the current (since it had twice the exposed area) as the planar conductor sample. Perhaps the additional current to the hemispherical conductor resulted as a consequence of having more of the conductor area standing away from the insulator plate so as not to be affected as strongly by insulator current

suppression before snapover. Also, the current jump magnitude for the hemispherical probe was roughly eight times (for snapover) and 11 times (for gas discharge) as large as the planar probe, while the current jump ratios for both snapover and gas discharge were similar in magnitude (see Section 4.13). These results for the current jump magnitudes and ratios are consistent with the absolute current measurements as discussed in Section 4.13.

xiv) Roughening the surfaces of the sample dielectrics on the order of 50 Fm to 100 Fm, either by abrasives or by applying a thin layer of randomly oriented cubic crystal MgO particles, inhibited the collection currents of both snapover and gas discharge. Coating the insulator surfaces with Aerodag^{TM} (colloidal microcrystalline graphite with a polymer binder base) did not fully suppress snapover or gas discharge (perhaps due to the polymer base), but increased the overall current collection to the sample by effectively increasing the conducting sample area (see Section 4.14).

xv) The glow that has been reported to accompany snapover was not captured on video or by a spectrometer. However, the optical spectrum of the glow accompanying what was believed to be either gas discharge (originating from the sample) or Paschen discharge (originating from the background gas) was recorded. From the spectrum, only argon lines could be clearly identified.

From these results, attempts to directly correlate primary snapover with the SE model of snapover were not successful for a number of reasons:

i) It was not always obvious whether primary snapover and gas discharge were driven by two completely different mechanisms or were both combined effects of SE emission and ionization of thermal or electron-induced desorption of surface materials.

ii) Insignificant current anomalies (jumps and slope increases) occurred at much lower

voltages (100 to 150 V) more representative of the insulator first crossover energies.

iii) Estimates of diffusion pump oil deposition rates suggested that the film thickness deposited by chamber contamination was much greater than the maximum escape depth of SE's in diffusion pump oil; this may have obfuscated any snapover dependence on sample dielectric type.

iv) Snapover inception voltages occurred at much higher voltages than simple interpretation of the SE model (based on computational and theoretical studies) suggests. As already explained, primary snapover voltages were $\sim$180 V higher than the associated first crossover energies of either sample dielectrics or diffusion pump oil.

v) SE values of the sample dielectric emission characteristics, including the first crossover energy, were not known with the necessary accuracy to verify snapover inception voltage dependence on dielectric first crossover energies.

vi) An inadequate number of samples were tested to conclusively rule out statistical dependence of primary snapover on dielectric first crossover energies.

vii) Snapover onset voltage and current jump magnitude exhibited some dependence on conductor type, which was not expected from the SE model.

viii) The snapover onset voltage of a hemispherical conductor was higher than for a planar conductor of similar material, in contradiction to the prediction of Hastings and Chang (1989) based on a SE model.

Although a detailed picture of the mechanism for snapover has not yet been clearly revealed by our study, many new insights into the phenomenon have been uncovered. To reiterate some of the key observations and results that are unique to this study:

i) To date, no comprehensive computational or theoretical model has included the combined effects of currents originating from: i) the plasma; ii) SE's; iii) BSE's; iv) finite insulator

surface conductivity; and v) desorption and ionization materials originating from the insulator (which seem to be just as important if not more important than pure SE contributions). Consequently, no model has been able to account for the multiple current jumps observed in measured I-V curves. Now that this is recognized, a suitable model may be developed that better simulates snapover data.

ii) Further attempts to perform ground-based studies of snapover dependence on insulator types may be seriously hampered by the prolific surface contamination (as compared to the SE mean escape depth) that exists in plasma chambers that operate at pressures of $\sim 10^{-6}$ to 10^{-4} Torr.

iii) Current jumps occurring at voltages between 600 to 1000 V (Paschen discharges) seemed to alter the surfaces of the insulators (perhaps permanently) as seen by the modified behavior of subsequent snapovers and gas discharges. In a previous study by Grier and McKinzie (1972), it was reported that current jumps occurring with voltages less than or equal to 10 keV could produce charring or melting of the insulator. In our study, it was observed that permanent material alterations may in fact occur at significantly lower voltages.

iv) Observations of the I-V profiles (Section 4.1), convergence between forward and reverse bias I-V curves (Section 4.5), and second derivative analysis of the reverse bias curves (Section 4.5) suggested that minor current collection mode transitions occurred at voltages well below the onset of any significant snapover at ~100 V, and may have been caused by immediate regions of the surrounding insulator reaching the first crossover energy and also by local sheath responses to immediate insulator charging.

v) Current collection before snapover is dependent on sample insulator and conductor materials, suggesting that finite surface conductivity of the surrounding insulator

(enhanced by adsorbed contaminants) or of oxide layers on the conductors may influence local plasma and insulator potentials before snapover–both of which are intimately connected with snapover onset voltages and current collection magnitudes. Additionally, after snapover the insulator type (but not the conductor) again influenced the overall sample current either because of differences in the SE yield properties of the insulators, or because of the relative surface roughness of the insulators.

vi) In order to further study snapover insulator SE yield dependence, consistent SE yield properties of the insulators must first exist in the literature (as indicated before, presently the variations in reported insulator first crossover energies for a given insulator are as large as the differences between different insulator values). Presently, up-to-date SE yield data on insulators are being measured at Utah State University.

vii) Although additional experiments need to be performed, the sample conductor type (aluminum or copper) seemed to affect both onset voltage and current jump magnitude of primary snapover and gas discharge as well as the overall current collection due perhaps to differences in oxide layer conductivity.

viii) Clear power law relationships between collected current and sample conductor diameter were found where the current before snapover, after snapover, and after gas discharge displayed power law coefficients to conductor diameter of roughly three, two, and one, respectively. For both snapover and gas discharge, power law coefficients of roughly two and one, respectively, for the current jump magnitudes were the same as the absolute currents following the corresponding current jumps (see Section 4.12). In future experimental investigations, smaller conductor sizes will be used to further verify this power law behavior.

ix) Finally, sample surface treatments to the surrounding dielectric were found to suppress

overall current collection as well as snapover and gas-discharge current jumps when roughened on the order of 50 Fm to 100 Fm most likely due to a SE inhibiting effect. These results could lead to possible mitigation strategies for the snapover parasitic power loss problem on spacecraft.

REFERENCES

Al'pert, Ya. L., A.V. Gurevich, and L.P. Pitaevskii, Space Physics with Artificial Satellites, (Consultant's Bureau, New York, 1965).

Brandon, S.T., R.L. Kessel, J. Enoch, and T.P. Armstrong, "Numerical simulations of positively-biased probes and dielectric-conductor disks in a plasma," J. Appl. Phys. 56 (11), 3215-3222 (1984).

Bruining, H., "Secondary electron emission," Philips Tech. Rev. 13 (3), 80 (1938).

Carruth Jr., M.R., "Plasma electron collection through biased slits in a dielectric," J. Spacecr. Rockets 24 (1), 79-85 (1987).

Chaky, R.C., J.H. Nonnast, and J. Enoch, "Numerical simulation of sheath structure and current-voltage characteristics of a conductor-dielectric disk in a plasma," J. Appl. Phys. 52 (12), 7092-7098 (1981).

Chang, W.Y., J.R. Dennison, J. Kite, and R.E. Davies, "Effects of evolving surface contamination on spacecraft charging," AIAA Paper 2000-0868, presented at the 38th AIAA Aerospace Sciences Meeting and Exhibit, Reno, NV (2000).

Chase, R.E., W.L. Gordon, and R.W. Hoffmon, Secondary Electron Emission Yield Annual Report for Period July 1, 1978 to June 30, 1979, Case Western Reserve University, Cleveland, OH, 1979 (unpublished).

Chung, M.S. and T.E. Everhart, "Simple calculation of energy-distribution of low-energy secondary electrons emitted from metals under electron bombardment," J. Appl. Phys. 45 (2), 707-709 (1974).

Cole, R.K., H.S. Ogawa, and J.M. Sellen Jr., "Operation of solar cell arrays in dilute streaming plasmas," AIAA Paper 69-262 (1969).

Davies, R.E., Measurement of Angle-Resolved Secondary Electron Spectra, Ph.D. dissertation, Utah State University, 1999.

Davies, R.E. and J.R. Dennison, "Evolution of secondary electron emission characteristics of spacecraft surfaces," J. Spacecr. Rockets 34 (4) (1997).

Davis, V.A. and B.M. Gardner, "Parasitic current collection by solar arrays in LEO," AIAA Paper 95-0594, presented at the 33rd AIAA Aerospace Sciences Meeting and Exhibit, Reno, NV (1995).

Dennison, J.R., J. Kite, W.Y. Chang, and R.E. Davies, "Absolute and differential spacecraft charging as a result of evolving surface contamination," presented at the 7th ESA Spacecraft Charging Conference, Noordwijk, The Netherlands, 2001 (unpublished).

Domitz, S. and J.C. Kolecki, "Effect of parasitic plasma currents on solar-array power output," NASA CP-2071, 358-375, 1979 (unpublished).

Ferguson, D.C., 2001a (private communication).

Ferguson, D.C., 2001b (private communication).

Ferguson, D.C., G.B. Hillard, D. Snyder, and N. Grier, "The inception of snapover on solar arrays: a visualization technique," AIAA Paper 98-1045, presented at the 36th AIAA Aerospace Sciences Meeting and Exhibit, Reno, NV (1998).

Gabriel, S.B., C.E. Garner, and S. Kitamura, "Experimental measurements of the plasma sheath around pinhole defects in a simulated high-voltage solar array," AIAA Paper 83-0311, presented at the 21st AIAA Aerospace Science Meeting and Exhibit,Reno, NV (1983).

Galofaro, J., B. Vayner, W. de Groot, D. Ferguson, C.D. Thomson, J.R. Dennison and R.E. Davies, "Inception of snapover and glow induced discharges," AIAA Paper 2000-0245, presented at the 38th AIAA Aerospace Sciences Meeting and Exhibit, Reno, NV (2000).

Goto, K. and K. Ishikawa, "Secondary electron emission from diffusion pump oils II.: δ-η Analysis for DC-705," Jpn. J. Appl. Phys. 7 (3), 226-231 (1968).

Grier, N.T., "High voltage surface-charged particles environment test results from space flight and ground simulation experiments," NASA TM-79184, 1-11, 1979 (unpublished).

Grier, N.T. and S. Domitz, "Current from a dilute plasma measured through holes in insulators," NASA TN D-8111, 1-26, 1975 (unpublished).

Grier, N.T. and D.J. McKinzie Jr., "Measured current drainage through holes in various dielectrics up to 2 kilovolts in a dilute plasma," NASA TN D-6663, 2-20, 1972 (unpublished).

Grier, N.T. and N.J. Stevens, "Plasma interaction experiment (PIX) flight results," NASA CP-2071, 295-314, 1978 (unpublished).

Hansen, W.N., 1999 (private communication).

Hastings D.E. and P. Chang, "The physics of positively biased conductors surrounded by dielectrics in contact with a plasma," Phys. Fluids B 1 (5), 1123-1132 (1989).

Hastings D.E. and H. Garret, in Spacecraft-Environment Interactions, edited by A.J. Dessler, J.T. Houghton, and M.J. Rycroft (Cambridge University Press, New York, 1996), pp. 142-203.

Hawley, R., "Solid insulators in vacuum: a review," Vacuum 18, 383-390 (1968).

Hendriks, B.H.W., G.G.P. van Gorkom, N. Lambert, and S.T. de Zwart, "Modes in electron-hopping transport over insulator sustained by secondary electron emission," J. Phys. D 30, 1252 (1997).

Hendriks, B.H.W., G.G.P. van Gorkom, A.T.M.H. van Keersop, and N. Lambert, "Dynamical behavior of electron hop transport over insulating surface," J. Appl. Phys. 85 (3), 1848-1856 (1999).

Hillard G.B. and D.C. Ferguson, "Solar array module plasma interactions experiment (SAMPIE): science and technology objectives," J. Spacecr. Rockets 30 (4), 488-494 (1993a).

Hillard G.B. and D.C Ferguson, "The SAMPIE flight experimental final technical requirements document," NASA TM-106224, 1993b (unpublished).

Kennerude, K.L., "High voltage solar array experiments," NASA CR-121280, 1974 (unpublished).

Kessel, R.L., R.A. Murray, R. Hetzel, and T.P. Armstrong, "Numerical simulation of positive-potential conductors in the presence of a plasma and a secondary-emitting dielectric," J. Appl. Phys. 57 (11), 4991-4995 (1985).

Krainsky, I., W. Lundin, W.L. Gordon, and R.W. Hoffmon, Secondary Electron Emission Yield Annual Report for Period July 1, 1980 to June 30, 1981, Case Western Reserve University, Cleveland, OH, 1981 (unpublished).

Krauss, A.R., "Localized plasma sheath model on dielectric discharge of spacecraft polymers," Air Force Weapons Laboratory Final Report AFWL-TR-88-37, 1989 (unpublished).

Lochte-Holtgreven, W., in Plasma Diagnostics, edited by H.F. Dylla (AIP Press, Woodbury, NY, 1995), pp. 668-731.

Mandell, M.J., 2000 (private communications).

Mandell, M.J. and I. Katz, "Potentials in a plasma over a biased pinhole," IEEE Trans. Nucl. Sci. NS-30 (6), 4307-4310 (1983).

Mandell, M.J., I. Katz, G.A. Jongeward, and J.C. Roche, "Computer simulations of plasma electron collection by PIX-II," J. Spacecr. Rockets 23, 512-518 (1986).

Miller, H.C., "Surface flashover of insulators," IEEE Trans. Electr. Insul. 24 (5), 765-786 (1989).

Moore, J.H., C.C. Davis, and M.A. Copeland, Building Scientific Apparatus, 2nd ed. (Addison-Wesley, Reading, MA, 1989), p. 335.

Mueller, C.W., "The secondary electron emission of pyrex glass," J. Appl. Phys. 16 453-458 (1945).

NASA Space and Environment Effects Branch, http://powerweb.grc.nasa.gov. (2001).

Nickles, N., R.E. Davies, and J.R. Dennison, "Applications of secondary electron energy-and angular-distributions to spacecraft charging," presented at the 6th International Spacecraft Charging Conference, Boston, MA, 1999 (unpublished).

Parker, L.W. and E.C. Whipple, "Theory of satellite electrostatic probe," Ann. Phys. 44 126-127 (1967).

Pillai, A.S. and R. Hackam, "Surface flashover of solid dielectric in vacuum," J. Appl. Phys. 53 (4), 2983-2987 (1982).

Snyder, D.B., "Dynamic interactions between ionosphere plasma and spacecraft,"presented at the 75th Anniversary U.R.S.I Symposium, Brussels, Belgium, 1995 (unpublished).

Stevens, N.J., "Interactions between spacecraft and the charged particle environment," NASA CP-2071, 268-294, 1979 (unpublished).

Stillwell, R.P., R.S. Robison, and H.R. Kaufman, "Current collection from the space plasma through defects in solar array insulation," J. Spacecr. Rockets 22 (6), 631-641 (1985).

Thiemann, H. and R.W. Schunk, "Particle-in-cell simulations of sheath formation around biased interconnectors in a low-earth-orbit plasma," J. Spacecr. Rockets 27 (5), 554-562 (1990a).

Thiemann, H. and R.W. Schunk, "Advanced model of solar array-plasma interactions," presented at the ESA Workshop on Space Environment Analysis, ESTEC, Noordwijk, The Netherlands, 1990b (unpublished).

Thiemann, H. and R.W. Schunk, "Computer experiments on arcing processes as observed in ground tests," J. Spacecr. Rockets 31 (6), 929-936 (1994).

Thiemann, H., R.W. Schunk, and K. Bogus, "Where do negatively biased solar arrays arc?," J. Spacecr. Rockets 27 (5), 563-565 (1990).

Thomas, S. and E.B. Pattison, "Range of electrons and contributions of back-scattered electrons in secondary production in aluminum," J. Phys. D 3 349-357 (1970).

Thomson, C.D., J.R. Dennison, R.E. Davies, B. Vayner, J. Galofaro, D. Ferguson, and W. de Groot, "Investigation of the first snapover of positively biased conductors in a plasma," AIAA Paper 2000-0869, presented at the 38th AIAA Aerospace Sciences Meeting and Exhibit, Reno, NV (2000).

Uman, M.A., Introduction to Plasma Physics, (McGraw-Hill, Inc., 1964), p. 114.

Vayner, B., C.V. Doreswamy, D.C. Ferguson, J.T. Galofaro, and D.B. Snyder, "Arcing on aluminum anodized plates immersed in low density plasmas," J. Spacecr. Rockets 35 (6), 805-811 (1998).

Vayner, B., J. Galofaro, D. Ferguson, and W. de Groot, "The conductor-dielectric junction in a low density plasma," NASA TM 1999-209408, 1-23, 1999 (unpublished).

Vayner, B., J. Galofaro, D.C. Ferguson, W. de Groot, C.D. Thomson, J.R. Dennison, and R. Davies, "A comprehensive study of the conductor-dielectric junctions in low density plasmas," AIAA Paper 2000-0871, presented at the 38th AIAA Aerospace Sciences Meeting and Exhibit, Reno, NV (2000).

Whetten, N.R. and A.B. Laponsky, "Secondary electron emission from MgO thin films," J. Appl. Phys. 30 (3), 432-435 (1959).

Willis, R.F. and D.K. Skinner, "Secondary electron emission yield behavior of polymers," Solid State Commun. 13, 685-688 (1973).

APPENDIX

June 25, 2001

Dale C. Ferguson
NASA Glenn Research Center
Mail Stop 302-1
21000 Brookpark Rd.
Cleveland, OH 44135
Phone: (216) 433-2298

Dear Dale:

I am in the process of preparing my Master's Thesis in the Physics Department at Utah State University. I have finished all of the essential editing, and I hope to have all other requirements completed by early August of 2001.

I am requesting your permission to include the attached material as shown for a figure in my thesis. This figure was prepared by your staff for the NASA Technical Memorandum 1999-209408. I will make acknowledgments and/or appropriate citations to your work as shown and any copyright and reprint rights information in a special appendix. The bibliography citation will appear at the end of the manuscript as shown. Please advise me of any changes you require.

Please indicate your approval of this request for the use of this figure by signing the space provided, and by attaching any other form or instruction necessary to confirm permission from NASA. If you have any questions, please call me at the number above.

If you are aware of any additional restrictions by NASA in reproducing this figure, please forward my request to the appropriate person or office.

Thank you for your cooperation,

Clint Thomson

I hereby give permission to Clint Thomson to reprint the following material in his thesis.

Description: Figure 9 (a) of the optical spectrum of gas-discharge glow in argon plasma, from: B. Vayner, J. Galofaro, D. Ferguson, and W. de Groot, "The conductor-dielectric junction in a low density plasma," NASA TM 1999-209408, 14 (1999).

Signed _____